The role of the signalling protein XLαs in cardiovascular control in mice

Thesis submitted in accordance with the requirements of the University of Liverpool for the degree of Doctor of Philosophy

By

Nicolas Nunn

December 2012

Abstract

Loss of the signalling protein XLαs in mice leads to a lean phenotype characterised by increased energy expenditure due to elevated sympathetic nervous system (SNS) stimulation of brown adipose tissue. XLαs is the protein produced from the *Gnasxl* transcript of the imprinted *Gnas* locus, and has a restricted expression pattern that includes a number of brain regions essential for SNS control of both energy expenditure and the cardiovascular system. However, it is unknown to what degree XLαs influences overall sympathetic tone, or how XLαs signalling in the brain causes these phenotypic changes.

Using arterial cannulation, anaesthetised *Gnasxl* knockout mice had elevated blood pressure, shown to be caused by increased SNS stimulation by a greater blood pressure response to the sympatholytic reserpine in knockouts. Using electrocardiogram (ECG) telemetry, conscious *Gnasxl* knockout mice had elevated heart rate at night, as well as a significant heart rate response to both reserpine and the parasympatholytic atropine. This supported the previous results showing elevated SNS stimulation of the cardiovascular system, but paradoxically also suggested elevated parasympathetic stimulation. Therefore, autonomic control of the cardiovascular system was investigated in further detail by analysing heart rate variability (HRV).

A number of HRV analyses were experimentally validated in wildtype mice. The most reliable method was the fast Fourier transform (FFT); high frequency (HF) power was used as a measure of parasympathetic activity, and low frequency (LF)/HF ratio was used as a measure of sympathetic activity. *Gnasxl* knockouts had a greater LF/HF response to reserpine, but an equivalent HF response to atropine, suggesting the mice had elevated SNS activity only. Additionally, knockouts had elevated LF/HF ratio at night, suggesting consistently elevated SNS output.

Neuronal signalling pathways that may be deregulated in *Gnasxl* knockouts were investigated by injection of MTII and Exendin-4, agonists to the melanocortin 3/4 and GLP-1 receptors, respectively. *Gnasxl* knockouts had a hypersensitive heart rate response both to centrally injected MTII in anaesthetised mice and peripherally injected Exendin-4 in conscious mice. The hypersensitivity to Exendin-4 was investigated further by HRV analysis, which showed that Exendin-4 had no effect on the SNS, but caused a potent reduction in parasympathetic activity in both wildtypes and knockouts.

Neuronal signalling changes in response to Exendin-4 were investigated by antibody staining for the early response gene c-fos. No significant differences were seen in overall numbers of activated neurones between wildtypes and knockouts in a number of brain regions including the nucleus of the solitary tract (NTS). Interestingly, neurones expressing XLαs showed no c-fos response to Exendin-4, except in the area postrema.

In summary, loss of XLαs in mice resulted in elevated SNS stimulation of the cardiovascular system, as well as hypersensitivity to Exendin-4 that was unlikely to be caused by increased activation of XLαs-deficient neurones.

Acknowledgements

Firstly, I need to thank my supervisors Dr Antonius Plagge and Dr Richard Barrett-Jolley, without whom this project would not exist. I also need to thank them for all their help and guidance, without which I wouldn't have succeeded.

Thanks to Katie Burton for teaching me to do immunohistochemistry, Claire Feetham for helping me with the *in vivo* experiments, especially the telemetry surgery, and Becky Lewis for always having a helpful word. Also thanks to the honours students Jennifer Martin and Jenny Kasper who helped with the c-fos immunohistochemistry.

Thanks to Kelly, and to my friends, especially Matt, who put up with me and helped keep me sane throughout my PhD.

Finally, thanks to the IMB for funding my project.

Contents

List of figures

List of tables

List of abbreviations

1°	primary
2°	secondary
α-MSH	alpha melanocyte stimulating hormone
AC	adenylate cyclase
aCSF	artificial cerebrospinal fluid
Arc	arcuate nucleus
ATP	adenosine-5'-phosphate
BAT	brown adipose tissue
BCIP	5-bromo-4-chloro-3-indolyl phosphate
bp	base pair
BP	blood pressure
cAMP	cyclic adenosine mono phosphate
ChAT	choline acetyl transferase
CNS	central nervous system
cre	cre recombinase
CSF	cerebrospinal fluid

DAB	3,3’-Diaminobenzidine
DAPI	4’,6’-diamino-2-phenylindole
DEM	data exchange matrix
DIG	digoxigenin
DMH	dorsomedial nucleus of the hypothalamus
dNTP	deoxyribonucleotide triphosphate
ECG	electrocardiogram
ECL	enhanced chemiluminescence
EDTA	ethylene diamine tetraacetic acid
ESC	embryonic stem cell
EtBr	ethidium bromide
EtOH	ethanol
FFT	fast Fourier transform
GABA	gamma-aminobutyric acid
Gad67	glutamate decarboxylase 67 kDa
GLP-1	glucagon-like peptide 1
GLP-1R	glucagon-like peptide 1 receptor
GPCR	g-protein coupled receptor

$G_s\alpha$	stimulatory g-protein alpha subunit
H_2O_2	hydrogen peroxide
HF	high frequency
HR	heart rate
HRP	horseradish peroxidise
HRV	heart rate variability
HSL	hormone-sensitive lipase
ICV	intracerebroventricular
IF	immunofluorescence
IHC	immunohistochemistry
ip	intraperitoneal
iv	intravenous
kb	kilobase (1,000 base pairs)
kDa	kilo Dalton (molecular weight X 1000)
KO	knockout
LC	locus coeruleus
LF	low frequency
LF/HF	low frequency to high frequency ratio

LH	lateral hypothalamus
loxP	locus of chromosomal crossover (x) in bacteriophage P1
m-/p+	knocked out on the maternal allele
m+/p-	knocked out on the paternal allele
MC3/4R	melanocortin 3/4 receptor
MeOH	methanol
mRNA	messenger ribonucleic acid
NE	norepinephrine
NBT	nitroblue tetrazolium
NP-40	nonidet P40
NTS	nucleus of the solitary tract
O/N	overnight
Oed-Sml	oedematous-Small
PBS	phosphate buffered saline
PCR	polymerase chain reaction
PFA	paraformaldehyde
P-HSL	phosphorylated hormone sensitive lipase
PK	Proteinase K

PKA	protein kinase A
PMSF	phenylmethylsulfonyl fluoride
PNS	parasympathetic nervous system
POMC	proopiomelanocortin
PVN	paraventricular nucleus of the hypothalamus
RMSSD	root mean square of successive differences
RPa	Raphe pallidus
RR	interval between two R peaks (of the ECG QRS spectrum)
RT	room temperature
sch1	schedule 1
SD	standard deviation
SDNN	standard deviation of normal RR intervals
SDS	sodium dodecyl sulphate
SDS-PAGE	sodium dodecyl sulphate polyacrylamide gel electrophoresis
SEM	standard error of the mean
SNS	sympathetic nervous system
SSC	sodium chloride-sodium citrate

TAE	tris-acetate-EDTA
TE	Tris EDTA buffer
TEMED	N,N,N',N'-Tetramethylethylenediamine
TH	tyrosine hydroxylase
Tris	tris(hydroxymethyl)aminomethane
TX	Triton X-100
UCP1	uncoupling protein 1
UV	ultraviolet
V	volts
v/v	volume over volume
VMH	ventromedial nucleus of the hypothalamus
w/v	weight over volume
WAT	white adipose tissue
WT	wildtype
XGal	5-bromo-4-chloro-3-indolyl b-D-galactopyranoside
XLαs	extra-large variant of the stimulatory g-protein alpha subunit

1 Introduction

1.1 Obesity and cardiovascular disease

Obesity is a major global health concern (Figure 1). According to the World Health Organisation (WHO), worldwide obesity has doubled since 1980 (www.who.int). In 2008, more than 1.4 billion adults were overweight, and 500 million were obese, which is more than 10% of the global adult population. This is caused by a global increase in high-energy foods and a decrease in physical activity. Obesity has a number of pathological consequences, including cardiovascular disease, diabetes, osteoarthritis and cancers; risk factors for these diseases increase with BMI. In fact, cardiovascular disease is the major cause of death worldwide, and was responsible for 30.5% of deaths in 2008.

Alterations in energy balance often correlate with effects to the cardiovascular system. For example, obesity is strongly correlated with hypertension and other forms of cardiovascular disease (Hall *et al.*, 2010). These changes are frequently associated with changes in autonomic control, (Matsumura *et al.*, 2003; Balthasar, 2009), in particular to the sympathetic nervous system (SNS) (Malpas, 2010). Animal models are useful for studying physiological control of energy balance, in particular transgenic mouse models are being used more and more. Disturbances to both energy balance and the cardiovascular system are relevant to this project and correlations will be investigated in Chapter 3, followed by further investigation in later chapters into the cardiovascular system.

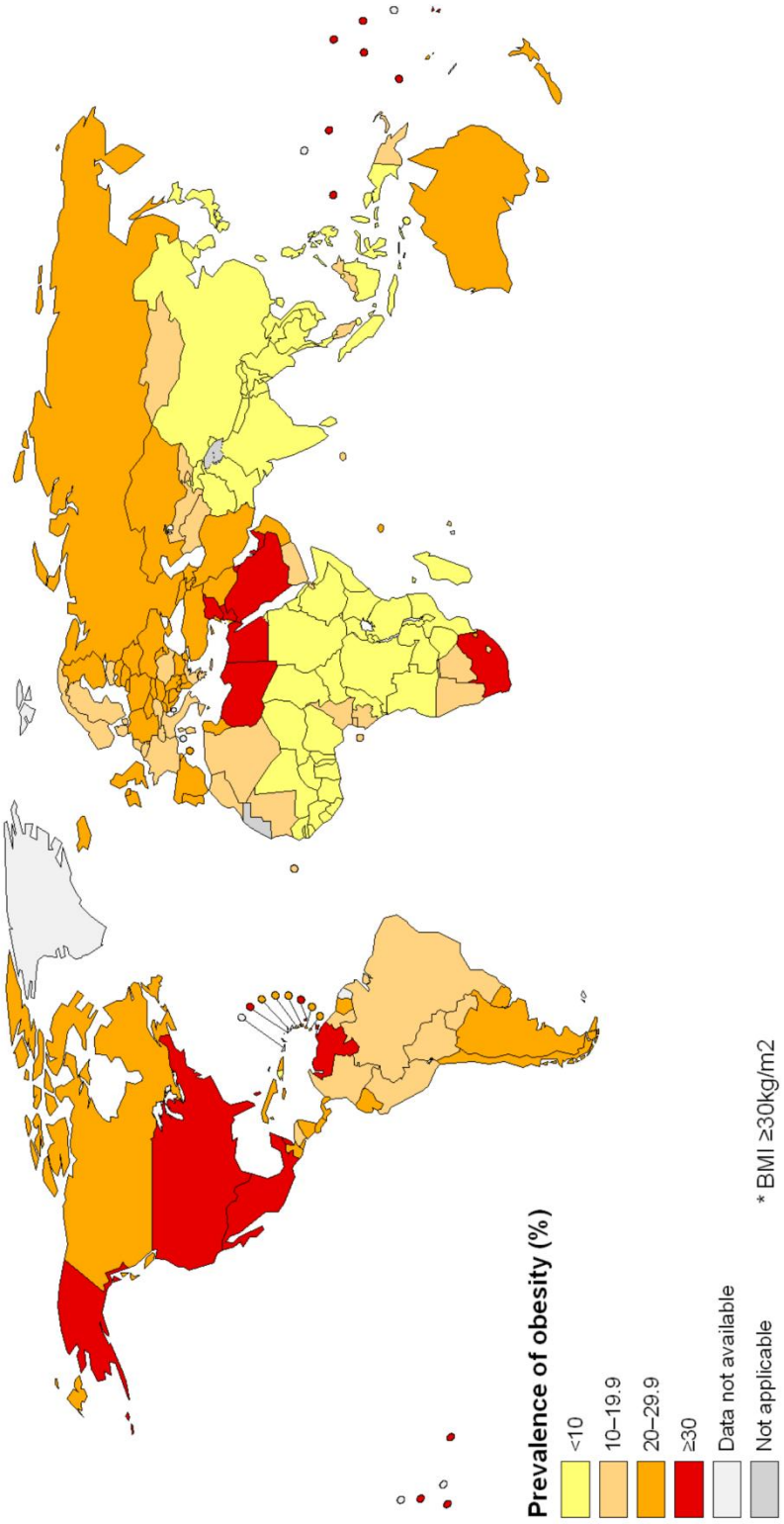

Figure 1.1. Prevalence of obesity worldwide.
Countries of the world are colour coded to indicate percentage obesity of the population, defined as those individuals with a BMI greater than or equal to 30 kg/m^2. Data are from 2008 (taken from WHO website October 2012: www.who.int)

1.2 The autonomic nervous system

The autonomic nervous system regulates animal physiology to maintain homeostasis of the body's systems, including the cardiovascular system and energy balance. A number of inputs feed into the central nervous system (CNS) where they are integrated, and the CNS exerts control via the two branches of the autonomic nervous system, the sympathetic and parasympathetic branches. The sympathetic nervous system (SNS) has classically been associated with the "flight or fight" response, and gives a stimulatory outcome to many peripheral tissues, for example increasing blood pressure and heart rate. The parasympathetic nervous system (PNS) opposes the SNS, and generally depresses peripheral effectors, for example decreasing blood pressure and heart rate. However, unlike the classic view of only acting in extreme situations, the SNS and PNS are constantly regulating homeostasis (Malpas, 2010).

1.2.1 Autonomic hierarchy

The autonomic nervous system is tightly controlled by a number of key brain regions, and the hierarchy of CNS control has been investigated in detail. The nucleus of the solitary tract (NTS) in the medulla is the primary site for information coming into the brain, via visceral afferents that synapse onto second order neurones in the NTS (Figure 1.2A) (Andresen & Paton, 2011).

There are also a few areas in the brain where the blood brain barrier (BBB) is "leaky", allowing hormones and other peripheral factors to cross. These are the circumventricular organs, and include the area postrema (AP) which lies alongside the NTS and the arcuate nucleus (ARC) in the hypothalamus.

These inputs provide constant updates concerning the homeostatic status of the body.

There are a number of brain regions crucial for initiation and control of SNS output (Figure 1.2B). Of particular importance to controlling SNS activity, is the paraventricular nucleus of the hypothalamus (PVN), which acts as a controlling hub of SNS outflow (Card & Sved, 2011). The PVN is subject to tonic GABAergic inhibition; sensitivity of the PVN neurones to GABA has been associated with elevated SNS activity and chronic heart failure (Patel, 2000; Zhang *et al.*, 2002; Li & Patel, 2003).

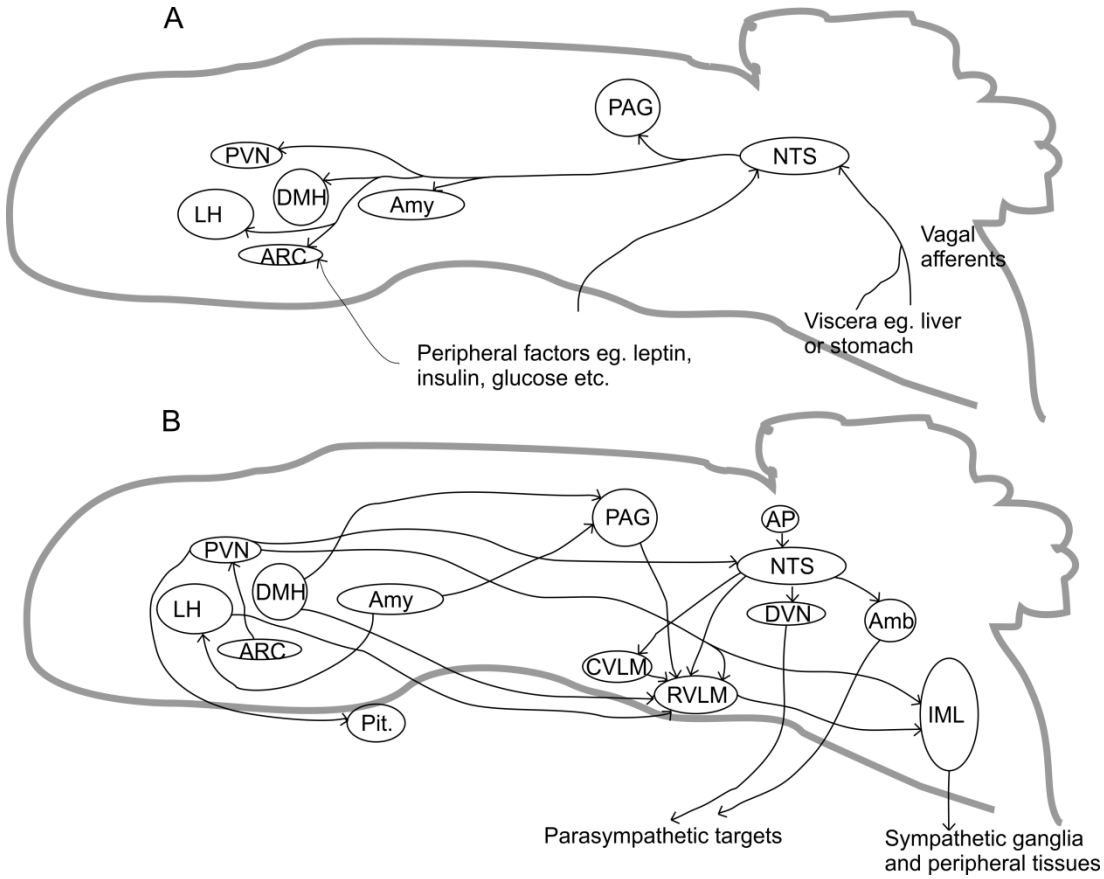

Figure 1.2. Central control of the autonomic nervous system.
(A) Diagram showing the main brain regions involved in receiving and integrating autonomic inputs, especially via the NTS.
(B) Diagram showing the main brain regions involved in initiation and control of the autonomic nervous system. Of particular important for SNS control is the PVN, and for SNS control of the cardiovascular system the RVLM. The NTS is especially important for control of the PNS.
Sizes and locations of brain regions are approximate.
Abbreviations used: PVN, paraventricular nucleus of the hypothalamus; DMH, dorsomedial nucleus of the hypothalamus; LH, lateral hypothalamus; ARC, arcuate nucleus; Amy, amygdala; PAG, periaqueductal grey; NTS, nucleus of the solitary tract; Pit., pituitary; CVLM, caudal ventrolateral medulla; RVLM, rostral ventrolateral medulla; AP, area postrema; Amb, ambiguus nucleus; DVN, dorsal vagal nucleus; IML, intermediolateralis of the spinal cord. Modified from (Andresen & Paton, 2011; Card & Sved, 2011; Stern, 2011).

1.2.2 Cardiovascular control

It is important for the body to be able to maintain blood pressure at a constant level despite, for example, changes in posture that cause a drop in pressure, and to maintain blood pressure during changes to cardiac output, such as during exercise. The demand for blood pressure elevation must be balanced against the destructive force of high pressure, and a number of homeostatic mechanisms are involved that include both short- and long-term control.

Blood pressure is determined by a combination of blood volume, force of contraction of the heart, and peripheral resistance. Blood pressure can be controlled by direct stimulation by the autonomic nervous system, for example of the heart or blood vessels, or by indirect signalling, for example control of the kidney by the renin-angiotensin system.

Autonomic control of the heart occurs via the SNS and the PNS, which provide stimulatory and inhibitory inputs, respectively (Figure 1.3A). Autonomic control of the vasculature is mainly by the SNS, which causes constriction of the vessels to increase peripheral resistance thereby increasing blood pressure (Figure 1.3B).

The major cause of short-term blood pressure control is mediated via the baroreflex (Dampney *et al.*, 2002); this consists of stretch sensitive baroreceptors in the aortic arch and the carotid body, which relay blood pressure information to the brainstem, specifically via the NTS and ventrolateral medulla. The baroreflex, initiated by either a decrease or increase in blood pressure, will result in reflex changes to both sympathetic

and parasympathetic output depending on the response required. There are also short-term “feed-forward” mechanisms which can alter blood pressure control depending on more complex behavioural activity (Dampney *et al.*, 2002). For example, anticipation of exercise results in increased cardiovascular stimulation.

Long-term blood pressure control depends largely upon the activity of the kidneys, with regards to retention of water and salt (Dampney *et al.*, 2005). The kidney is controlled by direct stimulation by the SNS, as well as indirectly by hormones including angiotensin II and vasopressin. These stimulate retention of salt and water, resulting in increased blood volume and therefore increased blood pressure. Renal sympathetic nerve activity is known to be increased in hypertension (Esler & Kaye, 1998). A number of CNS regions are known to be important for long-term blood pressure control, especially the rostral ventrolateral medulla (RVLM), and the hypothalamic PVN (Dampney *et al.*, 2005). There are also indications that the baroreflex can be involved in long-term blood pressure control (Thrasher, 2004).

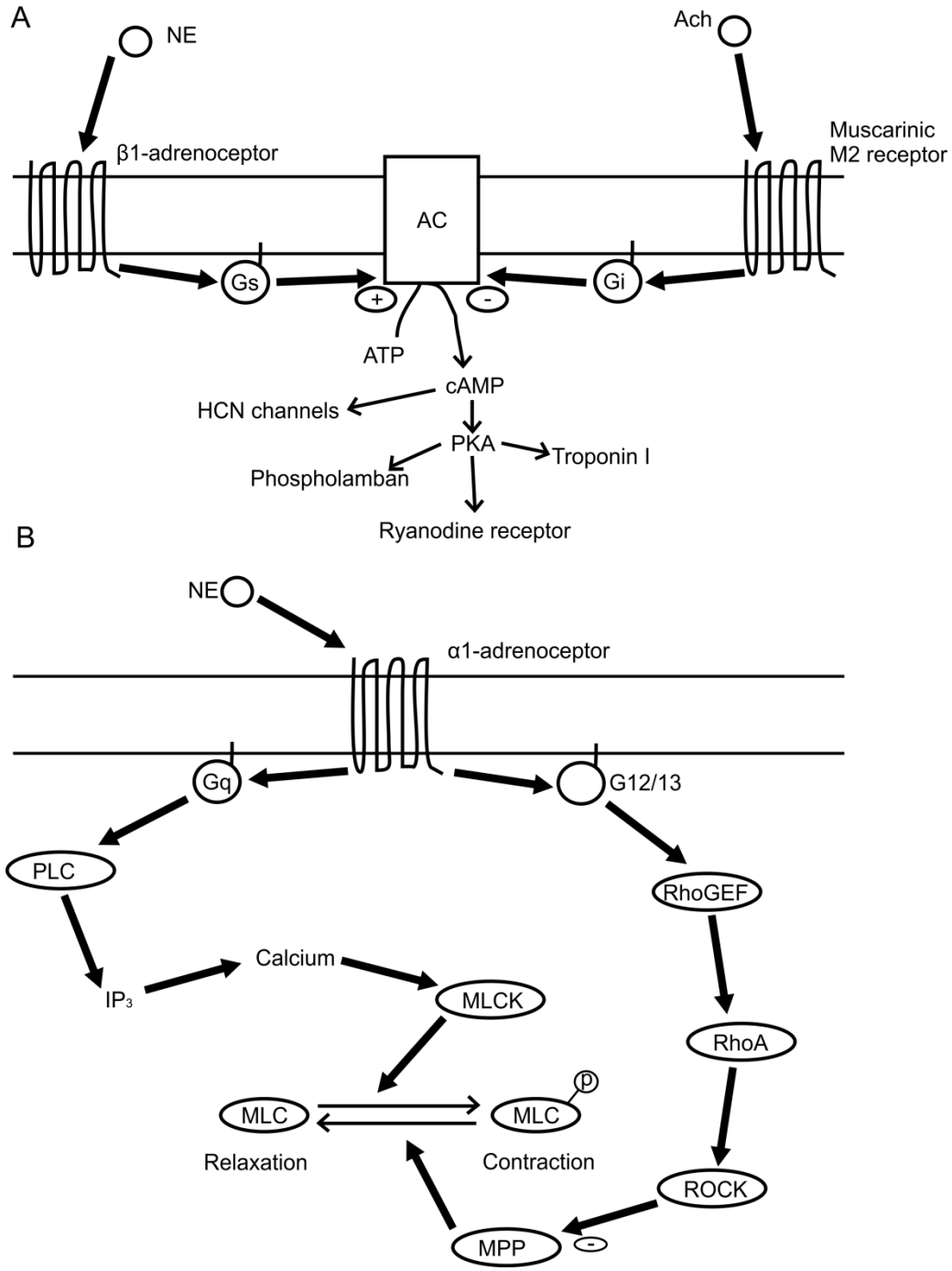

Figure 1.3. Control of heart and blood vessels by peripheral autonomic stimulation.
Diagram showing the main intracellular pathways involved in control of the cardiovascular system by sympathetic and parasympathetic innervation.
(A) The heart is heavily regulated by both the SNS and PNS, which release norepinephrine (NE) and acetylcholine (ACh), respectively, from the nerve terminals.
(B) The vasculature is heavily regulated by the SNS; NE increases contractility, thereby increasing peripheral resistance.
Modified from (Wettschureck & Offermanns, 2005).

1.2.3 Thermogenesis

Body heat is generated in mammals by basal metabolism, muscle activity (eg. shivering) and non-shivering thermogenesis. Non-shivering thermogenesis is especially important for maintenance of body temperature in small mammals (such as rodents), and in babies, and is mediated by brown adipose tissue (BAT). BAT has also been shown to be physiologically relevant in adults (Cypess *et al.*, 2009; Virtanen *et al.*, 2009), which means that control of thermogenesis might prove relevant to pharmacological control of energy expenditure in humans.

A number of brain regions play crucial control in the regulation of thermogenesis, including the preoptic area (POA), the DMH and the PVN. The POA contains temperature-sensitive neurones, and receives input from peripheral sensory pathways (Dimicco & Zaretsky, 2007). The DMH and PVN control SNS outflow downstream of the POA. Of particular importance to the control of thermogenesis is the DMH; injection of bicuculline methiodide (BMI), a $GABA_A$ receptor antagonist, into the DMH results in greatly increased body temperature due to increased BAT thermogenesis (Zaretskaia *et al.*, 2002).

It is interesting to note that, although the PVN is classically thought of as a stimulator of SNS activity, Madden and Morrison recently showed that BMI injection into the PVN not only causes a reduction in body temperature, it reverses the increases to SNS stimulation of BAT by BMI injection into the DMH (Madden & Morrison, 2009).

1.3 Hypothalamic control of energy balance

The hypothalamus was identified as a crucial part of the control of energy balance from early lesion experiments. Systematic lesions of the VMH, PVN and DMH resulted in obesity, whereas lesions to the LH resulted in hypophagia (Hetherington & Ranson, 1940; Brobeck *et al.*, 1943; Brobeck, 1946; Anand & Brobeck, 1951). This led to the proposal that the VMH functions as a "satiety centre", and the LH as a "hunger centre" (Gao & Horvath, 2008), whereas the DMH and PVN have a role in control of energy expenditure.

1.3.1 Leptin and melanocortins

Studies with the obese mouse models *ob/ob* and *db/db* led to the discovery of the hormone leptin, and the leptin receptor which is highly expressed in the hypothalamus (Zhang *et al.*, 1994). Leptin is an adipokine hormone released from white adipose tissue which signals the adipogenic status of the animal. The identification of leptin led to the discovery of downstream melanocortin signalling pathways in the hypothalamus.

Leptin acts on two primary populations of neurones in the arcuate nucleus, which have opposite effects on feeding. These are neurones expressing pro-opiomelanocortin (POMC), which are anorexigenic, and neurones expressing neuropeptide Y (NPY) and agouti-related protein (AgRP), which are orexigenic. POMC is a precursor for α-melanocyte stimulating hormones (α-MSH), which is an endogenous agonist for the melanocortin 3 and 4 receptors (MC3R and MC4R) (Adan *et al.*, 1994), whereas AgRP is an endogenous antagonist for the MC3/4R (Ollmann *et al.*, 1997).

POMC neurones in the Arc are activated by leptin, whereas NPY/AgRP neurones are inhibited by leptin; these are thought to be the primary central regulators of energy balance (Xu *et al.*, 2011). Furthermore, NPY neurones inhibit POMC neurones via GABA. In this way, leptin causes a potent stimulation of the MC3/4R in the hypothalamus by stimulating the activatory POMC neurones and inhibiting the inhibitory NPY/AgRP neurones. MC3/4R neurones are expressed in the Arc, PVN, LH and DMH (Mountjoy *et al.*, 1994; Sahm *et al.*, 1994), and activation of them results in reduced food intake, and elevated energy expenditure, as well as increased blood pressure and heart rate (Fan *et al.*, 1997).

1.3.2 MC4R control of energy balance

The circuitry of the melanocortin neurones has been investigated in detail. For example, neuroanatomical characterisation using fluorescent reporters showed that NPY neurones release GABA onto POMC neurones (Cowley *et al.*, 2001). It was also shown that the POMC and NPY neurones of the Arc project to a number of hypothalamic regions, including the PVN and the LH (Mountjoy *et al.*, 1994).

Balthasar *et al.* used a loxSTOPlox conditional knockin of the MC4R (the LoxTB mouse) to investigate the function of MC4R in specific nuclei. The LoxTB mice are functional knockouts of MC4R unless cre enzyme removes the STOP cassette. For example, using a Sim1-cre mouse line, Balthasar *et al.* re-introduced MC4R specifically into the PVN and amygdala of mice otherwise lacking MC4R (Balthasar *et al.*, 2005).

Mice lacking MC4R are normally obese, with increased food intake and reduced energy expenditure. However, re-introduction of the MC4R specifically into the PVN reduced the food intake back to normal levels, but energy expenditure remained low. This demonstrated that MC4R control of food intake and energy expenditure diverges, and that it is the MC4R in the PVN that is responsible for controlling food intake.

Another study used choline acetyl transferase (ChAT)-cre crossed to the lox-STOP-lox MC4R mouse rescues MC4R in cholinergic neurones of the IML layer of the spinal cord as well as the DMV. A second line Phox2b-cre rescued MC4R expression in parasympathetic neurones. It was found that MC4R rescue in parasympathetic neurones had no significant effects on energy expenditure or body weight, and that MC4R rescue in cholinergic neurones increased metabolic rate, and improved glucose and insulin control (Rossi *et al.*, 2011). Therefore, it is likely that MC4Rs in the IML regulate the liver responses to insulin, whereas MC4Rs expressed in the DMV might regulate insulin release.

There is an interesting role for GABA in the hypothalamic circuitry control energy balance. Selective deletion of the vesicular GABA transporter (VGAT), which is required for GABA release, from NPY/AgRP neurones results in elevated energy expenditure, which would be expected by disinhibition of the POMC neurones. A recent study by Vong *et al.* used conditional knockin mice to investigate the specific deletion of leptin receptor in GABAergic versus Glutamatergic neurones. They found that loss of leptin receptor from GABAergic neurones resulted in severe obesity, whereas loss

from Glutamatergic neurones had little effect on energy balance (Vong *et al.*, 2011).

The hindbrain also plays a significant role in the control of energy balance, particularly in the control of feeding. Particularly the NTS and DMV, which are involved in the satiety response to cholecystekinin (CCK) (Silver *et al.*, 1989), and requires input from the vagus (Smith *et al.*, 1985).

1.3.3 Cardiovascular control by leptin and melanocortins

Stimulation of POMC neurones by leptin results in activation of the SNS in control of the cardiovascular system in addition to the control of energy expenditure as discussed earlier. Activation of MC3/4R, particularly in the PVN, increases sympathetic nerve stimulation of the cardiovascular system, resulting in elevated blood pressure (Li *et al.*, 2012). It has also been shown that chronically increased circulating leptin can result in elevated blood pressure (Hall *et al.*, 2010).

1.4 The imprinted *Gnas* locus

$G_s\alpha$, the stimulatory g-protein alpha subunit, is a signalling protein that couples g-protein coupled receptors (GPCRs) to adenylate cyclase (AC) to produce the second messenger cAMP. $G_s\alpha$ is encoded by the mouse gene *Gnas*, which is part of the imprinted gene locus, also called *Gnas*.

1.4.1 Genomic imprinting

Genomic imprinting is a phenomenon which occurs in mammals that results in epigenetic silencing of a gene depending on whether it was maternally or

paternally inherited. Gene silencing typically occurs by germline DNA methylation of an imprinting control region, which constitutes a region of CpG motifs (often referred to as a CpG island). The methylation results in transcriptional silencing, which results in allele-specific silencing and produces parent-of-origin specific effects.

A number of imprinted genes have been identified in the mouse (Figure 1.4), and many cause growth defects, or developmental or behavioural abnormalities, when mutated. A recent study using high throughput transcriptional sequencing has shown that there may be many more imprinted genes than previously suspected (Gregg *et al.*, 2010).

1.4.2 *Gnas* locus

Gnasxl is part of the complex imprinted *Gnas* locus, which is highly conserved between mice and humans (*Gnas* in mice; *GNAS* in humans). Many different transcripts are produced from the locus, some encoding fully functioning proteins, some encoding truncated proteins, and some are non-coding (Figure 1.5) (Weinstein *et al.*, 2007). The two main proteins produced from the locus are $G_s\alpha$ and its splice variant XLαs. $G_s\alpha$ has long been known as the target of cholera toxin, and is essential for mediating normal cAMP signalling pathways, which are explained in further detail in a later section.

1.4.3 *GNAS* mutations in humans

Homozygous loss of $G_s\alpha$ is universally lethal, but heterozygous deletions or mutations cause a range of metabolic phenotypes in humans and mice (Weinstein *et al.*, 2007). Heterozygous loss of $G_s\alpha$ in humans (from either the

maternal or paternal allele) results in Albright's hereditary osteodystrophy (AHO) (Spiegel & Weinstein, 2004), which includes a number of developmental and neurobehavioural abnormalities. It is interesting to note that loss of $G_s\alpha$ specifically from the maternal allele results in a number of additional phenotypes, including severe obesity and multi-hormone resistance (Weinstein *et al.*, 2001). These additional phenotypes are caused by the tissue-specific imprinting of $G_s\alpha$, which is silenced from the paternal allele in a number of tissues, including the pituitary, thyroid and renal proximal tubules, and the PVN (Weinstein *et al.*, 2001; Chen *et al.*, 2009).

1.4.4 *Gnas* mutations in mice

Loss of $G_s\alpha$ has similar effects in mice as it does in humans. Loss of $G_s\alpha$ from the paternal allele in a *Gnas* exon 1 mutant has little effect in terms of metabolism, but the mice have a similar phenotype to the symptoms seen in human AHO patients, including subcutaneous ossification (Sakamoto *et al.*, 2009; Huso *et al.*, 2011). Furthermore, loss of $G_s\alpha$ from the maternal allele results in severe obesity, as well as glucose intolerance and insulin resistance and hormone resistance (Chen *et al.*, 2005).

A knockout model for the second exon of *Gnas* has an interesting imprinted phenotypic effect. Inheritance of a *Gnas* exon 2 deletion from the maternal allele (E2 m-/p+) has similar effects to the $G_s\alpha$-specific knockout for *Gnas* exon 1, including obesity, glucose intolerance and insulin resistance. However, inheritance of *Gnas* exon 2 deletion from the paternal allele (E2 m+/p-) has a largely opposite phenotype to the maternal inherited mutation, which includes decreased adiposity, glucose tolerance and insulin sensitivity

(Yu *et al.*, 2000). This is caused by loss of the paternally inherited *Gnasxl* transcript (Figure 1.5), and the phenotypic effects of paternal *Gnasxl* mutation are dominant over the heterozygous mutation of *Gnas* from the paternal allele.

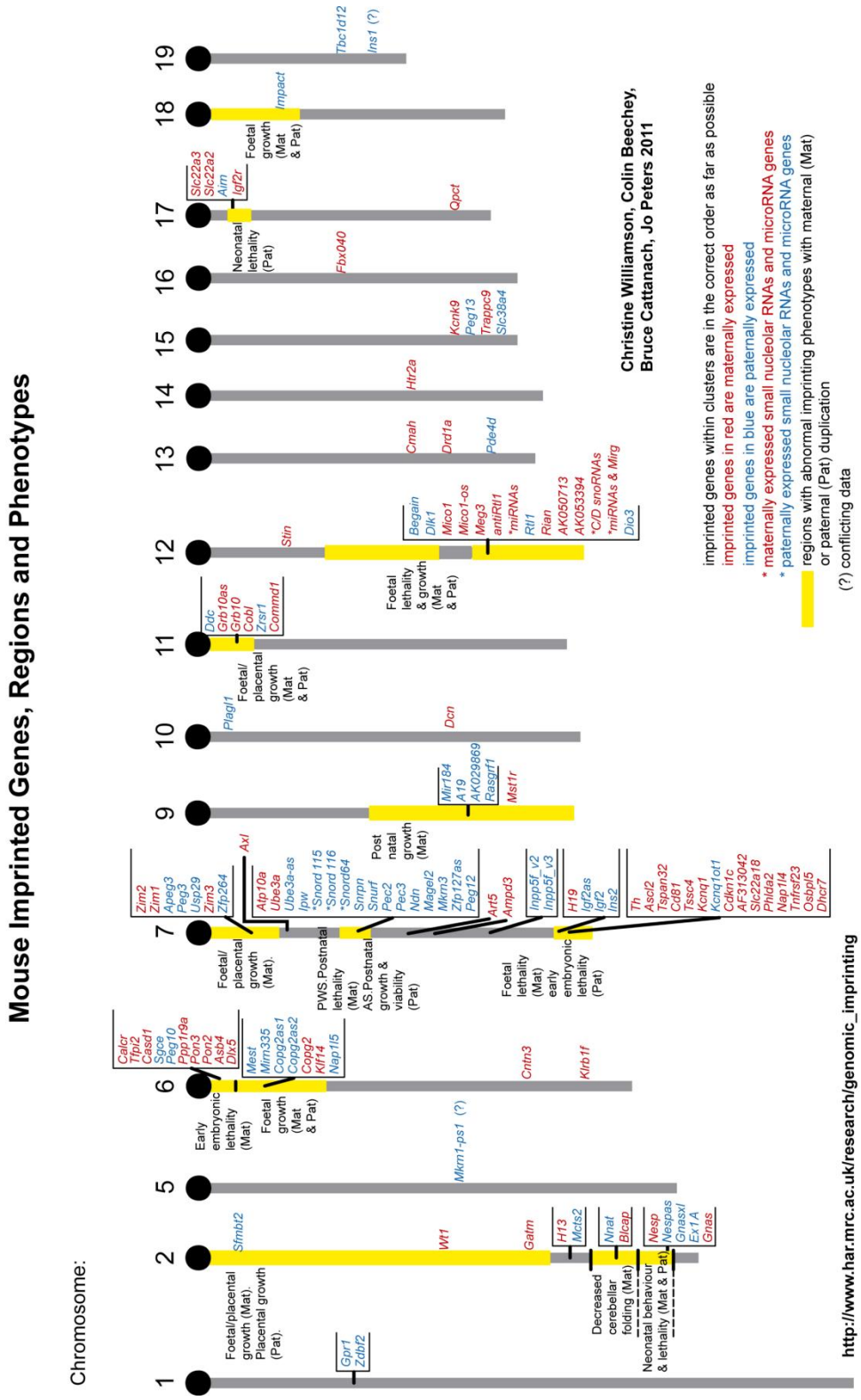

Figure 1.4. Known imprinted genes in the mouse.
A schematic of imprinted genes, grouped by location on the mouse chromosomes. The yellow blocks indicate regions of known imprinting phenotypes, and known genes are shown in blue (paternally expressed) and in red (maternally expressed). Taken from the MRC Harwell Mousebook (Williamson *et al.*, 2012).

1.5 *Gnasxl* and its product XLαs

1.5.1 *Gnasxl* is a splice variant of *Gnas*

Gnasxl is a splice variant of *Gnas*, and encodes the extra-large variant of $G_s\alpha$ (XLαs) (Kehlenbach *et al.*, 1994; Peters *et al.*, 1999). *Gnasxl* has its own unique promoter and first exon, and splices onto the same downstream exons 2-12 as *Gnas* (Figure 1.5). Unlike $G_s\alpha$ which is expressed ubiquitously, XLαs has a restricted expression pattern that includes distinct populations of neurones in the brain as well as peripheral tissues, and is known to change throughout development (Krechowec *et al.*, 2012).

In adult mice XLαs is expressed in the adrenal medulla, the intermediate pituitary and a number of brain regions including the hypothalamus (paraventricular, dorsomedial, lateral, arcuate and suprachiasmatic nuclei and the amygdala) as well as the hindbrain (the nucleus of the solitary tract, the gigantocellular reticular nucleus, the hypoglossal, the locus coeruleus and the Raphe Pallidus), and in the ventral motor neurones of the spinal cord (Pasolli *et al.*, 2000; Krechowec *et al.*, 2012).

The expression pattern changes slightly throughout developmental stages of a mouse. In neonates, there is no XLαs expression in the NTS or amygdala, but there is additional neonatal-specific expression in the laterodorsal tegmental nucleus (LDTg), as well as a number of peripheral tissues including the smooth muscle cells of blood vessel walls and the tongue.

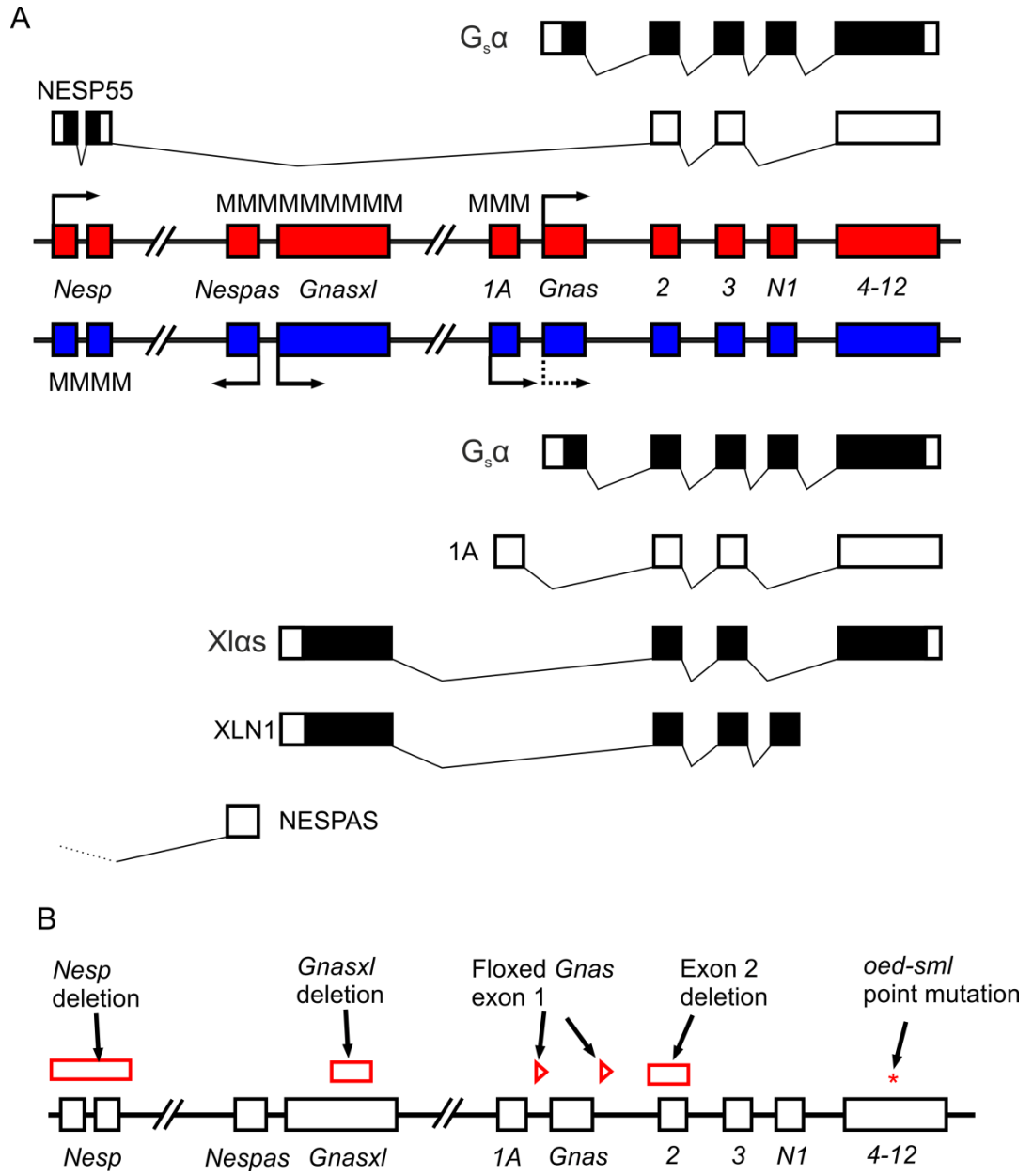

Figure 1.5. The complex imprinted *Gnas* locus.
(A) Diagram of the *Gnas* locus, showing the maternal (red) and paternal (blue) alleles, as well as the majority of the transcripts produced from the locus. Differential parent-of-origin methylation of the genomic alleles is shown as MMM, which results in silencing of that region of the locus. The arrows show which transcripts are transcribed from each allele; the dotted line for *Gnas* on the paternal allele indicates that it is silenced in a limited number of tissues, including the PVN. Alternative transcript splicing is shown, with coding (black) and non-coding (white) regions of exons. XLN1 is a neural-specific splice variant of XLαs. Modified from (Weinstein *et al.*, 2007).
(B) Diagram of the *Gnas* locus, showing the location of mutations in the various mouse models described.

1.5.2 *Gnasxl* knockout

Maternal inheritance of a *Gnasxl* knockout has no phenotypic effects; paternal inheritance has a phenotype very similar to the paternally inherited E2 mutant, including elevated energy expenditure and reduced fat mass.

The *Gnasxl* knockout phenotype has a shift from neonatal to adult stages, most likely due to the changing expression pattern of XLαs (Krechowec *et al.*, 2012). The neonatal phenotype includes defective suckling, leanness, inertia, hypoglycaemia, hypoinsulinaemia, elevated cAMP in BAT and a high mortality rate (Plagge *et al.*, 2004). The suckling defect is possibly due to an endogenous effect of XLαs expression in the tongue; XLαs expression in the tongue is lost in adulthood and so is this phenotype (Krechowec *et al.*, 2012).

The *Gnasxl* knockout phenotype has been studied in detail with respect to control of lipid deposition and metabolism; the mice have a lean phenotype with greatly reduced adiposity that is maintained from birth throughout life (Plagge *et al.*, 2004; Xie *et al.*, 2006).

Adult mice lacking XLαs have elevated energy expenditure, glucose tolerance, insulin sensitivity and markers of elevated stimulation of lipolysis and lipid oxidation in adipose tissue. This includes elevated mRNA levels of uncoupling protein 1 (UCP1), PPARγ and CREB in brown adipose tissue (BAT) (Xie *et al.*, 2006), which are markers of elevated SNS stimulation of BAT. Xie *et al.* also showed that *Gnasxl* knockouts have increased levels of excreted epinephrine and norepinephrine (NE) in urine, which suggests heightened SNS activity.

There is also evidence that the elevated lipolysis is not a cell autonomous effect in the adipose tissue. There was no difference in response to a β3-adrenoceptor agonist, which stimulates BAT lipolysis directly, between wildtypes and knockouts (Xie *et al.*, 2006). Therefore, the only possible cell-autonomous effect would have to be caused by a developmental problem with the BAT in knockouts. However, this would have to be caused indirectly, because XLαs is expressed in the blood vessels supplying BAT in neonates, not the brown adipocytes themselves (Krechowec *et al.*, 2012).

However, expression of XLαs in the blood vessels is lost in adulthood, so it is unlikely that loss of XLαs could affect signalling in later life (Krechowec *et al.*, 2012). It doesn't seem as if XLαs has any effect in humans, as AHO patients with paternally inherited *GNAS* mutations do not mirror the lean phenotype of *Gnasxl* knockout mice (Plagge *et al.*, 2008).

1.5.3 *Gnasxl* copy numbers

An interesting recent development in the investigation of XLαs is a study by Fernandez-Rebollo et al. which uses a mouse model of disrupted imprinting of the *Gnas* locus to investigate this from a different perspective (Fernandez-Rebollo *et al.*, 2012). The mouse model in question has a deletion of the Nesp55 transcript of the *Gnas* locus, which results in loss of methylation of the *Gnas* locus (Frohlich *et al.*, 2010). The Nesp55 transcript is encoded by the *Nesp* gene, and is responsible for maintaining the imprint marks of the *Gnas* locus, therefore loss of Nesp55 from the maternal allele results in it having the same imprint marks as the paternal allele. This results in

expression of *Gnasxl* from both alleles, as well as tissue-specific silencing of *Gnas* from both alleles.

Fernandez-Rebollo *et al.* then crossed these mice with paternally inherited *Gnasxl* mutation, thereby resulting in loss of *Gnasxl* back to a single copy number. Therefore, the effect of *Gnasxl* copy number could be investigated in the context of the hypocalcaemia, subcutaneous oedema and neonatal lethality of mice lacking both copies of $G_s\alpha$ from imprinted tissues. It is interesting to note that increasing the copy number of *Gnasxl* in this way resulted in decreased suckling and hypoglycaemia.

It is therefore very interesting that increasing *Gnasxl* copy number not only has a distinct phenotype, but that this phenotype has similar aspects to loss of *Gnasxl* (Plagge *et al.*, 2004). Therefore, not only is XLαs signalling important for its phenotypic effects, but the level of signalling is also important, and too much XLαs signalling can cause similar effects as too little XLαs signalling.

1.6 cAMP-regulated cell signalling

Regulated exocytosis, for example in neurones, is highly dependent upon Ca^{2+} which stimulates fusion of synaptic vesicles with the presynaptic membrane, thereby releasing the contents of the vesicle (in the case of a neurone, this could be a neurotransmitter such as glutamate or GABA). In a neuron, depolarisation of the membrane opens voltage-dependent calcium channels, which allows influx of Ca^{2+} from the extracellular environment, causing vesicle fusion. However, there are a number of factors that can

influence this process, including cAMP which has major functions in controlling exocytosis (Seino & Shibasaki, 2005).

cAMP is a second messenger that acts primarily via protein kinase A (PKA), but also has other effectors including Epac and cyclic nucleotide gated (CNG) channels.

1.6.1 PKA signalling

PKA is a protein kinase with diverse downstream targets that vary depending upon the cell type, but the primary effector is cAMP response element binding protein (CREB), which is a transcription factor activated by PKA which controls expression of genes under cAMP response element (CRE) transcription control. For example, SNS stimulation of BAT stimulates cAMP production, which activates PKA, which then activated CREB by phosphorylation. CREB then enters the nucleus of the cell, where it activates transcription of UCP1, which is required for BAT thermogenesis (Cannon & Nedergaard, 2004). A large number of genes contain the cAMP response element (CRE), and are therefore transcriptionally controlled by CREB, including neuropeptides, hormones and ion channels (for a review see (Lonze & Ginty, 2002)).

1.6.2 Epac signalling

Epac is a guanine nucleotide exchange factor (GEF) which is activated by cAMP and is expressed in a number of tissues, but particularly in brain and heart. There are a number of downstream effectors for Epac, involved in a number of cellular processes (Laurent *et al.*, 2012), but effects on exocytosis

may be mediated by Rab3, via the g-proteins Rim and Piccolo (Ozaki *et al.*, 2000). However, Epac has a lower affinity for cAMP than PKA, so it might be that Epac functions in microdomains in close proximity to the exocytic machinery where cAMP might accumulate to high concentrations in response to activation (Seino & Shibasaki, 2005).

1.6.3 Cyclic nucleotide gated channels

CNG channels are found in many cell types, including brain and heart. They are non-selective cation channels that allow influx of Ca^{2+} and Na^{+} in response to cyclic nucleotide binding. There are many variants of CNG channels that bind different cyclic nucleotides, but some are known to respond to cAMP; activation of CNG channels causes depolarisation and therefore activation of neurones (Seino & Shibasaki, 2005).

1.6.4 Adenylate cyclase

cAMP is produced by adenylate cyclase from ATP. Adenylate cyclase is stimulated by the stimulatory g-protein alpha subunit ($G_s\alpha$), and is inhibited by the inhibitory g-protein alpha subunit ($G_i\alpha$) (Wettschureck & Offermanns, 2005). These are members of the family of heterotrimeric g-proteins, so called because they act as trimers of α, β and γ subunits. There are a number of variants of each, including four families of Gα subunits which are known to couple to specific downstream signalling partners, for examples Gi and $G_s\alpha$ couple to adenylate cyclase, while Gqα stimulates phospholipase C (PLC)-β. There are also 5 variants of β subunit and 12 γ subunits. The β and γ subunits, although encoded separately, bind together strongly (with the exception of β-5) and act as a single unit. The expression of g-protein

variants is diverse, and some are expressed only in specific tissues (Wettschureck & Offermanns, 2005).

1.7 G-protein coupled receptors

Heterotrimeric g-proteins are regulated by the activity of g-protein coupled receptors (GPCRs), which are a large family of membrane proteins that all consist of 7 transmembrane loops. Under basal conditions, the α, β and γ subunits are bound in a heterotrimeric complex. Upon activation, the α subunit releases a bound GDP, and binds a GTP which causes a conformational change and the βγ subunits are released (Figure 1.6).The α and βγ subunits are then free to act on downstream signalling partners.

The GPCRs are a diverse family of receptors, and have been found to respond to factors as diverse as light, smells, and a range of neurotransmitters and hormones (Wettschureck & Offermanns, 2005). There are many known GPCRs in mammals, and for a number of these the endogenous ligand is not known, which are dubbed orphan receptors. Table 1.1 gives a list of many of the known GPCRs involved in cardiovascular and/or metabolic regulation, as well as the heterotrimeric g-protein(s) they are known to couple to.

The final major player in control of cAMP signalling is cAMP-specific phosphodiesterase (PDE), which degrades cAMP; intracellular targeting of PDEs can produce cAMP signalling microdomains by limiting the diffusion of cAMP away from the site of production.

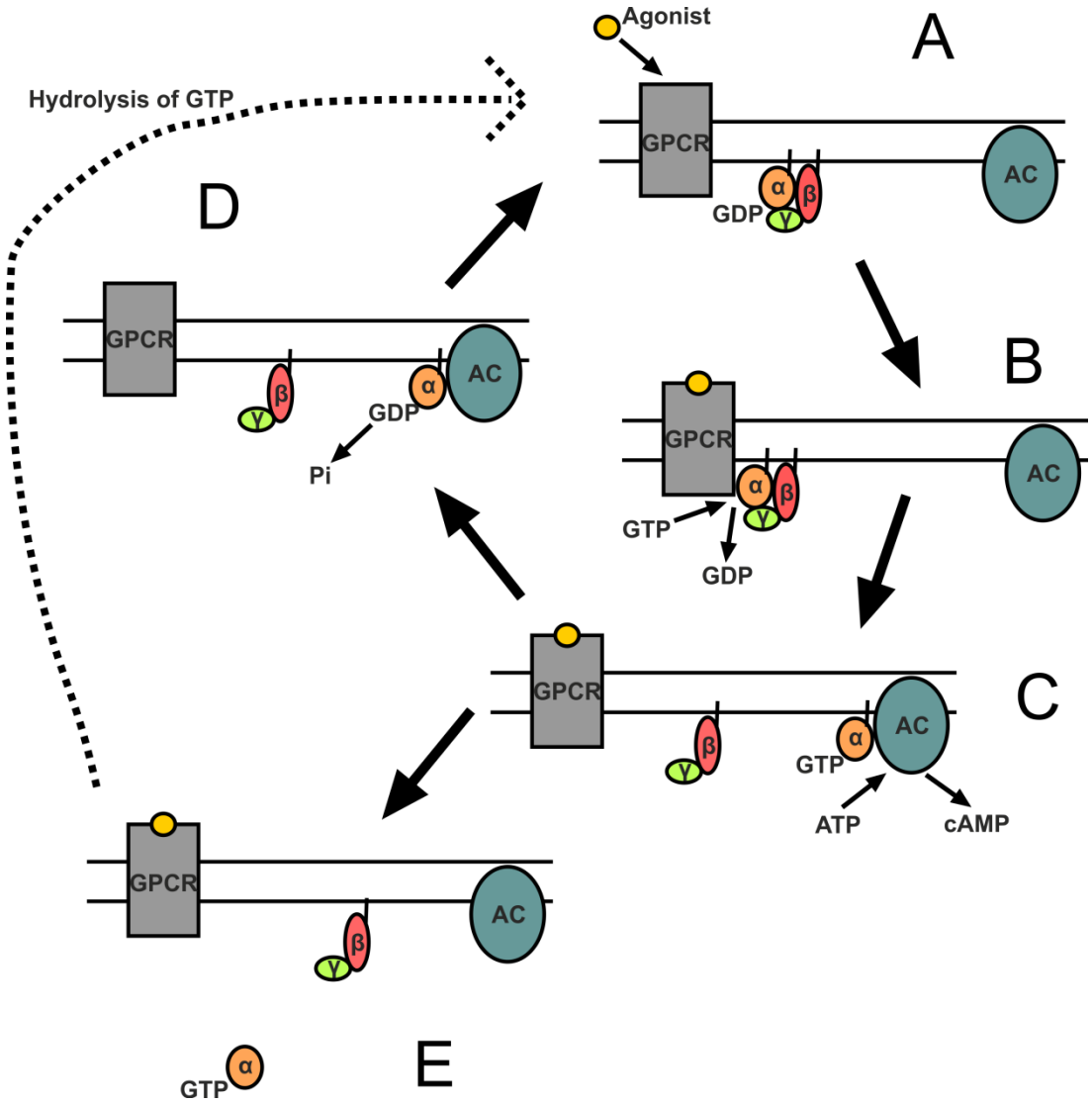

Figure 1.6. $G_s\alpha$ signalling.
Diagram showing intracellular $G_s\alpha$ signalling to produce cAMP in response to agonist.
(A) Before stimulation of the g-protein coupled receptor (GPCR) by an agonist, $G_s\alpha$ is bound to GDP and the heterotrimeric g-proteins (α, β and γ) are bound together in the inactive state.
(B) Agonist binding to the GPCR induces a conformational change, which causes $G_s\alpha$ to release GDP and bind GTP, thus activating $G_s\alpha$ and causing it to release the βγ subunits.
(C) GTP-bound $G_s\alpha$ migrates along the membrane and activates adenylate cyclase, stimulating it to produce cAMP from ATP. Additionally, some signals are mediated by the released βγ subunits via other targets.
(D) $G_s\alpha$ hydrolyses GTP back to GDP, releasing phosphate and returning $G_s\alpha$ to the inactive state.
(E) Continued activation of $G_s\alpha$ causes it to be redistributed to the cytoplasm, where it can no longer signal via AC. Hydrolysis of GTP allows $G_s\alpha$ to return to the plasma membrane for further signalling.
Modified from (Wettschureck & Offermanns, 2005).

GPCR	Endogenous agonist	Couples
$GABA_B$	γ-amino butyric acid (GABA)	$G_{i/o}$
D_1 and D_5	Dopamine	G_s
$5\text{-}HT_{4,6,7}$	Serotonin	G_s
A_{2A} and A_{2B}	Adenosine	G_s
CB_1 and CB_2	Anandamide	$G_{i/o}$
$Amy_{1,2,3}$	Amylin	G_s
$CGRP_1$	Calcitonin gene-related peptide (CGRP)	G_s, $G_{q/11}$
CRF_1 and CRF_2	Corticotrophin-releasing factor (CRF)	G_s
GLP-1R	Glucagon-like peptide 1 (GLP-1)	G_s
$MC_{1,3,4,5}$	Melanocortins (eg. α-MSH)	G_s
OX_1 and OX_2	Orexin	G_s
NK_1	Substance P (SP)	$G_{q/11}$
V_2	Vasopressin	G_s
PAC_1	Polyadenylate cyclase activating polypeptide (PACAP)	G_s

Table 1.1. Some known g-protein coupled receptors (GPCRs).
A number of GPCRs known to be involved in energy balance and/or cardiovascular control. Both the endogenous agonist and heterotrimeric g-protein signalling partner(s) are listed. Modified from (Wettschureck & Offermanns, 2005).

1.8 cAMP signalling by XLαs

1.8.1 XLαs protein domains

XLαs shares the main functional domains with $G_s\alpha$, which are encoded by the shared exons 2-12 (Figure 1.5) (Klemke *et al.*, 2000). Additionally the unique exon of $G_s\alpha$, which encodes part of the βγ binding domain, has highly conserved regions in XLαs (Figure 1.7) (Klemke *et al.*, 2000). Therefore, any potential differences in intracellular signalling between XLαs and $G_s\alpha$ are likely to be mediated by the N-terminal regions of the unique XLαs domain, be it by directly influencing binding partners, or by influencing intracellular localisation of XLαs.

The XLαs domain contains a number of recognisable domains, including a cysteine-rich region important for XLαs tethering to the membrane, a proline-rich region and other regions containing EPAA or AARA repeats (Klemke *et al.*, 2000). Although the early study by Klemke *et al.* suggested that XLαs is incapable of normal coupling between GPCRs and adenylate cyclase (Klemke *et al.*, 2000), a number of further *in vitro* studies have shown that XLαs is capable of coupling specific GPCRs, including β2-adrenoceptors (Bastepe *et al.*, 2002; Kaya *et al.*, 2009; Liu *et al.*, 2011).

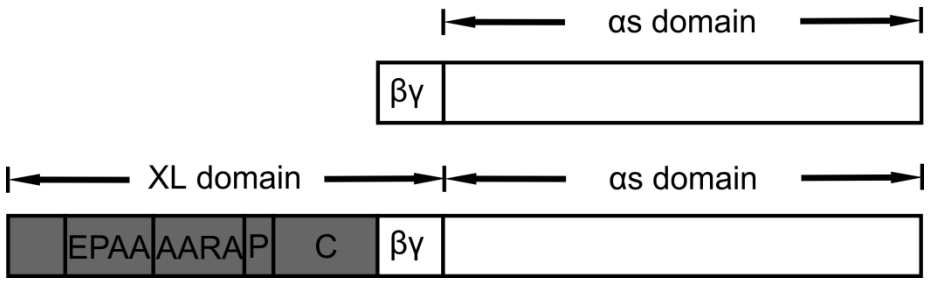

Figure 1.7. $G_s\alpha$ and XLαs protein domains.
$G_s\alpha$ and XLαs share the main signalling domain and regulatory regions of the C-terminal domain. Additionally, although coded separately, the βγ-binding domain is very similar between the two. However, XLαs has a large unique N-terminal domain, which includes a cysteine-rich region for membrane anchorage, a proline-rich region and regions of EPAA and AARA amino acid repeats. Modified from (Klemke *et al.*, 2000).

1.8.2 XLαs provides sustained signalling

Some minor differences have been discovered in signalling between XLαs and $G_s\alpha$; for example, it has recently been shown that XLαs remains at the plasma membrane following activation, resulting in sustained signalling and a prolonged cAMP signal (Liu *et al.*, 2011).

$G_s\alpha$ is known to become internalised following activation; sustained stimulation causes it to become redistributed from the plasma membrane to the cytoplasm (Wedegaertner *et al.*, 1996), which constitutes an important mechanism that limits activation of $G_s\alpha$ (Thiyagarajan *et al.*, 2002; Makita *et al.*, 2007). This is a reversible effect; loss of $G_s\alpha$ stimulation by removal of the GPCR agonist results in $G_s\alpha$ being trafficked back to the plasma membrane, ready for further signalling (Wedegaertner *et al.*, 1996) (Figure 1.6).

The recent study by Liu *et al.* showed that XLαs remains localised at the plasma membrane after activation, whereas $G_s\alpha$ is trafficked away from the membrane (Liu *et al.*, 2011). Liu *et al.* showed that XLαs is fully capable of coupling both parathyroid hormone receptor (PTHR) and β_2-adrenergic receptor (β_2-AR), and that stimulation of the PTHR resulted in a prolonged cAMP signal which was not seen after β_2-AR stimulation. This shows that there are definite differences not only in cAMP signalling by $G_s\alpha$ and XLαs, but also that XLαs can respond differently to different GPCRs. Whether this is caused by differences in XLαs binding affinity to the GPCR, different methods of desensitising the cAMP response of the different GPCRs, or by some other mechanism remains unclear.

It is possible that the main function of the XLαs-specific N-terminal domain is for maintaining XLαs at the plasma membrane following activation; there is a cysteine-rich region known to be responsible for targeting XLαs to the membrane by palmitoylation (Pasolli *et al.*, 2000). Therefore, it is possible that the effects of XLαs are caused by the dual effect of its expression in a particular population of neurones and its ability to cause extended activation of those neurones. For example, it might be that XLαs is expressed in GABAergic neurones in the hypothalamus, and is responsible for maintaining tonic GABA release onto PVN neurones.

However, there is a caveat with all these in vitro techniques, because it is a necessarily artificial system, ie. the proteins involved had to be added exogenously and overexpressed at high levels. Therefore, any conclusions drawn from such studies must take into account the fact that these are not necessarily at physiological expression levels and that many of the specific signalling partners or regulatory mechanisms may be absent, and all this could therefore influence the signalling properties.

It is possible that, while XLαs is capable of signalling via adenylate cyclase, its primary signalling partners in vivo constitute a different signalling pathway entirely, or that the cAMP signalling resulting from XLαs stimulation acts on specific downstream partners for example due to localisation in an intracellular microdomain.

Finally, there is the possibility that XLαs is capable of coupling the same upstream and downstream signalling partners as $G_s\alpha$, but its function in vivo is controlled by its expression pattern. This possibility is supported by the

highly restricted expression pattern of XLαs, as well as the changing phenotype between neonate and adulthood apparently caused by the changing expression pattern of XLαs (Krechowec *et al.*, 2012).

1.8.3 Structural binding of $G_s\alpha$

No crystal structure of XLαs exists, but the structure of $G_s\alpha$ has been determined to high accuracy (Sunahara *et al.*, 1997), and this is likely to reflect the structure of XLαs, excluding the bulky N-terminal XLαs domain. In addition, studies have determined the structure of $G_s\alpha$ in the inactive (GDP-bound) state and the mechanism of binding to the β2-adrenergic receptor (Figure 1.8A) (Chung *et al.*, 2011), as well as in the active (GTP-bound) state and the mechanism of binding to adenylate cyclase (AC) (Figure 1.8B) (Tesmer *et al.*, 1997). These structures of $G_s\alpha$ are therefore useful for visualising how the XLαs domain might function.

From the crystal structures of $G_s\alpha$ binding both to active β2-adrenergic receptor and to adenylate cyclase, it is clear that the N-terminal domain is situated at or near the interface with the opposing protein (Figure 1.8). Therefore, the XLαs-specific domain would be well placed to influence binding. In particular, with respect to binding AC, there doesn't appear to be any room for an additional bulky protein domain at the N-terminus if the proteins are expected to bind (Figure 1.8B). This might suggest that XLαs is, in principle, capable of binding both receptor and AC, but the bulky XLαs domain prevents it from binding AC as efficiently as $G_s\alpha$.

An early mouse model of the *Gnas* locus is the oedematous-small (*oed-sml*) mutation, which constitutes a point mutation in exon 6 of *Gnas/Gnasxl*,

resulting in a Valine to Glutamate mutation (Cattanach *et al.*, 2000).This has similar phenotypic effects to the E2 knockouts, including homozygous lethality. Maternally inherited *oed-sml* mutation is similar to E2 m-/p+, including subcutaneous oedema and increased fat mass; paternally inherited *oed-sml* mutation is similar to E2 m+/p-, including a lean phenotype and decreased fat mass. Therefore, this provides evidence that loss of the catalytic activity of XLαs is required for the *Gnasxl* knockout phenotype.

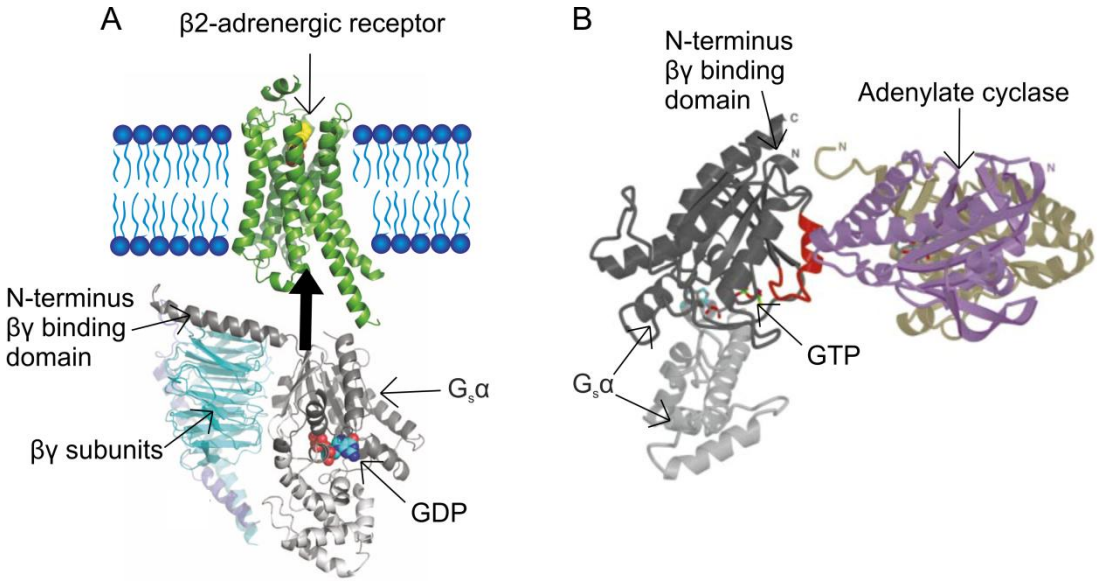

Figure 1.8. $G_s\alpha$ structure and binding.
Details of $G_s\alpha$ binding, using crystal structures.
(A) Binding of inactive GDP-bound $G_s\alpha$ heterotrimeric g-proteins to activated β2-adrenergic receptor. From this diagram it is clear that the bulky extra-large N-terminal XLαs domain could interfere with binding to the βγ subunits or the β-adrenergic receptor. Modified from (Chung *et al.*, 2011).
(B) Binding of active GTP-bound $G_s\alpha$ to the intracellular domain of adenylate cyclase (AC). It is also clear in this diagram that the bulky XLαs domain could interfere with binding to AC. Modified from (Tesmer *et al.*, 1997).

1.9 Neuronal signalling by $G_s\alpha$ and XLαs

1.9.1 Neuronal-specific knockout of $G_s\alpha$

A number of tissue-specific knockouts have been used to investigate the role of $G_s\alpha$ mutations in various tissues. It has been shown that loss of $G_s\alpha$ in peripheral tissues, including the liver, pancreas and adipose tissue, does not recapitulate the parent-of-origin effects of $G_s\alpha$ mutation (Chen *et al.*, 2011). However, loss of maternal $G_s\alpha$ specifically in the CNS causes the parent-of-origin effects of $G_s\alpha$ mutation on glucose and energy homeostasis (Chen *et al.*, 2009).

The maternally inherited brain-specific $G_s\alpha$ knockout (mBrGsKO) exhibited obesity, caused by decreased energy expenditure with no change in food intake. The mice were found to have decreased SNS activity and lowered blood pressure and heart rate. They were also hyperinsulinaemic and glucose intolerant. The food intake and energy expenditure responses to the MC3/4R agonist MTII were also investigated; mBrGsKO mice had a blunted increase in energy expenditure compared to wildtypes, but there was no effect on food intake.

It was also shown that expression levels of *Gnas* transcript was reduced in the PVN of mBrGsKO mice compared to paternal brain-specific knockout (pBrGsKO) mice, but not in other brain regions such as the hippocampus and NTS. These data suggest that the energy expenditure effects of mBrGsKO might be caused by loss of $G_s\alpha$ in the PVN, and therefore a loss of MC3/4R signalling in this nucleus, which indicates that MC3/4Rs couple via $G_s\alpha$.

1.9.2 PVN-specific knockouts of $G_s\alpha$

More recently, $G_s\alpha$ was deleted specifically in neuronal populations in the PVN, by crossing floxed *Gnas* mice with Sim1-cre mice to produce offspring with maternally deleted $G_s\alpha$ in PVN neurones (mPVNGsKO) (Chen *et al.*, 2012). These mice also suffered from obesity and reduced energy expenditure, but it was far milder than in the mBrGsKO mice, which means that only some of the actions of $G_s\alpha$ mediating energy balance are caused via the PVN.

Futhermore, Chen *et al.* showed that mPVNGsKO mice had elevated circulating insulin and triglycerides, but no changes were seen in the other serum chemistries investigated including fed and fasted glucose levels as well as leptin and free fatty acids. They also showed that the mPVNGsKO mice responded to cold exposure in the same way as wildtypes, but mBrGsKO mice had an impaired response, both in body temperature change and induction of UCP1 expression in BAT. This indicates that the alterations in thermogenesis caused by lack of $G_s\alpha$ in the brain are not caused by expression in the PVN.

However, the mPVNGsKO mice were found to have comparable reductions in blood pressure and heart rate as were seen in the mBrGsKO mice, suggesting that the cardiovascular effects of loss of $G_s\alpha$ in the brain are caused specifically by loss of expression in the PVN (Chen *et al.*, 2012).

1.9.3 Melanocortins signalling via $G_s\alpha$

$G_s\alpha$ couples the melanocortin 3 and 4 receptors (MC3/4R), which act in the CNS to decrease food intake and increase SNS activity and energy expenditure (Brito *et al.*, 2007; Nogueiras *et al.*, 2007). Mice lacking MC4R develop severe obesity, caused by increased food intake and decreased energy expenditure (Balthasar *et al.*, 2005).

Balthasar *et al.* showed that MC4R signalling in the PVN mediated specifically the food intake effects, with no effect to energy expenditure (Balthasar *et al.*, 2005). This is especially interesting in light of the mPVNGsKO mouse, where loss of $G_s\alpha$ in the PVN has no effect on food intake and minimal effects on energy expenditure (Chen *et al.*, 2012). However, the mPVNGsKO had decreased blood pressure and heart rate, similar to the BrGsKO, which suggests that the functions of $G_s\alpha$ in the PVN is in cardiovascular control.

Therefore the effects of $G_s\alpha$ and MC4R in the PVN do not necessarily match entirely, so there remains the possibility of other signalling pathways being involved; Chen *et al.* suggest that MC4R may couple to Gq in the PVN to cause the food intake changes.

1.10 Aims

The aims of this PhD are to investigate the effects of XLαs on autonomic control, specifically autonomic control of the cardiovascular system in adult *Gnasxl* knockout mice. Chapter 2 provides detail of the methods used, including arterial cannulation in anaesthetised mice with ICV drug injection,

ECG and heart rate monitoring in conscious mice by telemetry, heart rate variability (HRV) analysis and immunohistochemistry.

Chapter 3 will use blood pressure and heart rate monitoring, in anaesthetised and conscious animals, respectively. Autonomic control of the cardiovascular system in *Gnasxl* knockouts will also be investigated by cardiovascular responses to antagonists to the SNS and PNS.

Chapter 4 will examine autonomic control of the cardiovascular system in further detail by HRV analysis. A number of HRV analyses will be tested and validated in wildtype mice, followed by an exploration of HRV changes in mice lacking XLαs.

The aim of Chapter 5 is to investigate how loss of XLαs might impact on cardiovascular control by known neuropeptide signalling pathways, including GLP-1. This will be performed by ICV injections into anaesthetised mice and peripheral injections in conscious mice.

In Chapter 6, the neural pathways involved in XLαs signalling will be investigated by immunohistochemistry staining of the early response gene c-fos to an agonist of the neuronal GLP-1 signalling pathway. Furthermore, the involvement of XLαs-expressing neurones in the c-fos response will be investigated by immunofluorescence colocalisation.

Chapter 7 aims to identify a correctly targeted embryonic stem (ES) cell clone using Southern blotting for a conditional *Gnasxl* knockout, which could be used in the future to probe the effects of targeted deletion of XLαs.

Finally, Chapter 8 will review all the results presented in this thesis, provide overall conclusions, and give a speculative discussion of broader applications of the results as well as possible further experiments.

2 Methods

2.1 Buffers and solutions

2.1.1 General

PBS	Phosphate buffered saline (PBS) was made using PBS tablets (Sigma), according to the manufacturer's instructions.
10X TBS	100 mM Tris pH 7.5; 150 mM NaCl in H_2O.
20X SSC	3 M NaCl; 300 mM sodium citrate; pH 7.0 in H_2O.

2.1.2 Histology

4% PFA	Paraformaldehyde (PFA) was dissolved 4 % (w/v) in PBS, heated to 50 °C and 1 M NaOH added dropwise until the PFA dissolved.
DAB	3,3'-Diaminobenzidine (DAB; Sigma) was dissolved in PBS and sterile filtered. Just before use 0.1 % (v/v) H_2O_2 and 0.5 % (w/v) nickel chloride ($NiCl_2$) were added.
PBS-TX	0.25 % (v/v) Triton X-100 (Sigma) in PBS.
Blocking solution	10 % (v/v) normal serum and 0.25 % (v/v) Triton X-100 (Sigma) in PBS.

2.1.3 Protein gels and Western blotting

Protein lysis buffer	25 mM $NaPO_4$ pH 7.5; 25 mM NaF; 25 mM β-glycerolphosphate; 100 mM NaCl; 5 mM EGTA; 0.5 % (w/v) deoxycholate; 0.5 % (w/v) NP-40; 0.1 % (w/v) SDS; 0.01 % (w/v) sodium azide in H_2O. 0.5 mM PMSF, protease inhibitor cocktail (Sigma), phosphatase inhibitor cocktail (PhosStop; Roche) added just before use.
Resolving gel	10 % (v/v) acrylamide mix (29:1 acrylamide: bisacrylamide); 390 mM Tris pH 8.8; 0.1 % (w/v) SDS in H_2O. For polymerisation 0.1 % APS and 0.04 % TEMED were added.
Stacking gel	5 % (v/v) 29:1 acrylamide:bisacrylamide mix (Accugel; National Diagnostics); 100 mM Tris pH 6.8; 0.1 % (w/v) SDS (National Diagnostics) in H_2O. For polymerisation 0.1 % APS and 0.04 % TEMED were added.
SDS-PAGE electrophoresis buffer	25 mM Tris Base; 250 mM glycine; 0.1 % (w/v) SDS in H_2O.
Transfer buffer	25 mM Tris pH 8.3; 192 mM glycine; 20 % (v/v) MeOH in H_2O.
TBS-T	0.1 % (v/v) Tween20 in TBS.
Blocking solution	0.1 % Tween20 (v/v) and 5 % (w/v) skimmed milk

	powder in TBS.
Stripping buffer	62.5 mM Tris pH 6.8; 100 mM β-mercaptoethanol; 2 % (w/v) SDS in H_2O.

2.1.4 Southern blotting

Dig buffer 1	0.1 M maleic acid; 0.15 M NaCl; pH 7.5 in H_2O.
Dig buffer 3	0.1 M Tris pH 9.5; 0.1 M NaCl; 0.05 M $MgCl_2$ in H_2O.
10X blocking reagent	Blocking reagent (Roche) was dissolved 10 % (w/v) in Dig buffer 1.
Hybridisation buffer	5X SSC; 1X blocking reagent; 0.1 % (w/v) N-Lauroylsarcosine; 0.02 % (w/v) SDS in H_2O.
Wash buffer 1	2X SSC and 0.1 % (w/v) SDS in H_2O.
Wash buffer 2	0.1X SSC and 0.1 % (w/v) SDS in H_2O.
NBT stock	Nitro Blue Tetrazolium (NBT) dissolved 75 mg/ml in 70 % dimethylformamide.
BCIP stock	5-bromo-4-chloro-3-indolyl-phosphate (BCIP) dissolved 50 mg/ml in 70 % dimethylformamide.
NBT BCIP colour reagent	45 µl NBT stock and 35 µl BCIP added to 10 ml Dig buffer 3.

2.1.5 PCR and DNA electrophoresis

DNA lysis buffer	100 mM Tris pH 8.5; 5 mM EDTA; 200 mM NaCl; 0.2 %

	(w/v) SDS in H_2O.
TE	10 mM Tris pH 8.0 and 1 mM EDTA in H_2O.
TAE	40 mM Tris; 20 mM acetic acid; 1 mM EDTA in H_2O.

2.1.6 Injectables

Sterile saline	0.9 % (w/v) NaCl in H_2O, autoclaved.
aCSF	127 mM NaCl; 1.8 mM KCl; 1.2 mM KH_2PO_4; 2.4 mM $CaCl_2$; 1.3 mM $MgSO_4$; 26 mM $NaHCO_3$; 15 mM glucose in H_2O, as from (Belle *et al.*, 2009). Solution was oxygenated.

2.2 Animals

Mice were maintained on a 12 hour/12 hour light/dark cycle, with unlimited access to standard chow and water. All experiments were performed in accordance with Home Office animal use regulations.

2.2.1 Gnasxl knockouts

Gnasxl knockout mice were bred on a CD1 background. CD1 females (Charles River) were bred with male maternally inherited *Gnasxl* knockout ($Gnasxl^{m-/p+}$) carriers to produce paternally inherited *Gnasxl* knockout ($Gnasxl^{m+/p-}$) offspring. Offspring inherited the *Gnasxl* knockout allele according to standard Mendelian inheritance; half of offspring were wildtype, half were m+/p- knockouts.

2.2.2 Breeding survivors

Gnasxl knockout mice have low survival at birth – 0 % on an inbred C57/BL6 background, approximately 10 % on an outbred CD1 background (Plagge *et al.*, 2004). Survivability can be improved by culling of excess wildtypes one or two days after birth; culling was carefully controlled to leave paired wildtype-knockout offspring of each gender. Post weaning the knockouts no longer suffer from lethality effects, and become healthy, if lean, adults (Xie *et al.*, 2006).

2.2.3 Tissues

Tissues for Western blotting were rapidly dissected from mice culled by Schedule 1, placed on dry ice, and kept at -80 °C until use. For histology, adult mice were killed by transcardial perfusion: mice were terminally anaesthetised by pentobarbitone injection; following loss of paw-withdrawal reflex the chest cavity was opened by dissection, the right atrium of the heart cut, and the mouse was perfused with saline then 4 % PFA. The brain was then rapidly dissected and placed on 4 % PFA, and kept overnight at 4 °C on a rocker. The brains were then transferred to sterile 30 % sucrose solution to dehydrate the tissue.

2.2.4 Genotyping

Mice were genotyped by ear notches taken at weaning. Tissues were lysed by overnight incubation in DNA lysis buffer containing Proteinase K (100 µg/ml; Sigma) at 55 °C. Samples were then diluted 1:20 into sterile Elga water and heat denatured (15 minutes at 95 °C). 3 µl was taken for a 30 µl

PCR reaction containing the following: 1X GoTaq green buffer (Promega), dNTPs (200 µM each; Sigma), Primer XLF10 (0.83 µM), Primer XLR5 (0.83 µM), $MgCl_2$ (1.5 mM; Promega), 0.2 µl GoTaq (1 unit; Promega). The following PCR conditions were used, with 30 cycle of steps 2-4:

1. Hot Start 95 °C for 2 minutes
2. 45 seconds at 95 °C denaturing step
3. 45 seconds at 56 °C annealing step
4. 2 minutes at 72 °C elongation step
5. 5-minute final elongation step at 72 °C

Samples were run on a 2 % agarose gel for 40 minutes at 80 V, and visualised by Ethidium Bromide staining on a GelDock; knockouts were identified as having a double band.

Primer	Use	Sequence
XLF10	Genotyping PCR	GGAGCCAGGTCACTCTCAGC
XLR5	Genotyping PCR	CAGAAGCTGCCGCATTACCT
XL5' F1	Southern blotting	GGGTACCATGGCACTGGCCT
XL5' F3	Southern blotting	TTTCCTCCCAAAGGTAGC
XL5' R1	Southern blotting	GGAAGCAGTGAAGCAAACAT
XL5' R2	Southern blotting	GCAACAGATGACTGTGGAT
neo F1	Southern blotting	CCAGGTCCACTTCGCATATT
neo F2	Southern blotting	TGCTCCTGCCGAGAAAGTAT
neo R1	Southern blotting	ATACTTTCTCGGCAGGAGCA
neo R2	Southern blotting	AGAACTCGTCAAGAAGGCGA

Table 2.1. Primer sequences.
The primers used for genotyping PCR and for making Southern blot probes are detailed, including the base sequences.

2.3 Drug injections

All drugs for peripheral injection were made up in sterile 0.9 % saline, except for reserpine which was dissolved in 1 % acetic acid. They were injected at 50 µl volume, diluted according to the bodyweight of the mouse.

All drugs for intracranial injections were made up in aCSF, and injected at 1 µl for ICV injections.

2.4 Histology

2.4.1 Fixing and cutting

Tissues were embedded in OCT mounting medium (Thermo Scientific), sections were cut to 12 µm thickness on a Leica cryostat, placed on a Superfrost slide (Thermo Scientific) and kept at -80 °C until use.

2.4.2 Immunohistochemistry

2.4.2.1 Antibodies

Rabbit anti-c-fos Ab5 (1:50,000; Calbiochem), and the goat anti-rabbit VectaStain kit (Vector Laboratories).

2.4.2.2 Staining protocol

Immunohistochemistry (IHC) was performed for the early-response gene c-fos on 12 µm cryostat sections, using the Vectastain Elite® kit (Vector laboratories). Sections were removed from -80 °C storage, left for 10 minutes to warm up and air dry, then incubated with PBS for 5 minutes. Endogenous

peroxidise activity was then quenched by 5 minutes incubation with 0.3 % H_2O_2 in MeOH, followed by three 5-minute PBS washes.

Sections were blocked for 1 hour at room temperature in blocking solution (PBS-TX with 10 % normal goat serum), followed by an overnight incubation at 4 °C of rabbit anti-c-fos diluted 1:50,000 in blocking solution. After three 5-minute PBS washes, sections were incubated with biotinylated goat anti-rabbit (VectaStain) diluted 1:200 in blocking solution, according to the manufacturer's instructions. This was followed by three more 5-minute PBS washes, then incubation with the VectaStain Elite ABC reagent made up in PBS, according to the manufacturer's instructions (streptavidin-HRP conjugates).

After three more 5-minute PBS washes was the colour development step. In this case, DAB (Sigma) solution was used, containing 0.3 % H_2O_2 and 0.05 % (w/v) nickel chloride to produce a purple-black precipitate in the presence of HRP. After washing with PBS and H_2O, sections were dehydrated with an ethanol series, then cleared twice using HistoClear (National Diagnostics), and finally mounted with Eukitt (Fluka).

2.4.2.3 Microscopy and imaging

Brightfield images were taken using a Leica mz16 microscope.

2.4.3 Immunofluorescence

2.4.3.1 Antibodies

The following antibodies were used: rabbit anti-c-fos (1:2000; Calbiochem), goat anti-XLαs M14 (1:200; Santa Cruz), donkey anti-rabbit AlexaFluor 488

(1:1000; Invitrogen), donkey anti-goat AlexaFluor 594 (1:1000; Invitrogen), and finally the nuclear stain DAPI (0.1 µg/ml; Invitrogen).

2.4.3.2 Staining protocol

Immunofluorescence (IF) was used to stain for the early-response gene c-fos, and counter-stain for XLαs. As with the IHC, 12 µm cryostat sections were removed from -80 °C storage and left for 10 minutes at room temperature to warm up and dry out. Sections were incubated 5 minutes in PBS, then blocked for 1 hour at room temperature using blocking reagent (PBS-TX with 10 % normal Donkey serum).

Sections were then incubated overnight at 4 °C with primary antibodies against c-fos and XLαs diluted in blocking solution. Three 15-minute PBS washes were followed by 1 hour incubation at room temperature with the secondary antibodies and DAPI diluted in blocking solution. After three final 15-minute PBS washes, slides were mounted with Fluorogel (Electron Microscopy Sciences), air dried, sealed, and kept at 4 °C in the dark.

2.4.3.3 Microscopy and imaging

Epifluorescent images were taken using a Zeiss Axioskop 40 microscope with Axioskop Vision software.

2.5 Southern blotting

2.5.1 Lysates

Samples were lysed in lysis buffer with Proteinase K (100 µg/ml; Sigma) overnight at 55 °C. The DNA was then purified by isopropanol extraction.

Briefly, DNA was precipitated by addition of equal volume (ie. 500 µl) of isopropanol and thorough mixing by inversion, followed by a 1-minute spin at 12,000 rpm. The supernatant was removed, leaving the DNA pellet, which was cleaned twice by addition of ice cold 70 % EtOH, mixing, spinning, and removal of the supernatant, followed by drying at 37 °C to remove excess EtOH. 50 µl TE was then added, and left at 4 °C for at least a week to ensure complete dissolving of the DNA.

2.5.2 Restriction digests

20 µl of DNA sample was used in a 40 µl restriction digest with addition of the following: 4 µl 10X Fastdigest buffer (Fermetas), 15 µl H_2O and 1 µl of restriction enzyme. The enzymes used were all Fastdigest ® enzymes (Fermentas), and included BglI, BglII and SpeI. Digests were left overnight at 37 °C to ensure complete digestion of the DNA.

2.5.3 Gel

The full 40 µl restriction digest was loaded onto a 0.8 % TAE agarose gel, and run for approximately 18 hours at 40 V. 1kb (Invitrogen) and λHIII ladders were run alongside, and a photo was taken of the gel on a Geldoc with a fluorescent ruler to provide size references; DNA was visualised with ethidium bromide.

2.5.4 Transfer

The gel was washed for 15 minutes each in 0.25 M HCl, then in 0.5 M NaOH (twice) and finally in 1 M NH_4COOH (twice). The blot was then set up, using paper towels to draw up 1 M NH_4COOH through the gel, thereby transferring

the DNA onto an Amersham nylon Hybond membrane (GE Healthcare). The blot was left for 48 hours during which time the towels were changed regularly and the 1 M NH_4COOH was kept topped up. After blotting, the positions of the wells were marked on the membrane, and the DNA was crosslinked using 1200 µjoules of UV light.

2.5.5 Probe synthesis

Southern blot probes were synthesised by PCR using DIG-labelled UTP (Roche). Details of the primers used can be found in Table 2.1, but the PCR reaction was the same in all cases. Into each 50 µl reaction the following was added: 1 µl plasmid DNA, 36.5 µl H_2O, 5 µl 10X Dig Synth PCR buffer (Roche), 5 µl 10X Dig Synth dNTP mix (including DIG-UTP; Roche), 1 µl forward primer, 1 µl reverse primer, 0.5 µl polymerase (Roche). For the XL5' probe, the following PCR conditions were used, with 30 cycles of steps 2-4:

1. Hot Start 95 °C for 5 minutes
2. 30 seconds at 95 °C denaturing step
3. 30 seconds at 56 °C annealing step
4. 2 minutes at 72 °C elongation step
5. 2-minute final elongation step at 72 °C

For the Neo probe, the following PCR conditions were used, with 30 cycles of steps 2-4:

1. Hot Start 95 °C for 5 minutes
2. 45 seconds at 95 °C denaturing step
3. 45 seconds at 58 °C annealing step

4. 2 minutes at 72 °C elongation step
5. 2-minute final elongation step at 72 °C

The probes were cleaned up by running on a 1.7 % agarose gel, cut out on a transilluminator and purified from the gel using gel extraction columns (Qiagen). Briefly, the gel was dissolved in approximately 200 µl binding buffer per 100 mg of gel and incubated for 10 to 15 minutes at 55 °C until fully melted/dissolved. This was added to the spin column, left for 2 minutes at room temperature, and spun at 12,000 rpm for 1 minute. Flow-through was discarded and 500 µl wash solution added to the column before spinning again; flow-through was discarded again and the wash repeated, followed by a final spin. 60 µl pre-warmed elution buffer was added to the column, left for 5 minutes at 55 °C and spun to elute the probe, followed by repeating the elution step to obtain maximal product.

2.5.6 Probe hybridisation and staining

Several probe reactions were performed and pooled into each 50 ml probe mix in hybridisation buffer to provide high levels of staining. The membrane was equilibriated in 5x SSC for 3 minutes, then incubated for 1 hour at 68 °C in hybridisation buffer as a pre-hybridisation step, then hybridised overnight at 68 °C with the probe on a shaking platform. After hybridisation, the membrane was washed twice for 5 minutes in Wash buffer 1 at room temperature, twice for 20 minutes in Wash buffer 2 at 68 °C, then equilibriated for a few minutes in Dig buffer 1 at room temperature.

The membrane was blocked for 90 minutes at room temperature with Dig buffer 1 containing 1 % blocking reagent (Roche), followed by a 30-minute

incubation with alkaline phosphatase-linked sheep anti-Dig (Roche) diluted 1:5000 in Dig buffer 1 with 1 % blocking reagent. The membrane was then washed twice for 15 minutes with Dig buffer 1, then equilibriated for a couple of minutes in Dig buffer 3, followed by overnight incubation with NBT BCIP colour reagent at room temperature; the colour reaction was stopped by incubation with PBS for a couple of minutes.

2.6 Western blotting

2.6.1 Protein extraction

Adult interscapular BAT samples were homogenised in protein lysis buffer, then sonicated to disrupt DNA. Samples were kept on ice at all possible times during the protocol. Samples were spun for 10 minutes at 12,000 g at 4 °C. Protein concentration was determined using a Pierce® BCA protein assay kit (Thermo Scientific), and samples were kept at -80 °C until use.

2.6.2 Gel and transfer

PAGE gels were made by overlaying a resolving gel with a short stacking gel. Both were made up according to the recipes shown earlier; the 10 % APS and TEMED were added quickly just before being poured into the gel cassettes, and the gel was overlaid with isobutanol. Following polymerisation, the isobutanol and excess acrylamide were washed off with H_2O before addition of the next gel, or use for electrophoresis. 100 µg of each protein lysate was diluted to 10 µl with H_2O, then diluted 1:1 with 2x Laemlli protein loading buffer (National diagnostics), before being heat denatured by incubating for 3 minutes at 95 °C then quickly placing on ice.

Samples were loaded onto the PAGE gel along with a coloured protein ladder (Fermentas), and empty wells were filled with 1x Laemlli protein loading buffer. The gel was run in SDS-PAGE electrophoresis buffer at 10 mA until the samples reached the resolving gel, then run at 15 mA until the blue dye ran off the bottom of the gel. The gel was then blotted to an Amersham PVDF Hybond membrane (GE Healthcare) by electrotransfer, 30 V overnight at room temperature, in transfer buffer. The position of the wells was marked with a pencil.

2.6.3 Staining

The membrane was incubated for 10 minutes at room temperature with TBS-T before blocking for 1 hour at room temperature with blocking solution (TBS-T with 5 % (w/v) skimmed milk powder). The membrane was incubated overnight at 4 °C with rabbit anti-P-HSL against Ser563 (Cell Signalling Technology) diluted 1:250 in blocking solution, followed by three 12-minute TBS-T washes, then incubated for 1 hour at room temperature with goat anti-rabbit HRP (Jackson Laboratories) diluted 1:10,000 in blocking solution. After three more 12-minute TBS-T washes, samples were detected using Amersham ECL plus detection kit (GE Healthcare).

The detection reagent was made up according to the manufacturer's instructions, then incubated on the membrane for 5 minutes before exposure for 6 hours on Kodak X-ray film (Sigma). The membrane was then stripped by incubation for 30 minutes at 50 °C in stripping buffer, before being washed twice for 10 minutes with large volumes of TBS-T. HSL was then immunostained in the same was as P-HSL, except that the primary antibody

used was rabbit anti-HSL (Cell Signalling Technology), and was incubated for 1 hour at room temperature diluted 1:1000 in blocking solution, and the membrane was only exposed to X-ray film for 10 seconds.

2.7 Cannulations

Adult male *Gnasxl* knockout mice and wildtype siblings were anaesthetised with an appropriate dose of urethane-chloralose administered ip in saline. Following injection of the anaesthetic, the mice were returned to the cage for 3 minutes until they became unconscious; body temperature was immediately recorded by rectal probe before exposure to a heat source. Following the initial measurement, body temperature was monitored by rectal probe, and maintained at 37 ±0.5 °C by heat lamp. Following loss of the paw-withdrawal and eye-blink reflexes, the trachea was intubated to facilitate breathing.

The carotid artery was cannulated with stretched PP25 tubing filled with heparinised saline; blood pressure was measured by a pressure transducer connected to a Neurolog blood pressure amp. Raw blood pressure signal was split, so that raw blood pressure could be recorded, as well as a second signal that was AC coupled and amplified between 10 and 100 times depending on signal strength. Both raw and amplified blood pressure signals were digitised to PC using a CED 1401 interface (Cambridge Electronic Design, Cambridge, UK) and recorded on Spike2 at 5 kHz.

2.7.1 Heart beat detection from blood pressure signal

Heart rate was annotated from the AC coupled amplified blood pressure signal using Wabp from the Physionet suite of programs (Goldberger *et al.*, 2000). Briefly, the signal was analysed at 1/10th sampling frequency (ie. 500 Hz), and resampled to 125 Hz for optimal beat detection by Wabp. Annotated beats were then reverted to 10 times speed to give the actual heart rate.

2.7.2 Intracerebroventricular injections

Anaesthetised cannulated mice were placed in a mouse-adapted stereotaxic frame. The head was clamped in a level position and a hole was drilled at an appropriate location for the site of injection. Injections were performed using an appropriately sized Hamilton syringe according to the following stereotaxic coordinates relative to bregma, as determined from the Paxinos and Franklin adult mouse stereotaxic atlas (Paxinos & Franklin, 2001): intracerebroventricular (ICV) injection (0.2 mm caudal, 1.0 mm lateral, 3.5 mm vertical).

All drugs were dissolved in aCSF, and injected in 1 µl volume for ICV injections; liquid was expelled gradually over 30 seconds, and the syringe elevated 2 minutes following injection. The syringe was kept in place above the injection site during recording, and at the end of the experiment 1 % (w/v) Chicago blue dye (Sigma) was injected at the same injection coordinates and in the same volume as the drug. The mouse was then decapitated and the brain removed and placed in 4 % PFA. Following overnight fixation, the brain was cut to 300 µm on a vibratome to confirm correctly targeted injection by the location of blue dye.

2.8 Telemetry

Telemetry was used to record electrocardiogram (ECG) and locomotor activity from conscious freely moving mice. The transmitters used were ETA-F20 transmitters from DSI (Data Sciences International, MN, USA); biopotential and locomotor activity were recorded.

2.8.1 Telemetry surgery

ECG telemeters were implanted subcutaneously into adult male *Gnasxl* knockout mice and wildtype siblings, under isoflurane anaesthesia (Figure 2.1A). Appropriate areas of the mouse's skin were shaved and painted with videne antiseptic, and mice were given pre-operative subcutaneous injections of the analgesic buprenorphine (Temgesic, 1.5 mg/kg; Reckitt Benckiser, Slough, UK), the antibiotic enrofloxacin (Baytril, 0.2 ml/kg; Bayer AG, Leverkusen, Germany) and the anti-inflammatory meloxicam (Metacam, 100 µg/kg; Boehringer Ingelheim, Germany).

Incisions in the skin were made using a scalpel, and blunt dissection was used to create a pocket in the loose skin of the flank. The body of the transmitter was placed subcutaneously along the flank, and the electrodes were stitched in place to record electrical activity of the heart; one on the right pectoral muscle, the other by the diaphragm on the left side. Incisions were closed using individual sutures of 4/0 polysorb, which were subsequently glued with surgical superglue (Vetbond) to resist being chewed out by the mouse.

Surgery was performed under aseptic conditions. Following surgery mice were isolated and kept warm and monitored for recovery from anaesthesia; recording was started a minimum of 5 days after surgery.

2.8.2 ECG recording

Following recovery from surgery, ECG and locomotor activity were recorded (Figure 2.1B). Mice were housed individually, each above a DSI telemetry receiver pad, and kept at least a metre apart to prevent cross-talk of signals.

The ECG signal is transmitted as a short range FM signal from the transmitter, which is picked up by the receiver pad, where the ECG signal is AC coupled. The receiver pad is connected via an Ethernet cable to a DSI data exchange matrix (DEM), which provides power for the pads. En route to the DEM is a signal output adaptor, which extracts the ECG signal to a BNC output cable, which is connected to the interface, a CED micro1401 (Cambridge Electronic Design, Cambridge, UK). The signal is digitised by the CED interface, and recorded on a PC by Spike2 at 5 kHz.

Locomotor activity signal is initiated at the level of the receiver pad, which produces a binary signal burst after movement of the transmitter exceeds a certain threshold level. The activity signal was extracted directly from the Ethernet cable by splicing the relevant pin of the Ethernet cable to a BNC cable which was connected to the CED interface, where it was digitised and recorded at 100 Hz. Spike2 recording was automated to record continuously 24-hours a day.

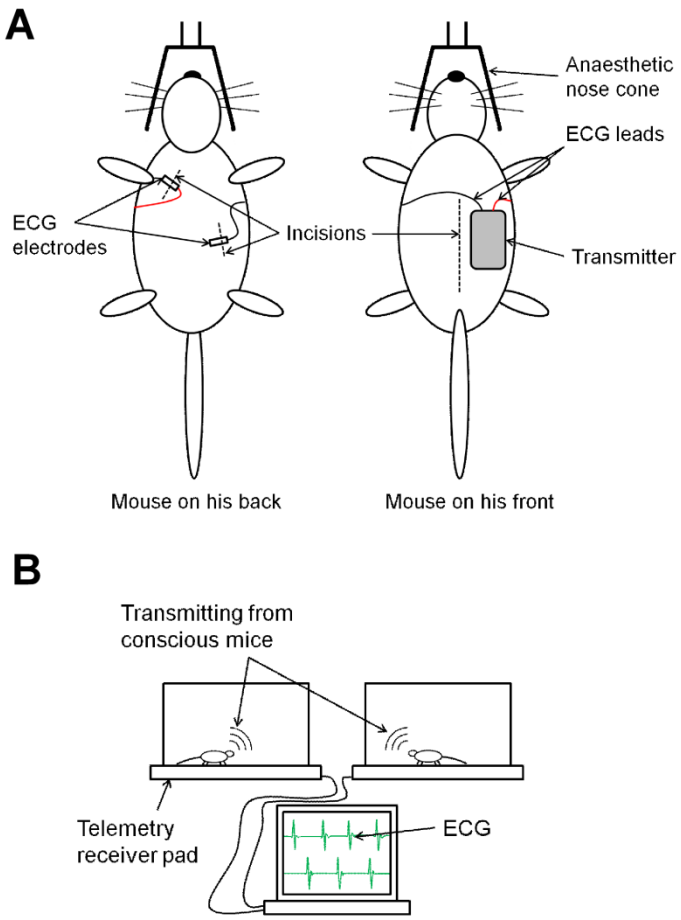

Figure 2.1. ECG telemetry surgery and recording in mice.
(A) ECG telemeters (DSI) were implanted subcutaneously in adult male mice under isoflurane anaesthesia.
(B) Following recovery ECG and locomotor activity were recorded from conscious freely moving mice.

2.8.3 Beat detection

A custom program was developed in Java script (Netbeans IDE) to annotate heart beats from ECG. The raw ECG signal was first cleaned up in Spike by the process of DCremove using a time constant of 20 ms. This subtracts the average of 10 ms either side from each data point, and has similar effects to a high pass filter.

The beat detection program recognises beats as regions of high variability. Specifically, a small window of ECG (2048 data points, ie. approximately 0.4 seconds) is analysed, and the data point with the highest standard deviation is considered (Figure 2.2). If the data point is above a threshold of 2 times the standard deviation of the data points in the window, it is annotated as a beat and 200 data points (ie. 0.04 s) either side are blanked. The program then tests the next point with the highest standard deviation, and continues until there are no more points above the threshold, before moving the window along and analysing further data points.

For analysis of circadian heart rate changes beats of more than 1000 bpm or less than 400 bpm, which are assumed to be ectopic or misread beats, are excluded. Heart rate responses to drug injections and heart rate variability are analysed directly from the raw heart beat annotation files, which contain heart beats annotated to a high degree of accuracy (ie. to within the sampling rate of 0.2 ms).

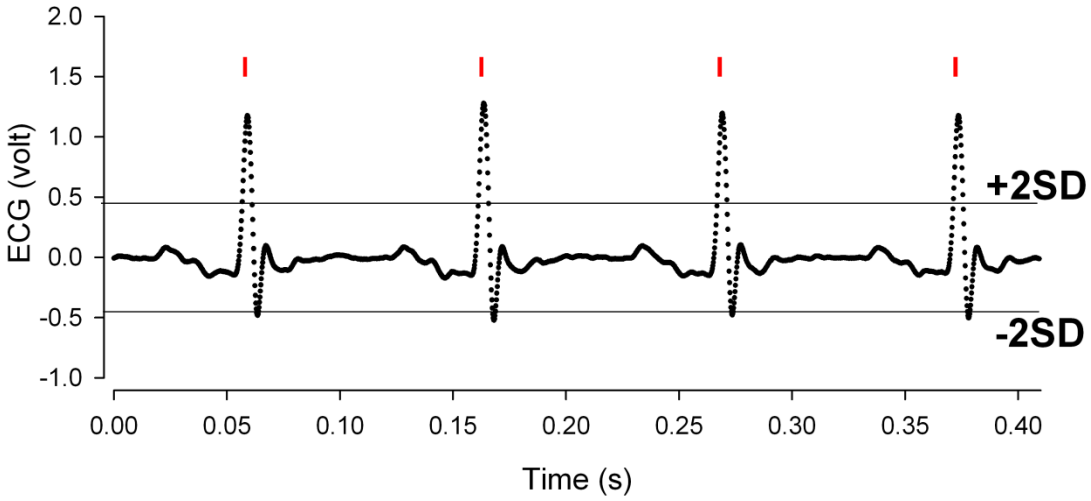

Figure 2.2. Heart beat detection from ECG.
The beat detection program recognises beats based on the most extreme points that lie outside 2 standard deviations from the mean, from a window of 2048 data points (ie. ~0.4s). Shown is one "window", with annotated beats shown as red bars, and the level of 2SD above and below the mean.

2.8.4 Heart rate variability

All heart rate variability (HRV) analyses were performed using Kubios HRV program (Niskanen *et al.*, 2004), except for Lomb transforms which were performed using the Lomb program from the Physionet suite (Goldberger *et al.*, 2000). In all cases, heart rate traces were visually inspected for 3-minute sections of clean and stable heart rate, which were then used for a number of HRV analyses.

The standard deviation of normal RR intervals (SDNN) was calculated as the standard deviation in ms of the 3-minute section of heart rate. The root mean square of successive differences (RMSSD) is calculated as the difference in ms between each successive RR interval, squared, averaged from the 3-minute period, and then square rooted. Poincaré plots were produced as each RR interval plotted against the following RR interval; the standard deviation was calculated at 45° rotation of each axis, producing SD1 and SD2 values (Figure 4.2Ai for a typical Poincaré plot).

Three different power spectral analyses were used. For fast Fourier transforms (FFTs) and autoregressive spectra, heart rate was resampled to 20 Hz. FFTs were performed using Welch's algorithm using 32-second windows with 50 % overlap. Autoregressive spectra were produced using a 32-order model. Lomb periodograms were produced from raw heart beat annotations, using the default settings on the Physionet Lomb program. The low frequency (LF) and high frequency (HF) bands were defined as 0.15-1.0 Hz and 1.0-5.0 Hz, respectively (see chapter 4 for validation). Raw HF power

was used as an indicator of parasympathetic activity, and LF/HF ratio was used as an indicator of sympathetic activity.

For further details of HRV and validation of the various analyses used, see chapter 4.

2.9 Statistics

Excluding representative plots for illustrative purposes, all graphs show mean ± standard error of the mean (SEM). For comparing basal physiological parameters between wildtypes and knockouts (for example in Figure 3.8 Aii), unpaired t-tests were used. For all other statistical analyses, paired t-tests were used. In figures 3.2 A, 3.2 B, 3.3 C and 3.8 B the differences in response were tested by paired t-test between wildtypes and knockouts, to account for the strictly dose-matched anaesthesia used. In all other cases, the responses were analysed by paired t-test within each genotype; in this way the response of each mouse was essentially paired with itself, to take into account variability in starting values, which can mask any drug effect.

3 Autonomic control of the cardiovascular system in mice lacking XLαs

3.1 Introduction

The sympathetic nervous system (SNS) plays a major role in the control of energy balance and the cardiovascular system (Hall *et al.*, 2010). Elevated sympathetic stimulation of adipose tissue activates lipolysis and, in brown adipose tissue (BAT), stimulates thermogenesis which results in increased metabolic rate (Cannon & Nedergaard, 2004).

Elevated sympathetic stimulation of the cardiovascular system results in elevations to blood pressure and heart rate; for example elevated blood pressure in the Schlager hypertensive mouse is caused by increased SNS activity (Davern *et al.*, 2009). Chronic elevations to SNS activity have been identified as characteristic of a number of cardiovascular diseases, including chronic heart failure (Fisher *et al.*, 2009).

3.1.1 Elevated SNS in animal models

Animal models in which there is a global increase in SNS activity, resulting in a lean animal with hypertension, include mice with artificial overexpression of leptin (Ogawa *et al.*, 2002) or α-MSH (Savontaus *et al.*, 2004), as well as

knockouts for the central nervous system renin-angiotensin system (Takahashi *et al.*, 2011).

Another mouse model of hypertension, the Schlager hypertensive mouse, is known to be caused by elevated SNS activity (Davern *et al.*, 2009), but no metabolic changes have so far been reported. Interestingly, the brain renin-angiotensin system contributes little to the hypertensive phenotype of the Schlager mouse (Palma-Rigo *et al.*, 2011), so there are clearly multiple parallel system that control the SNS effects on the cardiovascular system.

Mouse models can have more selective effects, for example increasing just cardiovascular SNS stimulation in the Schlager hypertensive mouse (Davern *et al.*, 2009) or modifying energy expenditure without affecting the cardiovascular system (Tallam *et al.*, 2005). It is therefore of interest to investigate effects to the cardiovascular system in lean *Gnasxl* knockout mice.

3.1.2 The SNS in *Gnasxl* knockouts

Adult mice lacking XLαs have elevated sympathetic stimulation of the brown and white adipose tissues, which results in increased metabolism (Xie *et al.*, 2006). However, the effects to the cardiovascular system are unknown, although it has been previously suggested that the mice have a global increase in SNS activity (Xie *et al.*, 2006).

The aim of this chapter is to investigate the cardiovascular phenotype of *Gnasxl* knockout mice, in particular investigating SNS control of the

cardiovascular system, as well as a brief investigation into the physiological effects of elevated SNS stimulation of the adipose tissue.

The hypothesis, that *Gnasxl* knockout mice suffer from a global increase in SNS activity that causes hypermetabolism and hypertension, is strongly supported by the neuronal expression pattern of XLαs. This includes the PVN, DMH, Arc, Raphe pallidus and the NTS (Pasolli *et al.*, 2000; Pasolli & Huttner, 2001; Krechowec *et al.*, 2012). XLαs expression in these brain regions, especially the DMH and PVN which are critical for control of the SNS (Loewy, 1991; Coote, 2007; Dimicco & Zaretsky, 2007; Nunn *et al.*, 2011), mean it is well placed to be controlling global SNS activity.

3.1.3 XLαs versus G_sα

There is an interesting dichotomy between XLαs and its splice variant G_sα concerning control of metabolism and the cardiovascular system. The mRNA transcripts *Gnasxl* and *Gnas*, which encode the proteins XLαs and G_sα, respectively, are oppositely imprinted – *Gnasxl* is silenced on the maternal allele (Hayward *et al.*, 1998; Peters *et al.*, 1999; Plagge *et al.*, 2004) while *Gnas* is silenced on the paternal allele, but only in certain cell types (Peters *et al.*, 1999; Plagge *et al.*, 2008; Chen *et al.*, 2009).

Mice lacking XLαs or G_sα have functionally opposite phenotypes; loss of XLαs results in a lean phenotype with hypermetabolism, glucose tolerance and insulin sensitivity (Xie *et al.*, 2006), whereas loss of G_sα results in an obese phenotype with hypometabolism, glucose intolerance and insulin resistance (Chen *et al.*, 2005). It therefore stands to reason that the signalling proteins function in an antagonistic manner, and that any further

phenotypic effects are likely to be opposite between the two genotypes. As more is known about the *Gnas* knockout, certain predictions can be made about the *Gnasxl* knockout.

Firstly, it has been shown, using a tissue- and maternal allele-specific knockout of $G_s\alpha$, that the metabolic effects of $G_s\alpha$ are caused specifically by loss of the signalling protein in the brain (Chen *et al.*, 2009). Therefore, this might suggest that XLαs also functions in the brain to cause an opposite metabolic phenotype.

Secondly, loss of $G_s\alpha$ in the brain results in a hypotensive phenotype, with reduced heart rate and a global decrease in SNS activity (Chen *et al.*, 2009). Therefore, one might predict that loss of XLαs may result in hypertension, with increased heart rate and a global increase in SNS activity.

Thirdly, the brain-specific *Gnas* knockout is resistant to an agonist to the melanocortin 3/4 receptors (MC3/4R) (Chen *et al.*, 2009), which stimulate the SNS and energy expenditure (Haynes *et al.*, 1999; Kuo *et al.*, 2004; Tallam *et al.*, 2005; Tallam *et al.*, 2006; Corander *et al.*, 2009; Rossi *et al.*, 2011). Therefore, loss of XLαs might result in increased sensitivity to a melanocortin agonist.

Finally, mice with $G_s\alpha$ conditionally mutated in the PVN retain the cardiovascular phenotype of maternal brain-specific $G_s\alpha$ knockouts, but not the metabolism effects (Chen *et al.*, 2012). Therefore, the cardiovascular effects of XLαs deletion might be expected to be caused by loss of XLαs from the PVN.

3.1.4 Aims

This chapter will investigate effects to the cardiovascular system in adult male *Gnasxl* knockout mice, focussing on indicators of sympathetic activity. This includes blood pressure monitoring in anaesthetised mice and heart rate monitoring in conscious mice, as well as injection of reserpine and atropine as antagonists to the autonomic control of the cardiovascular system. Additionally, body temperature control in *Gnasxl* knockouts will be briefly examined.

3.2 Methods

A number of approaches were used to investigate control of the cardiovascular system in *Gnasxl* knockout mice. All experiments were performed on adult male knockouts and wildtype siblings. The anaesthetic urethane was used for terminal anaesthetic recordings, as this is documented to have minimal cardiotropic effects compared to other injectable anaesthetics (Carruba *et al.*, 1987; Janssen *et al.*, 2004), and the dose was more tightly regulatable compared to inhalation anaesthetics.

Additionally, α-chloralose was added to the urethane to provide improved anaesthesia at lower dosages of urethane (Dalkara *et al.*, 1995; Kass *et al.*, 1998), and furthermore, the urethane-chloralose was strictly dose-matched within sibling groups to equalise any detrimental effects of the anaesthesia on the cardiovascular system.

The other technique used to record cardiovascular parameters was electrocardiogram (ECG) telemetry, from which heart rate and locomotor activity were recorded from conscious freely moving mice.

In conjunction with the recording of cardiovascular parameters by cannulation and telemetry, reserpine was used to inhibit sympathetic activity, specifically SNS stimulation of the cardiovascular system.

Reserpine inhibits the vesicular monoamine transporter, thereby inhibiting noradrenaline packaging into neurotransmitter vesicles in sympathetic nerve terminals giving a global reduction in sympathetic stimulation of peripheral tissues (Carlsson *et al.*, 1963; Iversen *et al.*, 1965).

Reserpine was therefore used as a “pure” sympatholytic, as it lacks the off-target effects of other global sympatholytics such as hexamethonium, pentolinium, or clonidine, or the “narrow” effects of targeted sympatholytics such as propranolol or prazosin (Bakris & Frohlich, 1989). Reserpine was dissolved in 1 % acetic acid solution, and injected 2 mg/kg ip in anaesthetised mice and 1 mg/kg ip in conscious mice.

Atropine was used as a classic parasympatholytic, to inhibit parasympathetic stimulation of the cardiovascular system (Katona & Jih, 1975), as an antagonist to the muscarinic acetylcholine receptor. It was injected at 2 mg/kg ip in conscious mice.

Further details of the methods used can be found in chapter 2.

3.3 Results

3.3.1 Arterial cannulation in anaesthetised mice

Cannulation was initially performed using urethane anaesthesia on adult male *Gnasxl* knockouts and wildtype siblings. However, there was high variability in recorded blood pressure, most likely due to the high and variable doses of urethane needed to achieve full anaesthesia, with the result that no significant differences were seen between knockouts and wildtypes (data not shown).

The experiment was therefore repeated using a mixed anaesthetic of urethane and α-chloralose in strictly dose-matched sibling groups (Figure 3.1 for representative data).

3.3.1.1 Basal cardiovascular parameters in anaesthetised Gnasxl knockout mice

Under urethane-chloralose anaesthesia, *Gnasxl* knockouts were found to have elevated blood pressure compared to dose-matched sibling wildtypes (Figure 3.2A; 62 ±5 vs 47 ±5 mmHg, KO vs WT, $p \leq 0.05$ by paired t-test, n=8), but there was no difference seen in the heart rate (Figure 3.2B; 565 ±21 vs 555 ±30 bpm, KO vs WT, n=8).

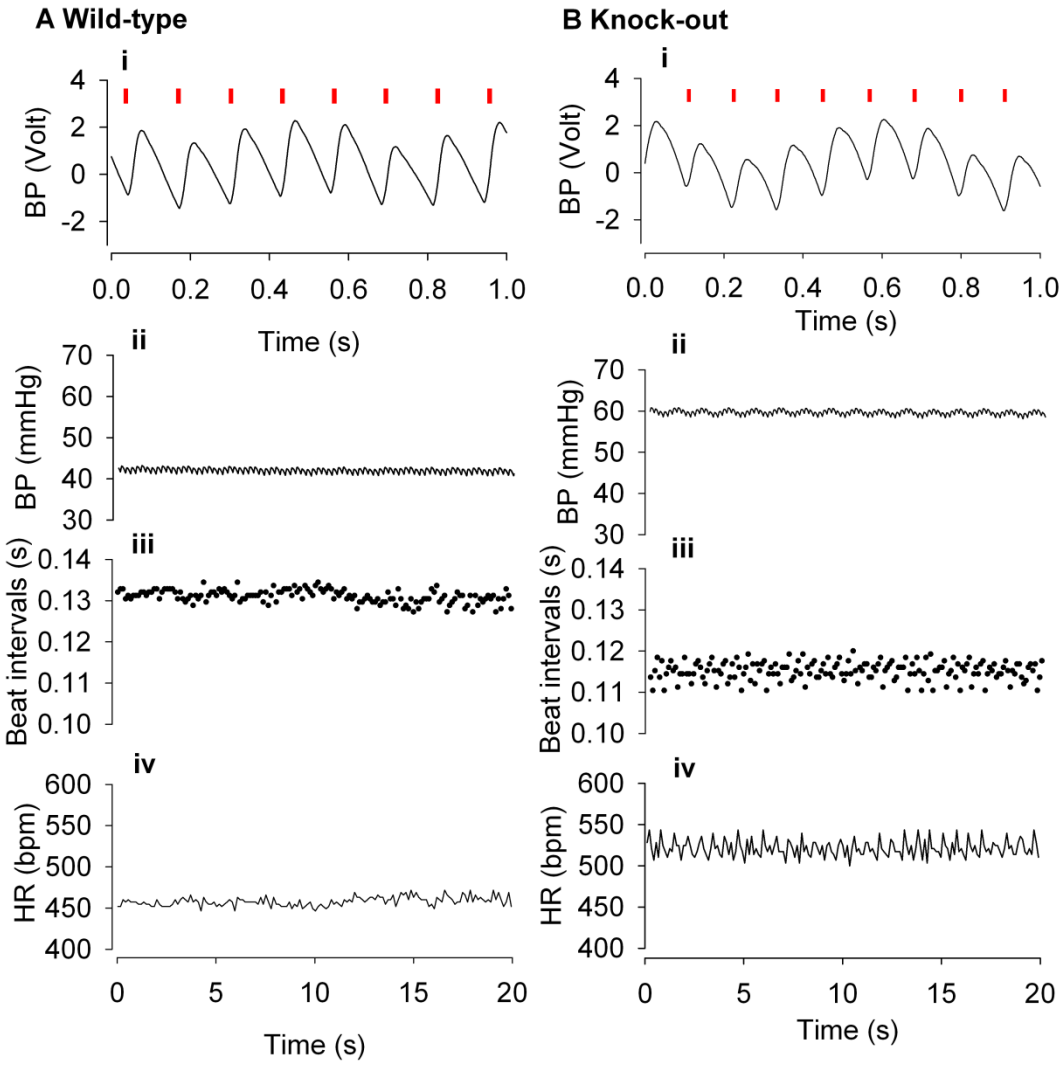

Figure 3.1. Typical blood pressure and heart rate traces in anaesthetised *Gnasxl* knockout mice and wildtype siblings.
Blood pressure was recorded in urethane-chloralose anaesthetised *Gnasxl* knockout mice (B; right) and wildtype siblings (A; left).
(i) Typical blood pressure trace recorded at high resolution. Signal was AC coupled and amplified 10-100 times, depending on signal strength. Heart beats were annotated using Wabp from the Physionet suite of programs; beat annotations are shown as red bars.
(ii) Typical raw unamplified blood pressure trace recorded by DC coupling.
(iii) Heart beat intervals associated with the shown blood pressure trace.
(iv) Instantaneous heart rate as calculated from the interval series shown.

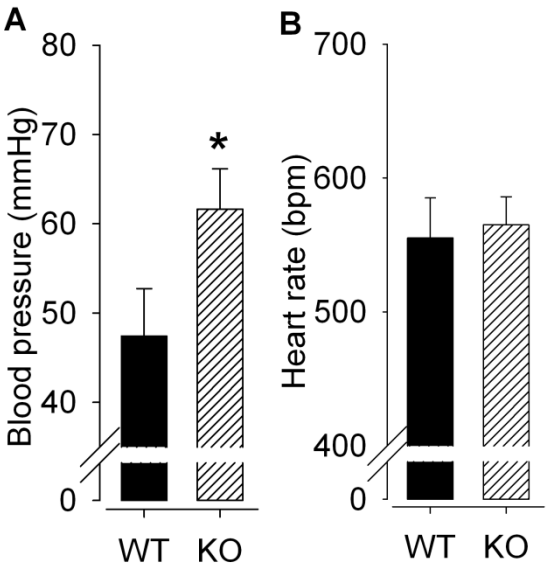

Figure 3.2. Basal cardiovascular parameters in anaesthetised *Gnasxl* knockout mice and wildtype siblings.

Blood pressure and heart rate were recorded in urethane-chloralose anaesthetised *Gnasxl* knockout mice and dose-matched wildtype siblings.
(A) Mean basal blood pressure was significantly elevated in *Gnasxl* knockout mice (*p≤0.05 by paired t-test, n=8).
(B) There was no significant difference in mean basal heart rate between wildtypes and knockouts.

3.3.1.2 Blood pressure responses to reserpine in anaesthetised Gnasxl knockouts

In order to determine whether the elevated blood pressure seen in the knockouts was due to increased SNS stimulation of the cardiovascular system, the mice were injected with the sympatholytic reserpine at 2 mg/kg ip. Both wildtypes and knockouts had a similar response to vehicle (Figure 3.3A), but knockouts had a more pronounced response to reserpine than wildtypes (Figure 3.3B).

This is more objectively visible when the blood pressure is averaged before injection, after vehicle injection, and after reserpine injection (Figure 3.3C). It is clear from this that the blood pressure drops to a similar extent in wildtypes and knockouts after vehicle injection, but the knockouts have a greater response to reserpine.

To take into account this gradual decrease in BP over time, the response to reserpine was calculated as blood pressure response to reserpine relative to the blood pressure response to vehicle; this was calculated individually for each mouse, so each mouse was its own internal control. In this way, knockouts were found to have a significantly greater response to reserpine compared to dose-matched sibling wildtypes (Figure 3.3D; -7.0 ±1.3 vs -0.5 ±1.9 mmHg, KO vs WT; $p \leq 0.05$ by paired t-test, n=5).

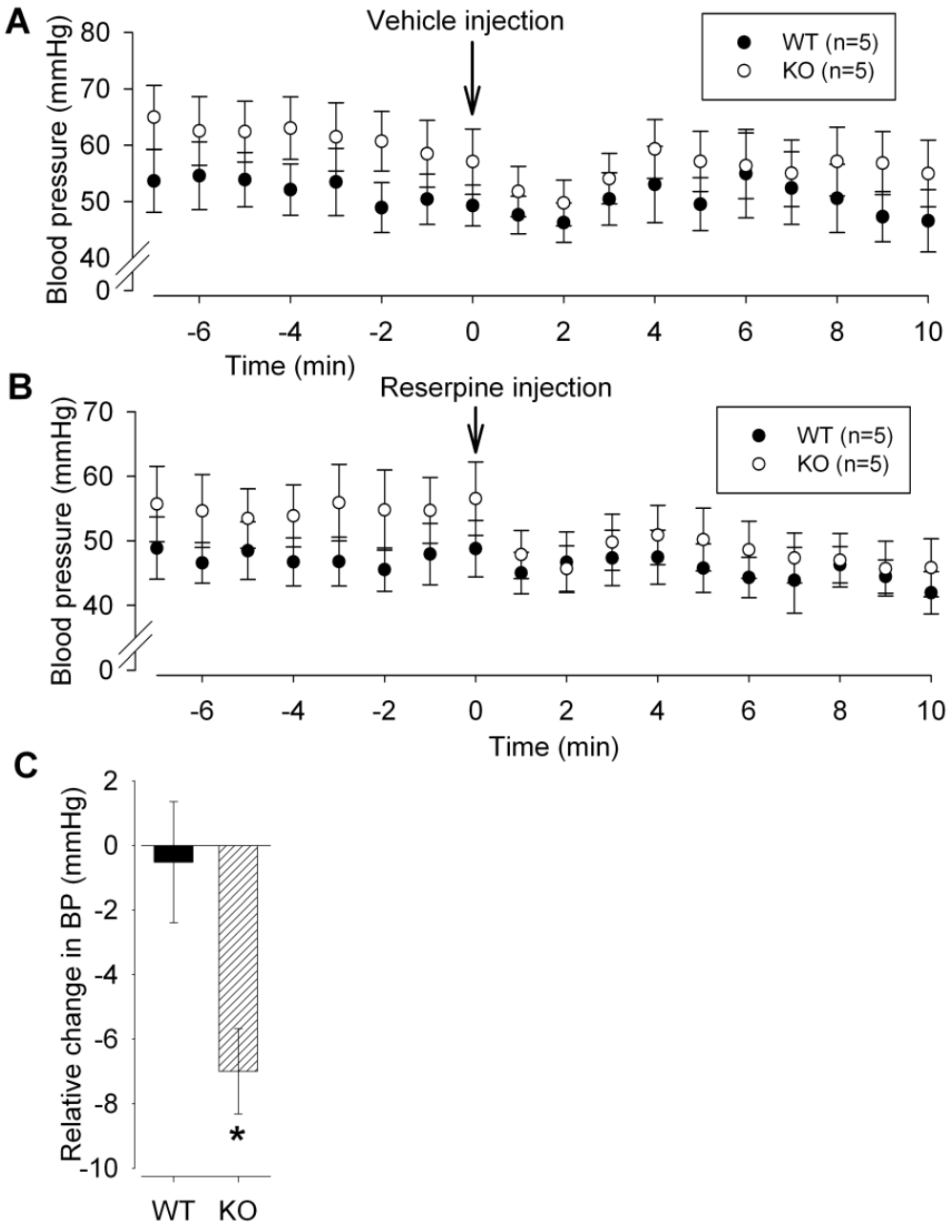

Figure 3.3. Cardiovascular response to reserpine in anaesthetised *Gnasxl* knockout mice and wildtype siblings.
Blood pressure was recorded in urethane-chloralose anaesthetised *Gnasxl* knockout mice and dose-matched wildtype siblings.
(A) Blood pressure responses to vehicle over time.
(B) Blood pressure responses over time to reserpine 2 mg/kg ip.
(C) Due to the highly variable and declining blood pressure, responses were calculated as blood pressure change after reserpine relative to the change after vehicle (ie. blood pressure decrease after reserpine minus decrease after vehicle, individually for each mouse). In this way, knockouts had a significantly greater relative blood pressure response to reserpine compared to wildtypes (*p≤0.05 by paired t-test; responses were paired between dose-matched siblings).

3.3.2 ECG telemetry in conscious mice

Radiotelemetry was used to record ECG from conscious freely-moving animals (Figure 3.4 for representative data); this avoided the potentially significant effects to the cardiovascular system of the anaesthesia used in the earlier experiments.

3.3.2.1 Heart rate in conscious Gnasxl knockout mice

Circadian changes in heart rate and locomotor activity were investigated in adult knockouts (3.5A/C). Knockouts had significantly elevated heart rate at night (Figure 3.5B; 630 ±14 vs 590 ±10 bpm KO vs WT, $p \leq 0.05$ by t-test, n=12), but there were no significant differences in daytime heart rate (Figure 3.5B) or in locomotor activity at any time (Figure 3.5D). Autonomic control of the cardiovascular system was investigated by injection of reserpine and atropine as sympathetic and parasympathetic antagonists, respectively.

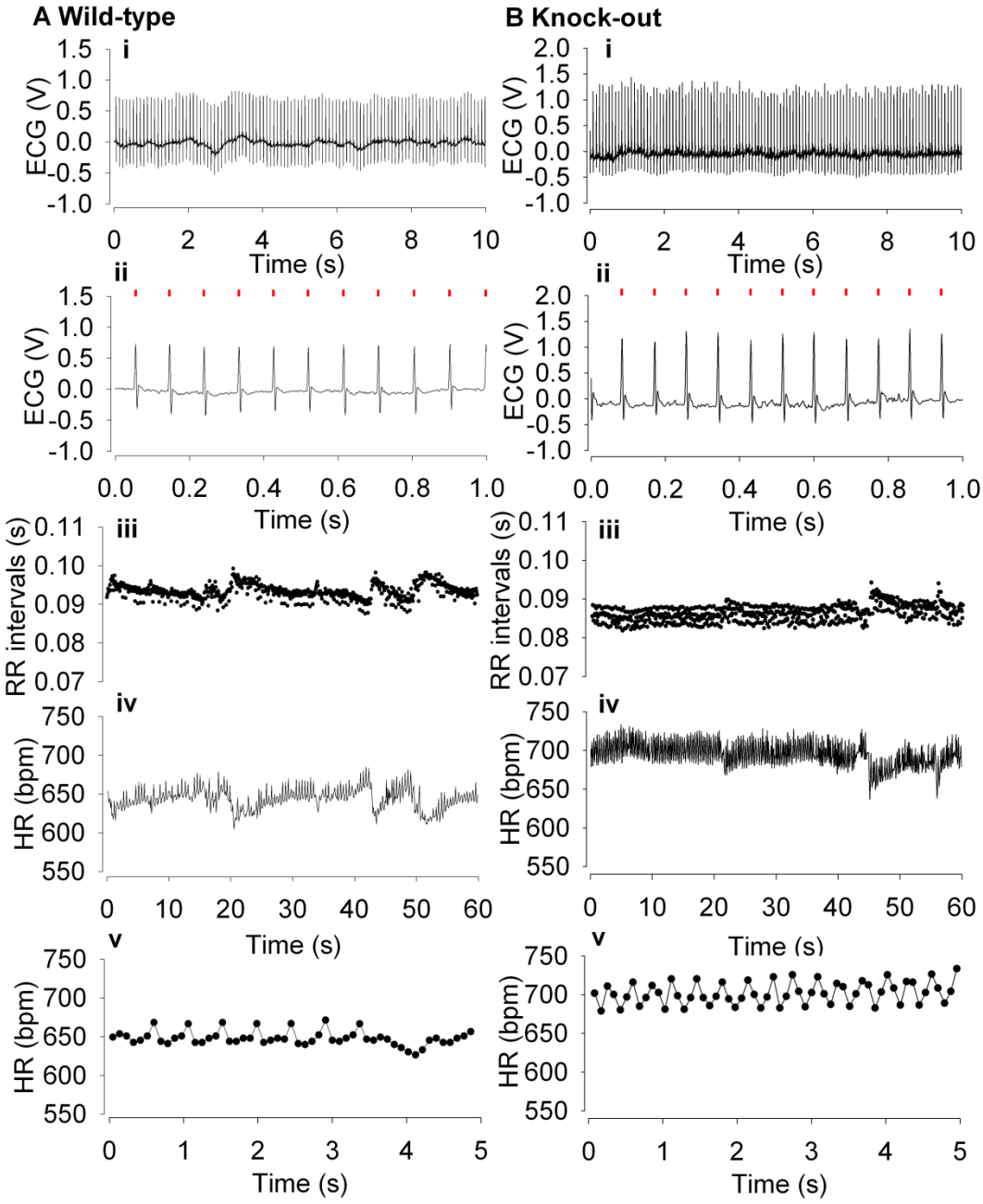

Figure 3.4. Typical ECG and heart rate traces in conscious *Gnasxl* knockout mice and wildtype siblings.
ECG was recorded at high resolution from conscious freely moving adult *Gnasxl* knockout mice (B; right) and wildtype siblings (A; left) using radiotelemeters.
(i) Typical raw ECG trace from the active night period.
(ii) Zoomed in region of the same ECG trace showing beat architecture. Heart beats were annotated using a custom program (red bars).
(iii) Typical heart beat interval series.
(iv) Instantaneous heart rate as calculated from the beat interval series shown.
(v) Zoomed in region of the same instantaneous heart rate trace showing substantial heart rate variability over time.

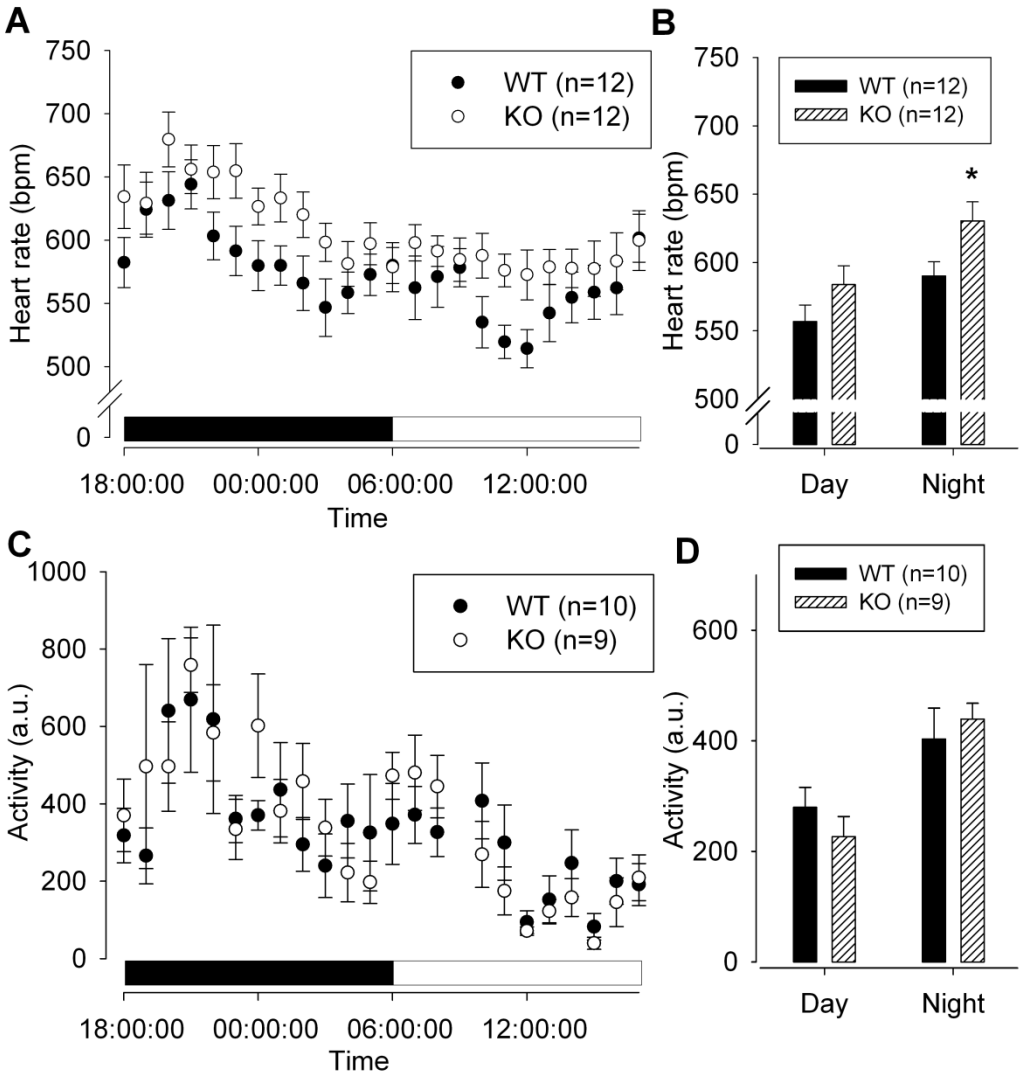

Figure 3.5. Circadian heart rate and activity in conscious *Gnasxl* knockouts.

Heart rate and activity were measured continuously by telemetry from conscious freely moving adult *Gnasxl* knockouts and wildtype siblings.

(A) Circadian variation in heart rate, averaged into 1-hour bins over 24 hours.

(B) Knockouts showed significantly elevated heart rate at night (*p≤0.05 by t-test, n=12).

(C) Circadian variation in locomotor activity, averaged into 1-hour bins over 24 hours.

(D) No significant changes were seen in average activity measures between wildtypes and knockouts.

3.3.2.2 Sympathetic control of heart rate in conscious Gnasxl knockout mice

The origin of the elevated heart rate in knockouts was investigated by injecting reserpine ip at 1 mg/kg. Heart rate response to reserpine over time for wildtypes and knockouts is shown in Figure 3.6A. On average, reserpine caused a significant decrease in heart rate in knockouts (Figure 3.6B; 531 ±23 to 455 ±12 bpm, $p \leq 0.05$ by paired t-test, n=8), but not in wildtypes (Figure 3.6B; 516 ±21 to 471 ±41 bpm, n=8). There was no significant difference in average heart rate response to reserpine between the two genotypes (Figure 3.6C; -73 ±30 vs -42 ±46 bpm, KO vs WT, n=8).

3.3.2.3 Parasympathetic control of heart rate in conscious Gnasxl knockout mice

Parasympathetic control of the cardiovascular system in *Gnasxl* knockouts was investigated by injection of atropine 2 mg/kg ip. Heart rate response to atropine over time for wildtypes and knockouts is shown in Figure 3.7A. On average, atropine significantly increased heart rate in knockouts (Figure 3.7B; 551 ±16 to 591 ±19 bpm, $p \leq 0.05$ by paired t-test, n=6), but not in wildtypes (Figure 3.7B; 533 ±28 to 552 ±17 bpm, n=6). There was no significant difference in average heart rate response to atropine between the two genotypes (Figure 3.7C; 40 ±11 vs 19 ±21 bpm, KO vs WT, n=6).

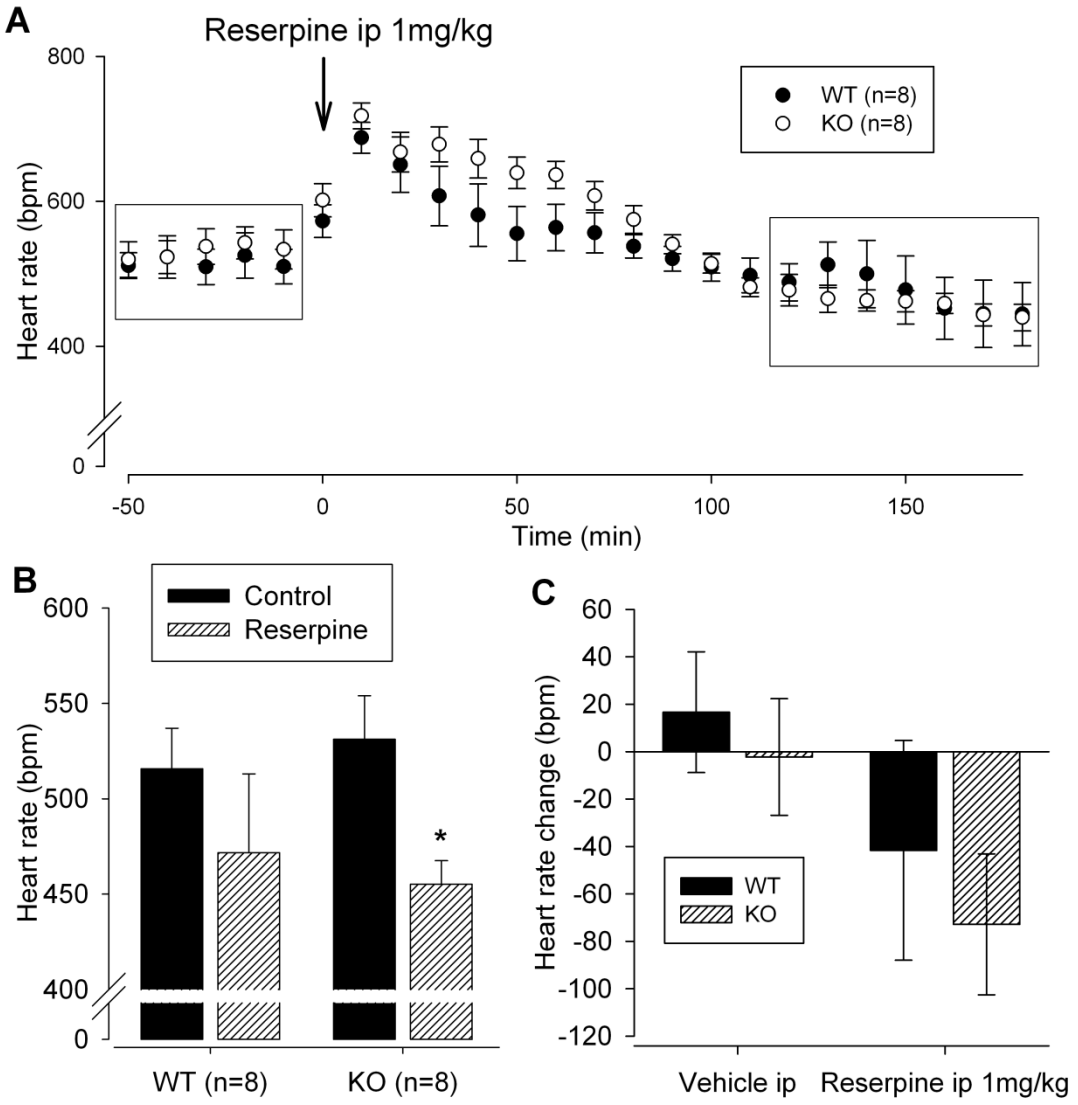

Figure 3.6. Heart rate responses to reserpine in conscious *Gnasxl* knockout mice.
Heart rate was recorded using ECG telemetry from conscious *Gnasxl* knockout mice and wildtype siblings. The sympatholytic reserpine was injected at 1 mg/kg ip.
(A) Heart rate response to reserpine over time.
(B) Knockouts had a significant decrease in heart rate in response to reserpine (*p≤0.05 by paired t-test, n=8), which was not seen in wildtypes.
(C) Heart rate responses to reserpine compared to vehicle responses in wildtype and knockouts.

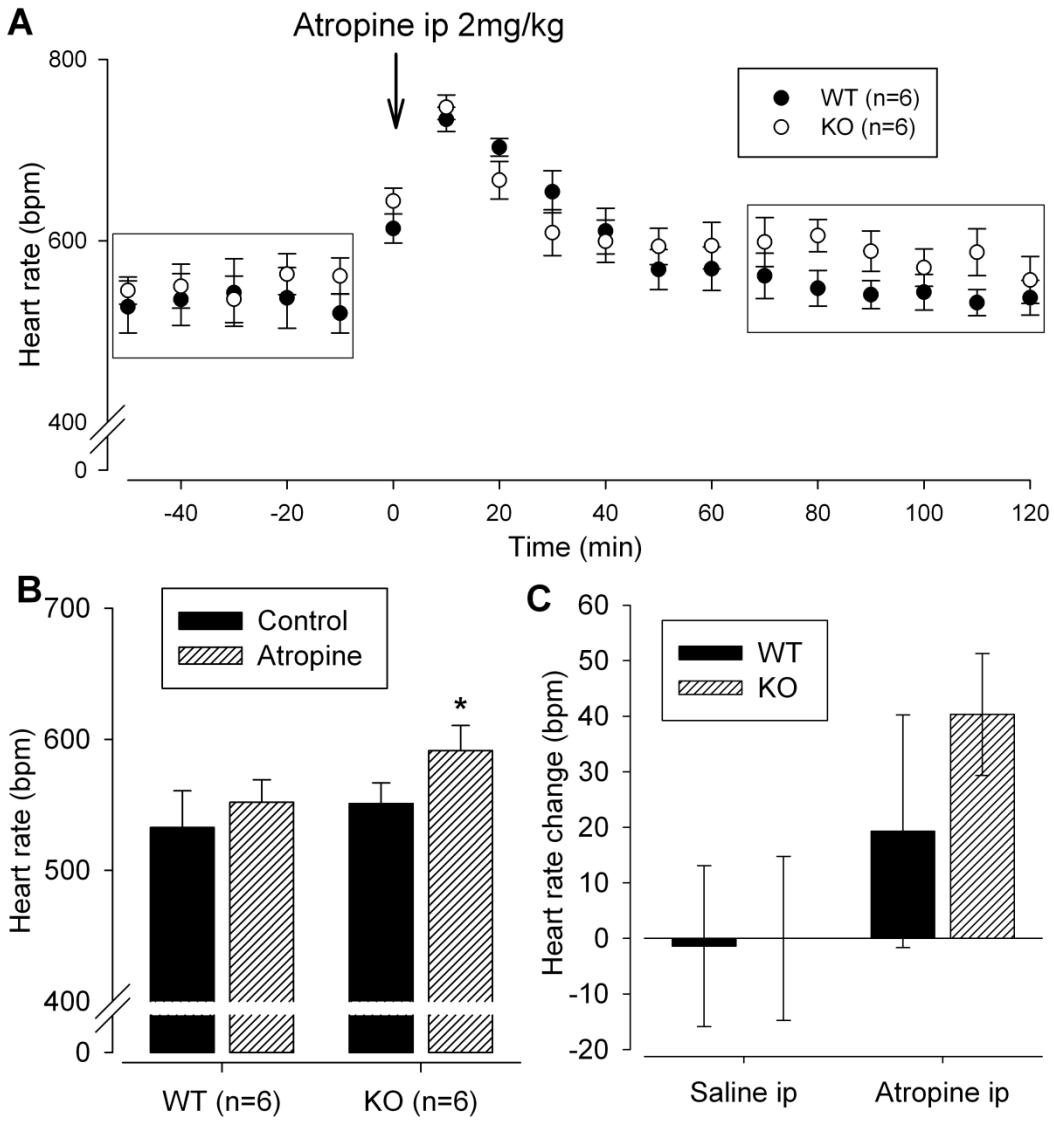

Figure 3.7. Heart rate responses to atropine in conscious *Gnasxl* knockout mice.

Heart rate was recorded using ECG telemetry from conscious *Gnasxl* knockout mice and wildtype siblings. The parasympatholytic atropine was injected at 2 mg/kg ip.

(A) Heart rate response to atropine over time.

(B) Knockouts had a significant increase in heart rate in response to atropine (*p≤0.05 by paired t-test, n=6).

(C) Heart rate responses of atropine compared to saline in wildtypes and knockouts.

3.3.3 Thermogenesis control in Gnasxl knockout mice

Gnasxl knockout mice have previously been shown to have elevated brown adipose tissue (BAT) expression of uncoupling protein 1 (UCP1), the BAT-specific uncoupling protein (Xie *et al.*, 2006). BAT expression levels of UCP1 increase in response to SNS stimulation of BAT (Cannon & Nedergaard, 2004), so this suggests first that *Gnasxl* knockouts have elevated SNS stimulation of the BAT, suggesting in turn that they have elevated thermogenesis, and therefore elevated core body temperature.

BAT signalling changes in *Gnasxl* knockouts were explored by Western blot to investigate phosphorylation changes to hormone sensitive lipase (HSL), which is known to control rates of lipolysis in response to SNS stimulation of BAT (Cannon & Nedergaard, 2004). Western blot for P-HSL compared to HSL is shown in Figure 3.8Ai. No significant changes were seen when the bands were quantified using pixel densitometry (Figure 3.8Aii; 1.2 ±0.7 vs 0.9 ±0.2 ratio P-HSL/HSL, WT vs KO n=2).

The physiological effects of the *Gnasxl* knockout on body temperature were also investigated. Body temperature was recorded following loss of consciousness precisely 3 minutes after injection of urethane-chloralose anaesthesia. Knockouts were found to have significantly elevated body temperature compared to dose-matched sibling wildtypes (Figure 3.8B; 38.1 ±0.3 vs 36.9 ±0.4 °C, KO vs WT, $p \leq 0.05$ by paired t-test, n=7).

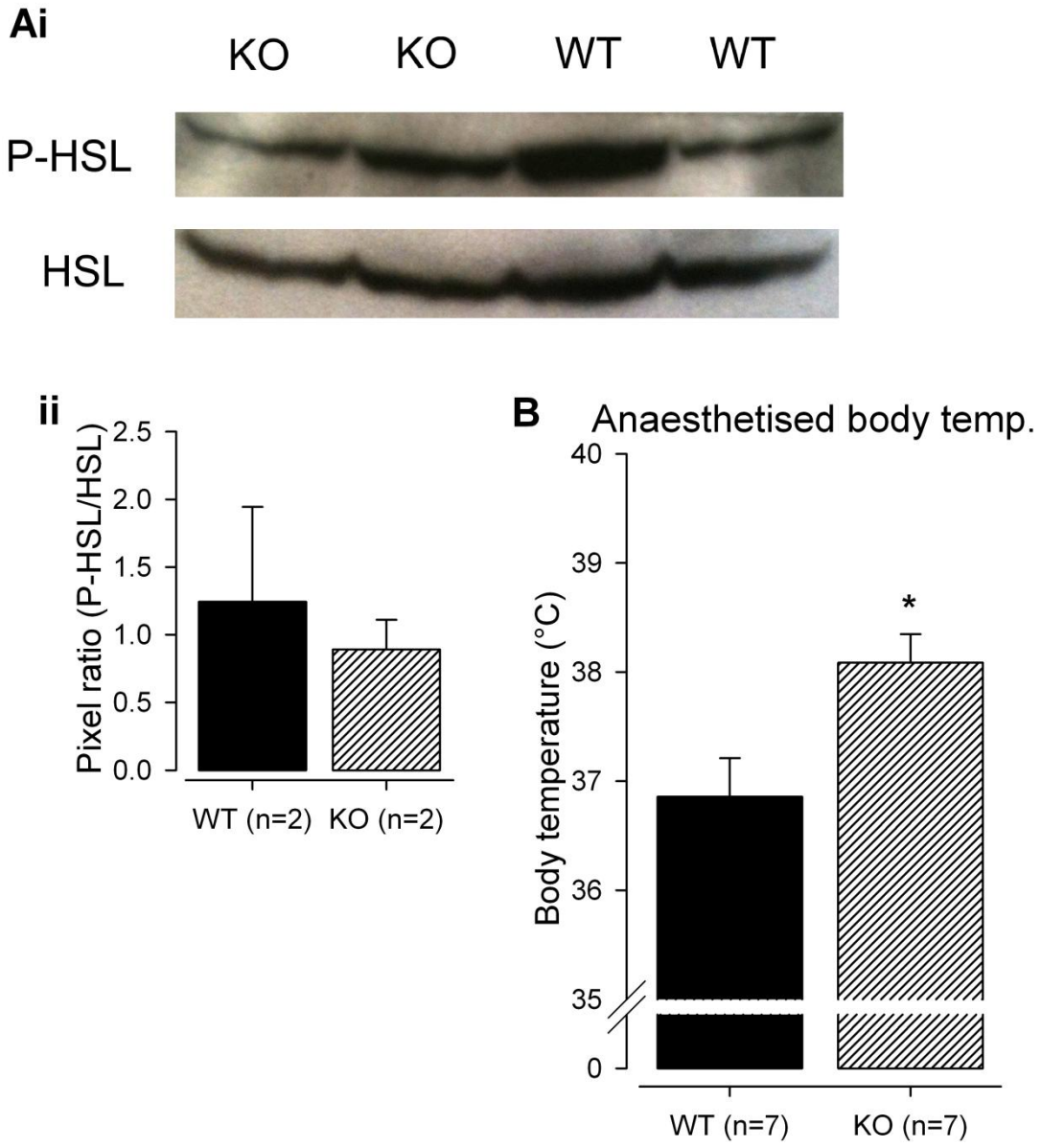

Figure 3.8. Physiological control of thermogenesis in *Gnasxl* knockout mice.
(A) Hormone-sensitive lipase phosphorylation levels in brown adipose tissue of *Gnasxl* knockouts and wildtype siblings were investigated by western blot (i). Phosphorylation levels, quantified using ImageJ (ii), were unchanged in *Gnasxl* knockouts compared to wildtype siblings (n=2).
(B) Body temperature was significantly elevated in urethane-chloralose anaesthetised *Gnasxl* knockouts compared to dose-matched wildtype siblings (*p≤0.05 by paired t-test, n=7).

3.4 Discussion

Xie *et al.* showed that mice lacking XLαs have a hypermetabolic phenotype caused by elevated SNS stimulation of the brown and white adipose tissues (Xie *et al.*, 2006). They postulated that the elevated SNS activity might be a global effect (Xie *et al.*, 2006), which would affect other tissues such as the cardiovascular system. This hypothesis is supported by the restricted expression pattern of XLαs in the brain, which includes a number of regions crucial for control of the SNS (Krechowec *et al.*, 2012). The aim of this chapter was to investigate this hypothesis in detail, focussing on autonomic control of the cardiovascular system in adult *Gnasxl* knockout mice.

Firstly blood pressure was recorded in adult *Gnasxl* knockout mice to provide an indication of overall cardiovascular stimulation. Non-invasive tail plethysmography system was first trialled in conscious mice, and while wildtype mice gave clear readings, *Gnasxl* knockouts did not (data not shown). There are a number of potential causes for this: perhaps the knockouts had poor blood circulation to the tail, or maybe they didn't respond in the same way as the wildtype mice to being housed at 30 °C for taking measurements, or maybe they responded differently to the stressful environment of being restrained.

As with the Schlager mice (Davern *et al.*, 2010), it is likely that the *Gnasxl* knockout mice might have an elevated stress response. Due to these problems with measuring cardiovascular parameters in conscious mice by non-invasive plethysmography, cannulation was used in anaesthetised mice.

Arterial cannulation was used to record arterial pressure in real time, providing basal blood pressure and heart rate data, as well as blood pressure responses to reserpine. Following a pilot cannulation experiment, it was found that the anaesthetic was having a substantial effect on the cardiovascular system (data not shown). Therefore, the anaesthetic was modified to include α-chloralose so as to reduce the concentration of urethane required for full anaesthesia (Dalkara *et al.*, 1995; Kass *et al.*, 1998). Additionally the mice were strictly dose-matched by anaesthetic between sibling groups, to balance any potential detrimental effects to the cardiovascular system.

Under these conditions, knockouts were found to have elevated blood pressure (Figure 3.2A), as well as a greater response to the sympatholytic reserpine (Figure 3.3D). No difference was seen in basal heart rate (Figure 3.2B) or in the heart rate response to reserpine (data not shown).

The increased basal blood pressure in *Gnasxl* knockouts suggests the mice have elevated cardiovascular stimulation, and the inhibition of peripheral sympathetic nerve activity by reserpine indicates this is caused by elevated SNS stimulation of the heart and vasculature. The principle behind this experiment is similar to that used by Davern *et al.* to investigate SNS control of the cardiovascular system in Schlager hypertensive mice, where the ganglionic blocker pentolinium was used to inhibit SNS activity (Davern *et al.*, 2009).

However, rather than pentolinium which blocks both SNS and PNS ganglia, reserpine was used because it inhibits specifically outflow from sympathetic

nerves. Davern *et al.* found that the elevated blood pressure in Schlager hypertensive mice was abolished after ganglionic blockade, after which the hypertensive mice had comparable blood pressure to wildtypes. A similar result was seen here, where the elevated blood pressure in the *Gnasxl* knockouts was counteracted by reserpine, quantified as a significantly greater blood pressure response. However, the Schlager study was performed on conscious mice, avoiding the potentially detrimental effects of anaesthesia on cardiovascular parameters.

Using ECG telemetry in conscious freely moving mice, adult male *Gnasxl* knockout mice were found to have elevated resting heart rate at night (Figure 3.5B). It is interesting to note that at certain time points during the day *Gnasxl* knockouts appear to have elevated blood pressure, but it is consistently higher at night, suggesting this is the time that the biggest phenotypic effects occur. This might be expected in a model of elevated SNS activity, as the sympathetic activity increases at night.

Reserpine and atropine were used to investigate the relative contributions of the opposing branches of the autonomic nervous system to the elevated heart rate. As with the anaesthetised mice, conscious mice were found to have a greater response to reserpine, which caused a significant decrease in heart rate in knockouts but not in wildtypes (Figure 3.6B).

Interestingly, the knockouts were also found to have a greater response to atropine, which caused a significant increase in heart rate in knockouts but not in wildtypes (Figure 3.7B). This suggests that the knockout mice

paradoxically have elevated tonic stimulation of the cardiovascular system by both the SNS and PNS.

However, these results do not necessarily mean that the mice have elevated sympathetic and parasympathetic nerve activity, as the effects might have a peripheral cause, for example varying levels of peripheral receptor expression (Young & Davisson, 2011). Therefore, this will be investigated further in the next chapter by analysis of heart rate variability in *Gnasxl* knockouts, as an indirect marker of sympathetic and parasympathetic nervous system stimulation of the cardiovascular system.

Although it has been mentioned that XLαs likely affects central SNS control by its expression in such regions as the PVN and DMH, it is also possible that XLαs has a direct effect on the PNS, as it is also expressed in brain regions crucial for PNS control, including the NTS and the nucleus ambiguus (Krechowec *et al.*, 2012).

Gnasxl knockout mice have previously been shown to exhibit markers of elevated metabolism, in particular elevated BAT lipolysis (Xie *et al.*, 2006), but the physiological effects have never been documented. Loss of XLαs had no significant effects on hormone-sensitive lipase (HSL) phosphorylation in BAT (Figure 3.8A), which is a marker of the degree of SNS-mediated lipolysis (Egan *et al.*, 1992; Cannon & Nedergaard, 2004).

However, *Gnasxl* knockouts were found to have elevated core body temperature (Figure 3.8B). The elevated body temperature fits with the concept of *Gnasxl* knockouts having elevated SNS stimulation of the BAT causing increased thermogenesis, resulting in the lean phenotype. It is

possible that the very low levels of HSL phosphorylation resulted in inaccurate quantification; very high levels of protein had to be loaded onto the gel in order to have a signal produced (ie. 100 µg of protein, compared to the usual 20-40 µg).

In summary, the phenotype of *Gnasxl* knockout mice is shown here to include elevated blood pressure, heart rate and body temperature, which would suggest a systemic change to cause such consistent effects. Furthermore, the changes to the cardiovascular system appear likely to be caused by elevated SNS stimulation, although possible changes to the PNS remain less clear.

The data support the hypothesis first described by Xie *et al.* (Xie *et al.*, 2006) that *Gnasxl* knockout mice have a systemic increase in SNS activity that is responsible for the metabolic phenotype previously described, as well as the cardiovascular phenotype described here. This implies that XLαs functions in the CNS to inhibit SNS outflow, resulting in elevated SNS activity when XLαs is knocked out. In the next chapter, autonomic control of the cardiovascular system in *Gnasxl* knockouts will be investigated in more detail by HRV analysis in conscious mice.

4 Autonomic control of heart rate variability in mice lacking XLαs

4.1 Introduction

In the previous chapter it was shown that mice lacking the signalling protein XLαs have elevated blood pressure and heart rate, with the likely explanation that this is caused by increased sympathetic nervous system (SNS) stimulation of the cardiovascular system. The aim of this chapter is to investigate this further using heart rate variability (HRV) analysis, as an indirect measure of the degree of autonomic stimulation of the cardiovascular system by the SNS and parasympathetic nervous system (PNS).

4.1.1 CNS control of the cardiovascular system

Heart rate and blood pressure are tightly controlled by the CNS, as well as other hormonal and peripheral factors (Figure 4.1) (Malliani *et al.*, 1991; Parati *et al.*, 1995; Parati *et al.*, 2006). Of particular importance is the balance between the sympathetic and parasympathetic branches of the autonomic nervous system.

Factors controlling the cardiovascular system cause variations in blood pressure and heart rate, which are known to occur at characteristic frequencies (Akselrod *et al.*, 1981). For example, it is known that cardiovascular control by the PNS occurs at high frequencies, and the SNS dominates lower frequency oscillations. However, the exact origin of the

slower oscillations remain unclear. Firstly is the central oscillator theory, which postulates that the sympathetic rhythms are generated by brain stem circuits. Secondly is the baroreflex theory, which suggests that the delay in feedback of the baroreflex loop results in oscillations to sympathetic and parasympathetic control of the cardiovascular system (Papaioannou, 2007).

In humans, HRV has been extensively analysed, and the methods for evaluating HRV have been standardised (Camm *et al.*, 1996). In fact, HRV is used as a diagnostic tool in investigations into cardiovascular disease, for example for diagnosing autonomic neuropathy (Ewing *et al.*, 1985), or for detecting changes to HRV which occur before a cardiac event, for example predicting ventricular tachycardia in patients with coronary heart disease (Huikuri *et al.*, 1993).

4.1.2 HRV analysis

Investigations into autonomic control in mice using HRV analysis are common due to the widespread use of transgenic and genetically modified mice (Uechi *et al.*, 1998; Ecker *et al.*, 2006; Senador *et al.*, 2009; Griffioen *et al.*, 2011). However, in mice, and other laboratory animals, HRV parameters have not been thoroughly standardised, although some efforts have been made in that direction (Gehrmann *et al.*, 2000; Thireau *et al.*, 2008).

The use of HRV analysis to quantify autonomic activity is a controversial topic (Goldstein *et al.*, 2011), but a number of reports show that HRV can give an accurate indication of autonomic activity (Farah *et al.*, 2006; Baudrie *et al.*, 2007; Laude *et al.*, 2008). The main benefit of HRV analysis is that it is non-invasive, and therefore can be used in conscious freely moving animals,

and it doesn't require culling of the animal, and therefore can be used to give responses to drugs or other interventions (Young & Davisson, 2011).

4.1.3 Aims

A number of different HRV analyses will be explored in this study, including standard time-domain analyses and power spectral analysis using fast Fourier transforms (FFTs). However, due to the inconsistencies in the HRV analyses reported in the literature, these methods will first be empirically verified using reserpine and atropine to inhibit cardiovascular regulation by the SNS and PNS, respectively. Once validated, HRV will be used to investigate in detail the control of autonomic stimulation of the cardiovascular system in *Gnasxl* knockout mice, with a high degree of confidence.

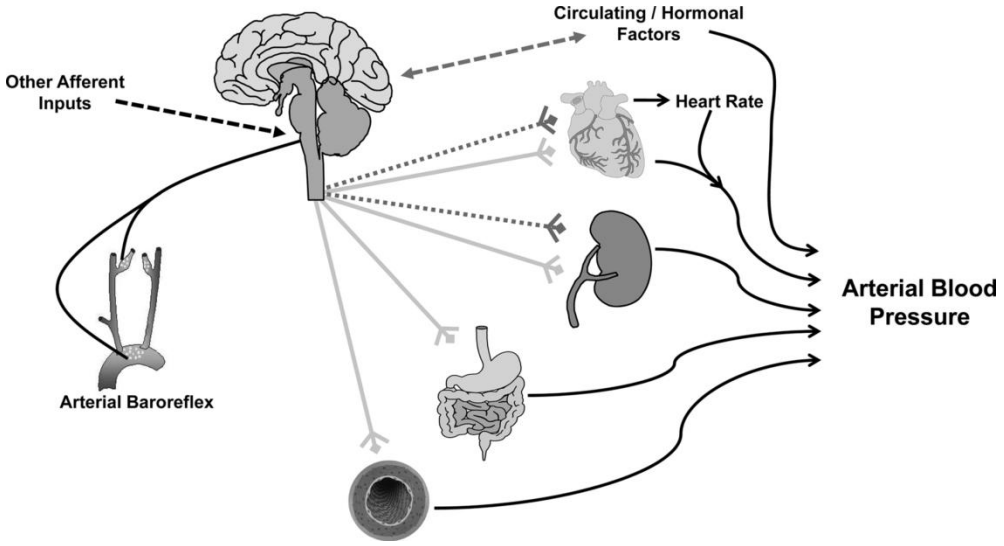

Figure 4.1. The complexities of cardiovascular control by the CNS.
Blood pressure control is mediated by a number of systems, including the heart, kidneys and vasculature. CNS control is exerted by the autonomic nervous system, including the sympathetic (light grey) and parasympathetic (dark grey dashed) nervous systems, as well as hormonal control, for example vasoactive substances released from the pituitary. The CNS is controlled by a number of inputs, including the baroreflex. Taken from (Young & Davisson, 2011).

4.2 Methods

Adult male *Gnasxl* knockout mice and wildtype siblings were implanted with electrocardiogram (ECG) telemeters. ECG was recorded at high frequency (5 kHz) and heart beats were annotated to within 0.2 ms accuracy. HRV analysis was performed using Kubios HRV program (Niskanen *et al.*, 2004), except for Lomb spectra, which were produced using the Lomb application from the Physionet suite of HRV programs (Goldberger *et al.*, 2000). For further details see chapter 2.

4.3 Results

4.3.1 Validating methods of HRV analysis

A number of methods for analysing HRV were tested by injection of reserpine and atropine, to investigate control by the sympathetic and parasympathetic nervous systems, respectively.

4.3.1.1 Time domain HRV analyses

The most straightforward methods for analysing HRV are so-called time domain measures, including the standard deviation of normal RR intervals (SDNN) and the root mean square of successive differences (RMSSD) (Camm *et al.*, 1996). SDNN is simply the overall standard deviation of heart beat intervals over a time period, and gives a crude estimate of long-term changes to the heart rate, ie. giving information about SNS control. RMSSD quantifies the degree of beat-to-beat variation in a heart rate series,

providing information of short-term changes to the heart rate, ie. about the PNS.

A typical resting RR interval series is shown in Figure 4.2Ai, with the associated SDNN and RMSSD values. Following reserpine injection and loss of SNS input to the cardiovascular system (Figure 4.2Aii), SDNN drops but the RMSSD remains high. On the other hand, following atropine injection and loss of PNS input (Figure 4.2Aiii), SDNN remains high and RMSSD drops.

These responses were quantified for a sample of wildtype mice, showing a significant decrease in SDNN (Figure 4.2B; 5.8 ±0.1 to 4.0 ±0.7 ms; $p \leq 0.05$ by paired t-test, n=8), but not RMSSD (Figure 4.2B; 3.5 ±0.4 to 3.0 ±0.4 ms; n=8) after reserpine injection. After atropine injection, there was a significant decrease in RMSSD (Figure 4.2C; 2.8 ±0.3 to 1.6 ±0.4 ms; $p \leq 0.05$ by paired t-test, n=6), with no significant change to SDNN (Figure 4.2C; 4.9 ±0.5 to 3.6 ±0.2 ms; n=6).

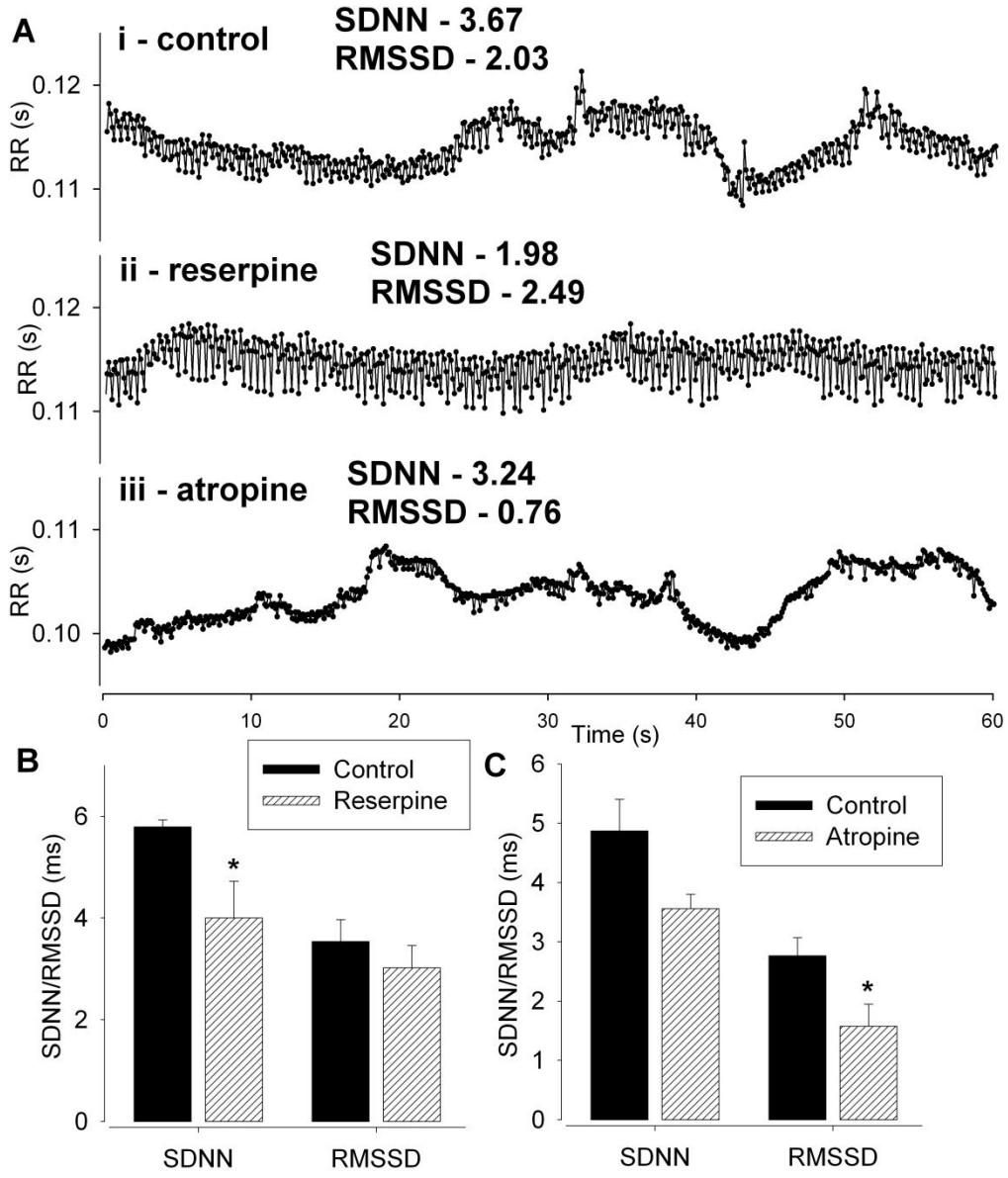

Figure 4.2. Time domain HRV analysis.
Heart rate was recorded from conscious CD1 wildtype mice at high resolution (within 0.2 ms). HRV analysis using the time domain measures standard deviation of normal RR intervals (SDNN) and root mean square of successive differences (RMSSD) were validated by injection of reserpine ip at 1 mg/kg to inhibit SNS activity and injection of atropine ip at 2 mg/kg to inhibit PNS activity. SDNN and RMSSD were calculated from 3-minute sections of clean and stable heart rate; the units of both are in ms.
(A) Typical RR interval series over 60s in control conditions (i), after reserpine injection (ii) and after atropine injection (iii). SDNN and RMSSD values for those time series are shown; note the reduction in SDNN after reserpine and the reduction in RMSSD after atropine.
(B) SDNN was significantly reduced after reserpine injection (*p≤0.05 by paired t-test, n=8).
(C) RMSSD was significantly reduced after atropine injection (*p≤0.05 by paired t-test, n=6).

4.3.1.2 Nonlinear HRV analysis

Nonlinear HRV parameters can provide more in depth detail into heart rate control. In this study, the nonlinear HRV parameter investigated was Poincaré analysis, in which an RR interval series is plotted on a scatter plot, with each interval plotted on the x-axis against the following interval on the y-axis (Figure 4.3Ai for a typical example in a wildtype mouse). This plot shows a distribution of the beat-to-beat variation in heart rate, and can provide information about long- and short-term HRV effects depending upon the distribution of the data. This is quantified by calculation of the standard deviation at 45° angles of the axes (see Figure 4.3Ai).

SD1 quantifies beat-to-beat variation, and is therefore a marker of short-term PNS activity. SD2 quantifies overall variation throughout the RR series, and is therefore indicative of long-term SNS activity. Accordingly, reserpine injection causes a reduction in SD2 (Figure 4.3Aii for typical example), whereas atropine injection causes a reduction in SD1 (Figure 4.3Aiii for typical example).

These responses were quantified for a sample of wildtype mice, showing a significant decrease in SD2 (Figure 4.3B; 7.7 ±0.2 to 5.2 ±1.0 ms; $p \leq 0.05$ by paired t-test, n=8), but not SD1 (Figure 4.3B; 2.5 ±0.3 to 2.1 ±0.4 ms; n=8) after reserpine injection. After atropine injection, there was a significant decrease in SD1 (Figure 4.3C; 2.0 ±0.2 to 1.1 ±0.3 ms; $p \leq 0.05$ by paired t-test, n=6), with no significant change to SD2 (Figure 4.3C; 6.5 ±0.8 to 4.9 ±0.3 ms; n=6).

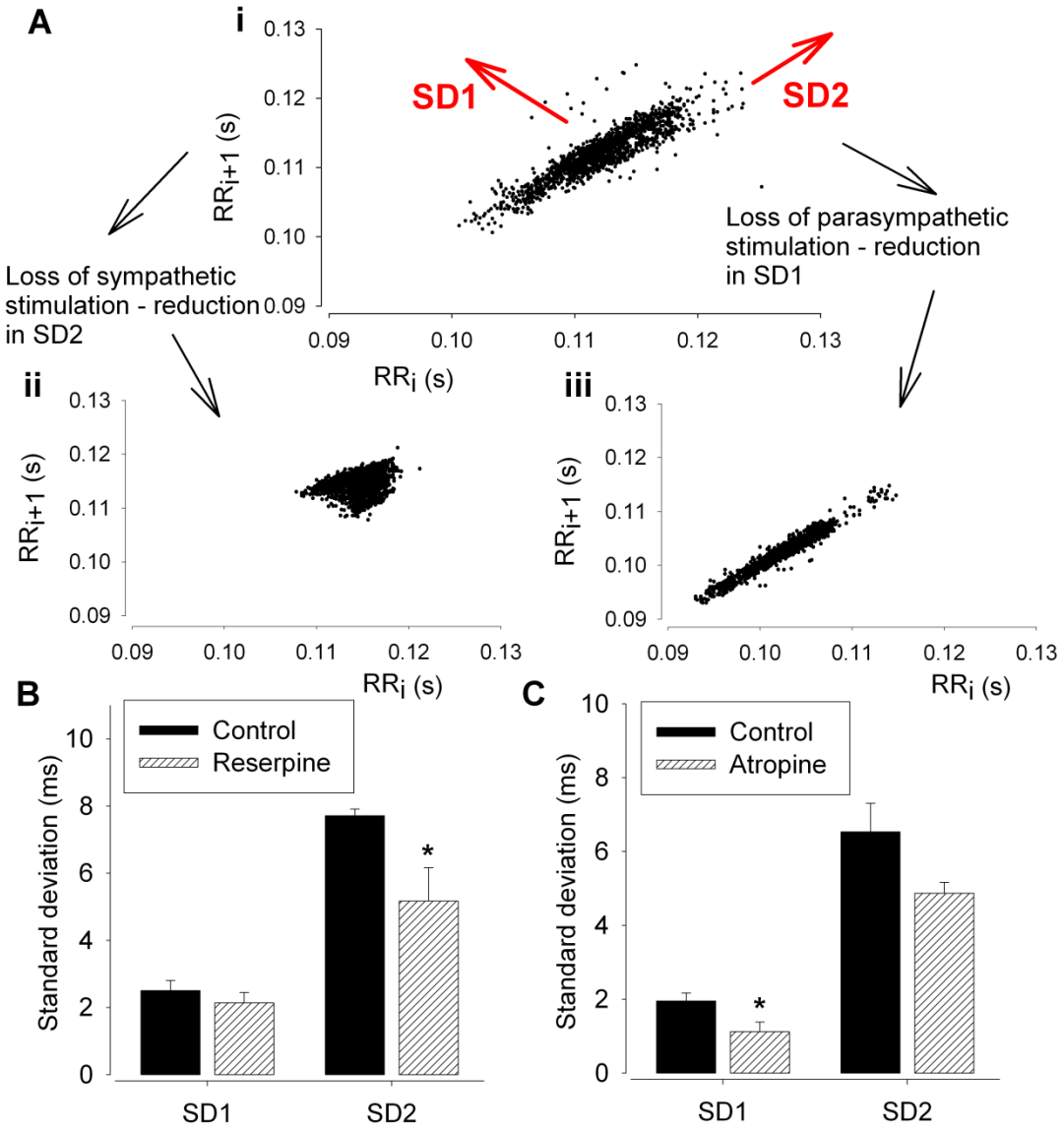

Figure 4.3. Nonlinear HRV analysis using Poincaré plots.
Heart rate was recorded from conscious CD1 wildtype mice at high resolution (within 0.2 ms). HRV analysis using nonlinear Poincaré analysis was validated by injection of reserpine ip at 1 mg/kg to inhibit SNS activity and injection of atropine ip at 2 mg/kg to inhibit PNS activity. Poincaré plots were produced by plotting each RR interval on the x-axis against the successive RR interval on the y-axis. The standard deviation was calculated at 45° angles of the axes to give the values SD1 and SD2, from 3-minute sections of clean and stable heart rate.
(A) Typical Poincaré plots in adult CD1 mice under control conditions (i), after reserpine injection (ii) and after atropine injection (iii). Note the reduction of SD2 after reserpine and the reduction in SD1 after atropine.
(B) SD2 was significantly reduced after reserpine injection (*p≤0.05 by paired t-test, n=8).
(C) SD1 was significantly reduced after atropine injection (*p≤0.05 by paired t-test, n=6).

4.3.1.3 Frequency domain HRV analyses

There is arguably far more information to be gained about heart rate control by HRV analysis in the frequency domain. This involves producing power spectra, which graphically represent the degree of variability across a range of frequencies. A number of methods can be used, including fast Fourier transforms (FFTs), autoregressive spectra and Lomb transforms.

Pilot investigations showed Kubios HRV program to be the most intuitive and user friendly method, as well as providing a visual interface that facilitated analysis (Niskanen *et al.*, 2004), and was therefore used for HRV analysis by FFT and autoregressive spectra. In each case the heart rate trace was visually inspected for 3-minute sections of clean and stable heart rate.

Heart rate was resampled at 20Hz; FFTs were performed using Welch's periodogram with 32-second windows with 50 % overlap, and autoregressive spectra were produced using a 32-order model. Lomb power spectra were produced from raw non-resampled heart rate data using Physionet (Goldberger *et al.*, 2000).

Power spectral analysis has the added complication that the frequencies of heart rate variability that correspond to sympathetic and parasympathetic activity in the mouse are inconsistent in the literature. Therefore, as part of this investigation, the frequencies associated with the SNS and PNS were empirically determined by injection of reserpine and atropine, respectively.

The high frequency (HF) domain is reported to reflect only PNS stimulation; this region is commonly reported to extend from around 1.5 Hz up to 5.0 Hz

(Thireau *et al.*, 2008), with the condition that the breathing peak be included. In this study, the breathing peak was occasionally found to lie as low as 1.2 Hz, so the lower boundary for the HF band was set to 1.0 Hz in order to guarantee inclusion of the breathing peak.

The low frequency (LF) domain is reported to reflect both SNS and PNS stimulation; the lower boundary can be between 0.15 and 0.4 Hz, and the upper boundary will generally correspond to the lower boundary of the HF region (Thireau *et al.*, 2008). Recently, a thorough investigation by Baudrie *et al.* into the optimal LF frequency bandings in mice gave a range of 0.15 – 0.60 Hz (Baudrie *et al.*, 2007).

In agreement with this LF range, it was found in this study that virtually all power spectral density was lost in the LF region down to 0.15 Hz following reserpine injection (see for example Figure 4.4Aii); therefore this was chosen as the lower cut-off. The chosen bandings were therefore: LF 0.15 – 1.0 Hz, HF 1.0 – 5.0 Hz, and these were used for validating HRV analysis by FFT, autoregressive and Lomb power spectra. Similar results were found for each of these methods, as detailed below.

Typical FFT power spectra are shown under resting conditions (Figure 4.4Ai), after reserpine injection showing loss of LF power (Figure 4.4Aii), and after atropine injection showing loss of both LF and HF power (Figure 4.4Aiii).

These responses were quantified for a sample of wildtype mice, showing that after reserpine injection both LF power (Figure 4.4B; 4.3 ±0.9 to 1.2 ±0.4 ms^2/Hz; $p \leq 0.05$ by paired t-test, n=8) and LF/HF ratio (Figure 4.4B; 1.2 ±0.3

to 0.5 ±0.1; p≤0.05 by paired t-test, n=8) were significantly reduced with no change to HF power (Figure 4.4B; 4.5 ±0.9 to 3.5 ±0.9 ms^2/Hz; n=8). Following atropine injection, both LF power (Figure 4.4C; 2.8 ±0.5 to 0.7 ±0.3 ms^2/Hz; p≤0.05 by paired t-test, n=6) and HF power (Figure 4.4C; 3.0 ±0.6 to 1.2 ±0.5 ms^2/Hz; p≤0.05 by paired t-test, n=6) were significantly reduced, with no change to LF/HF ratio (Figure 4.4C; 1.5 ±0.2 to 1.1 ±0.3; n=6).

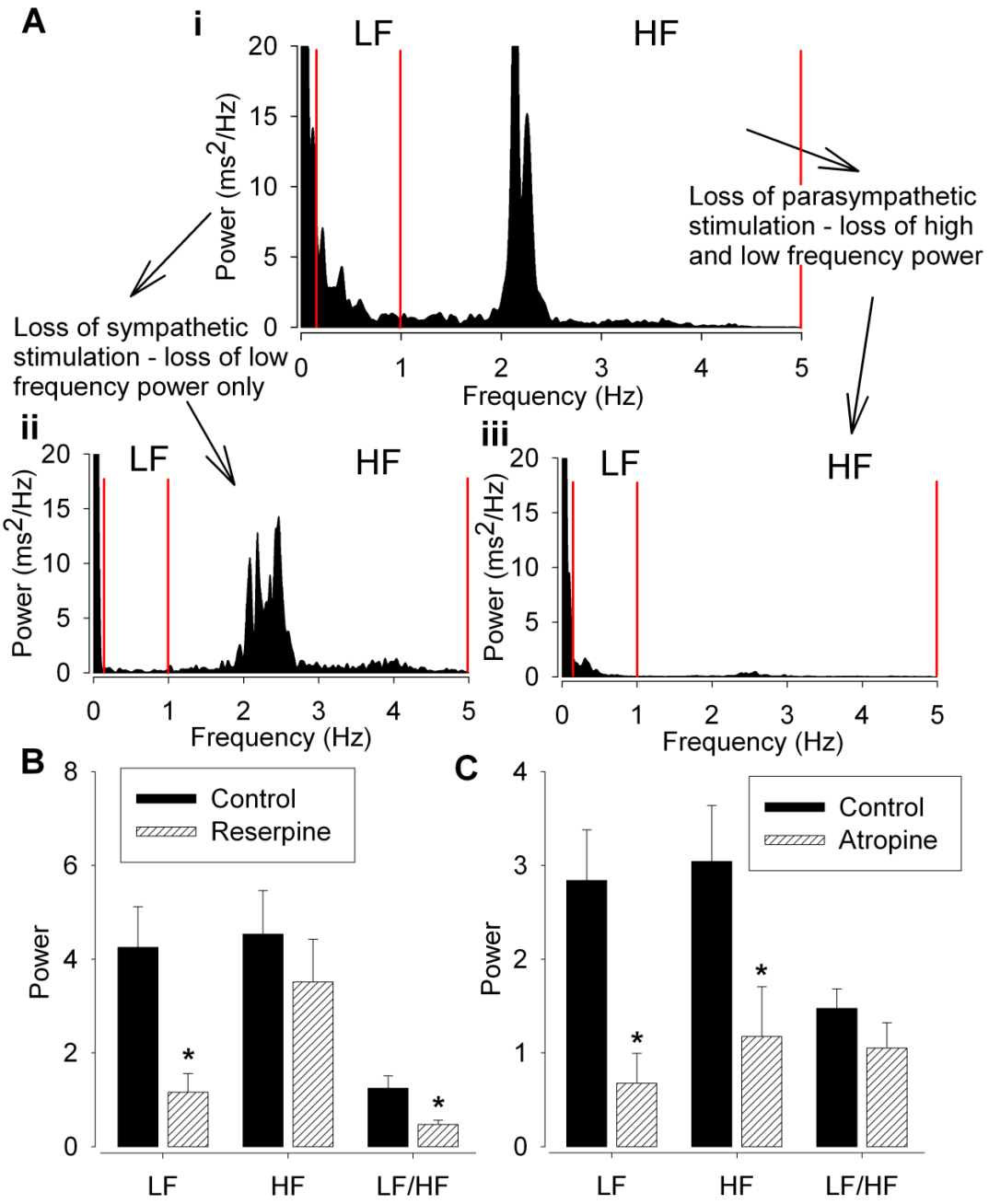

Figure 4.4. Frequency domain HRV analysis by fast Fourier transform. Heart rate was recorded from conscious CD1 wildtype. Frequency domain HRV analysis using fast Fourier transform (FFT) was validated by injection of reserpine ip at 1 mg/kg to inhibit SNS activity and injection of atropine ip at 2 mg/kg to inhibit PNS activity. FFT spectra were produced from 3-minute sections of clean and stable heart rate resampled at 20 Hz using Welch's algorithm with 32-second windows with 50 % overlap.
(A) Typical FFT spectra under control conditions (i), after reserpine injection (ii) and after atropine injection (iii). Note the breathing peak at ~2.2 Hz in the high frequency (HF) region and the total loss of power spectral density in the low frequency (LF) region down to 0.15 Hz.
(B) LF power and LF/HF ratio were significantly reduced after reserpine injection (*p≤0.05 by paired t-test).
(C) LF and HF power were significantly reduced after atropine injection (*p≤0.05 by paired t-test).

Typical autoregressive spectra are shown under resting conditions (Figure 4.5Ai), after reserpine injection showing loss of LF power (Figure 4.5Aii), and after atropine injection showing loss of LF and HF power (Figure 4.5Aiii).

These responses were quantified for a sample of wildtype mice, showing that after reserpine injection both LF power (Figure 4.5B; 4.1 ±0.8 to 1.1 ±0.3 ms^2/Hz; $p \leq 0.05$ by paired t-test, n=8) and LF/HF ratio (Figure 4.5B; 1.3 ±0.3 to 0.5 ±0.1; $p \leq 0.05$ by paired t-test, n=8) were significantly reduced with no change to HF power (Figure 4.5B; 4.5 ±0.9 to 3.5 ±0.9 ms^2/Hz; n=8). Following atropine injection, both LF power (Figure 4.5C; 2.7 ±0.5 to 0.6 ±0.3 ms^2/Hz; $p \leq 0.05$ by paired t-test, n=6) and HF power (Figure 4.5C; 3.0 ±0.6 to 1.2 ±0.5 ms^2/Hz; $p \leq 0.05$ by paired t-test, n=6) were significantly reduced, with no change to LF/HF ratio (Figure 4.5C; 1.4 ±0.2 to 0.9 ±0.2; n=6).

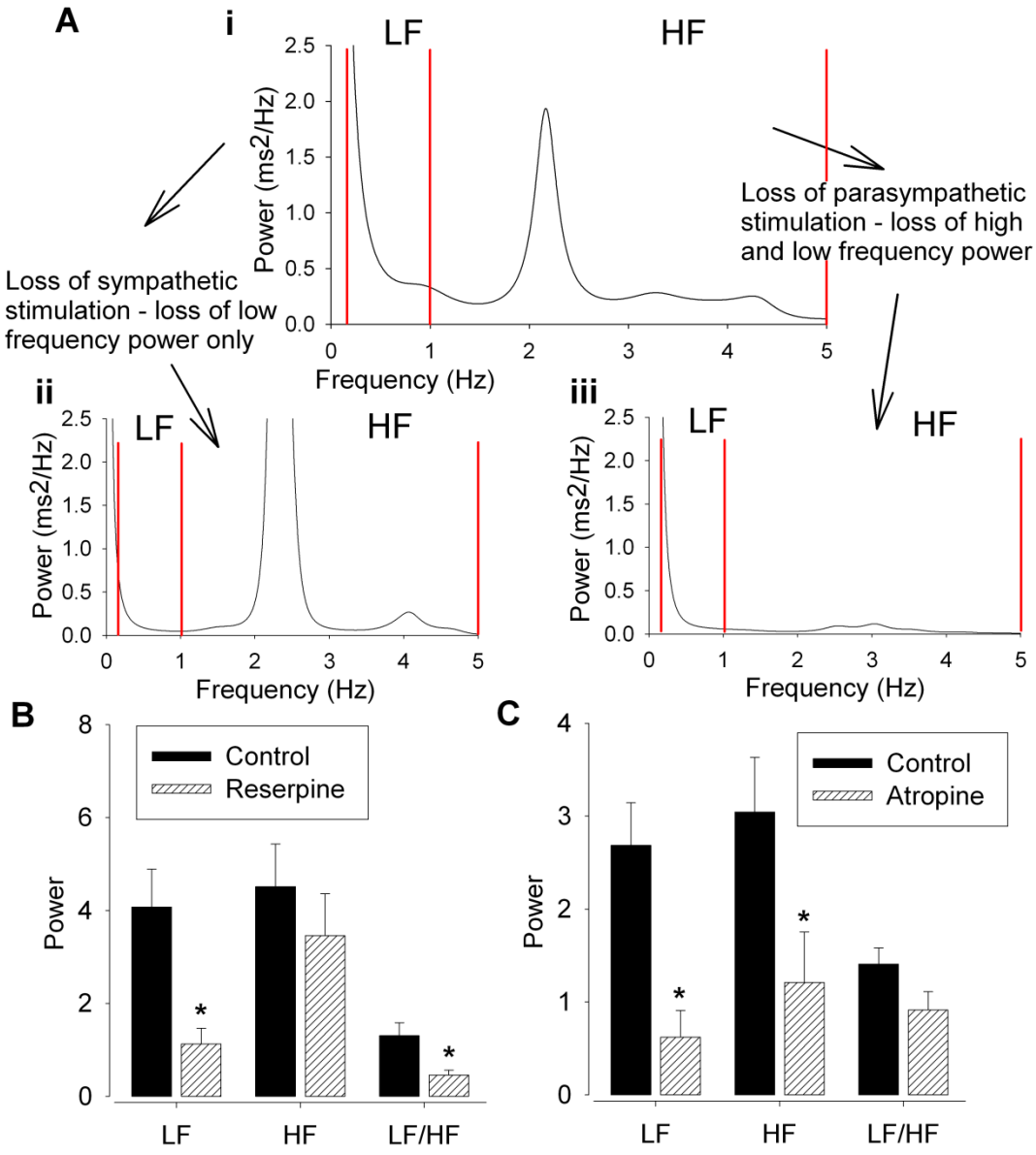

Figure 4.5. Frequency domain HRV analysis using autoregressive power spectra.

Heart rate was recorded from conscious CD1 wildtype mice at high resolution (within 0.2 ms). Frequency domain HRV analysis using autoregressive spectra was validated by injection of reserpine ip at 1 mg/kg to inhibit SNS activity and injection of atropine ip at 2 mg/kg to inhibit PNS activity. Autoregressive spectra were produced from 3-minute sections of clean and stable heart rate resampled at 20 Hz using a 32-order model.

(A) Typical autoregressive spectra under control conditions (i), after reserpine injection (ii) and after atropine injection (iii). Note the breathing peak at ~2.2 Hz in the high frequency (HF) region and the almost complete loss of power spectral density in the low frequency (LF) region down to 0.15 Hz.

(B) LF power and LF/HF ratio were significantly reduced after reserpine injection (*p≤0.05 by paired t-test).

(C) LF and HF power were significantly reduced after atropine injection (*p≤0.05 by paired t-test).

Typical Lomb power spectra are shown under resting conditions (Figure 4.6Ai), after reserpine injection showing loss of LF power (Figure 4.6Aii), and after atropine injection showing loss of LF and HF power (Figure 4.6Aiii).

These responses were quantified for a sample of wildtype mice, showing that after reserpine injection both LF power (Figure 4.6B; 4.5 ±0.9 to 1.2 ±0.4 ms^2/Hz *10^6; p≤0.05 by paired t-test, n=8) and LF/HF ratio (Figure 4.6B; 1.2 ±0.3 to 0.4 ±0.1; p≤0.05 by paired t-test, n=8) were significantly reduced with no change to HF power (Figure 4.6B; 5.3 ±1.0 to 4.3 ±1.1 ms^2/Hz *10^6; n=8). Following atropine injection, both LF power (Figure 4.6C; 2.5 ±0.7 to 0.6 ±0.3 ms^2/Hz *10^6; p≤0.05 by paired t-test, n=6) and HF power (Figure 4.6C; 3.0 ±0.8 to 1.3 ±0.6 ms^2/Hz *10^6; n=6) were significantly reduced, with no change to LF/HF ratio (Figure 4.6C; 1.0 ±0.2 to 0.7 ±0.2; n=6).

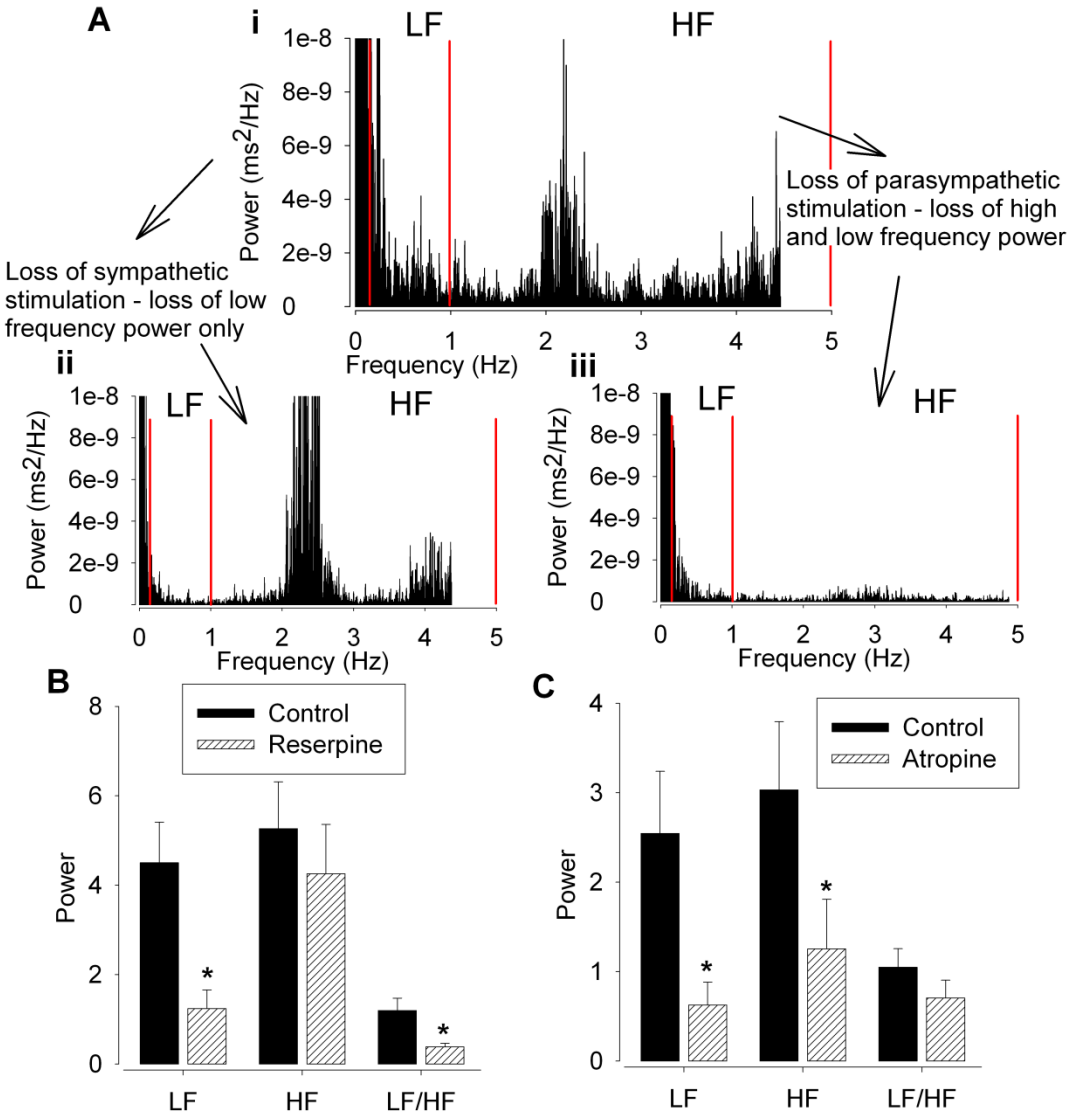

Figure 4.6. Frequency domain HRV analysis using Lomb power spectra.
Heart rate was recorded from conscious CD1 wildtype mice at high resolution (within 0.2 ms). Frequency domain HRV analysis using Lomb power spectra was validated by injection of reserpine ip at 1 mg/kg to inhibit SNS activity and injection of atropine ip at 2 mg/kg to inhibit PNS activity. Lomb spectra were produced from 3-minute sections of clean and stable heart rate using the Lomb periodogram, using native (ie. non-resampled) heart rate.
(A) Typical Lomb spectra under control conditions (i), after reserpine injection (ii) and after atropine injection (iii). Note the breathing peak at ~2.2 Hz in the high frequency (HF) region and the almost complete loss of power spectral density in the low frequency (LF) region down to 0.15 Hz.
(B) LF power and LF/HF ratio were significantly reduced after reserpine injection (*p≤0.05 by paired t-test).
(C) LF and HF power were significantly reduced after atropine injection (*p≤0.05 by paired t-test).
LF and HF powers in (B) and (C) are shown as ms^2/Hz *10^6.

The HRV changes calculated here by power spectral analysis fit previously reported HRV analyses in mice, where HF power is indicative of parasympathetic stimulation of the cardiovascular system, and LF/HF ratio is indicative of sympathovagal balance (Young & Davisson, 2011). These parameters were therefore considered valid for use in HRV analysis in *Gnasxl* knockout mice.

However, the remainder of this chapter uses FFT's to further analyse HRV control in *Gnasxl* knockout mice, because these are most commonly used in the literature, they are much easier to produce than Lombs, and they were more reliable than autoregressive spectra (LF/HF decreased a lot after atropine using autoregressive spectra, p=0.085).

4.3.2 HRV control in conscious Gnasxl knockout mice

Heart rate variability (HRV) was investigated in conscious *Gnasxl* knockout mice using fast Fourier transforms (FFTs), which were fully validated for analysis of parasympathetic activity and sympathovagal balance. HF power was used as an indicator of PNS activity, and LF/HF ratio was used as an indicator of SNS activity, specifically as a marker of sympathovagal balance.

4.3.2.1 HRV responses to reserpine in conscious Gnasxl knockouts

Reserpine caused a decrease in LF/HF ratio over time in both wildtypes and knockouts (Figure 4.7A). This was a significant decrease in both wildtypes (Figure 4.7B; 1.38 ±0.31 to 0.47 ±0.09, p≤0.05 by paired t-test, n=8) and knockouts (Figure 4.7B; 1.39 ±0.22 to 0.26 ±0.06, p≤0.05 by paired t-test, n=8). However, the percentage decrease in LF/HF ratio was significantly

greater in knockouts compared to wildtypes (Figure 4.7C; -80 ±5 vs -48 ±13 % KO vs WT, p≤0.05 by t-test, n=8).

4.3.2.2 HRV responses to atropine in conscious Gnasxl knockouts

Atropine caused a decrease in HF power over time in both wildtypes and knockouts (Figure 4.8A). This was a significant decrease in both wildtypes (Figure 4.8B; 3.0 ±0.6 to 1.2 ±0.5 ms^2/Hz, p≤0.05 by paired t-test, n=6) and knockouts (Figure 4.8B; 2.7 ±0.7 to 0.6 ±0.2 ms^2/Hz, p≤0.05 by paired t-test, n=6). However, there was no significant difference in % decrease between wildtypes and knockouts (Figure 4.8C; -61 ±16 vs -77 ±6 % in WT vs KO, n=6).

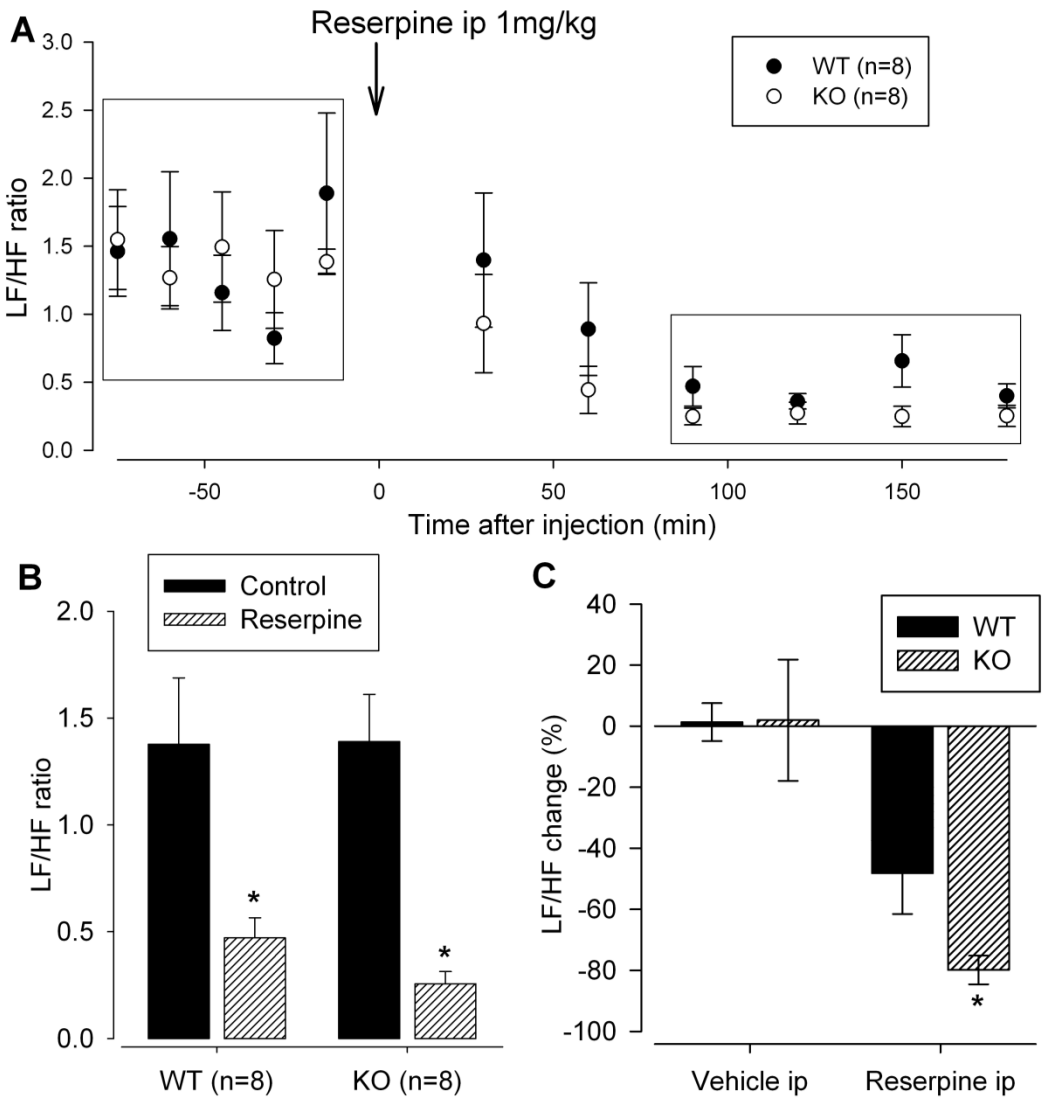

Figure 4.7. HRV responses to reserpine in conscious *Gnasxl* knockout mice.

Heart rate was recorded from conscious *Gnasxl* knockout mice and wildtype siblings at high resolution (within 0.2 ms). FFT spectra were produced from 3-minute sections of clean and stable heart rate resampled at 20 Hz using Welch's algorithm with 32-second windows with 50 % overlap. The LF/HF ratio was used as an indicator of sympathetic stimulation of the cardiovascular system, and was calculated using the bandings LF 0.15-1.0 Hz, HF 1.0-5.0 Hz. Reserpine was injected at 1 mg/kg ip.

(A) LF/HF response to reserpine over time.

(B) Both wildtypes and knockouts had a significant drop in LF/HF ratio in response to reserpine (*p≤0.05 by paired t-test, n=8).

(C) Knockouts had a significantly greater relative decrease in LF/HF ratio in response to reserpine than wildtypes (*p≤0.05 by t-test, n=8).

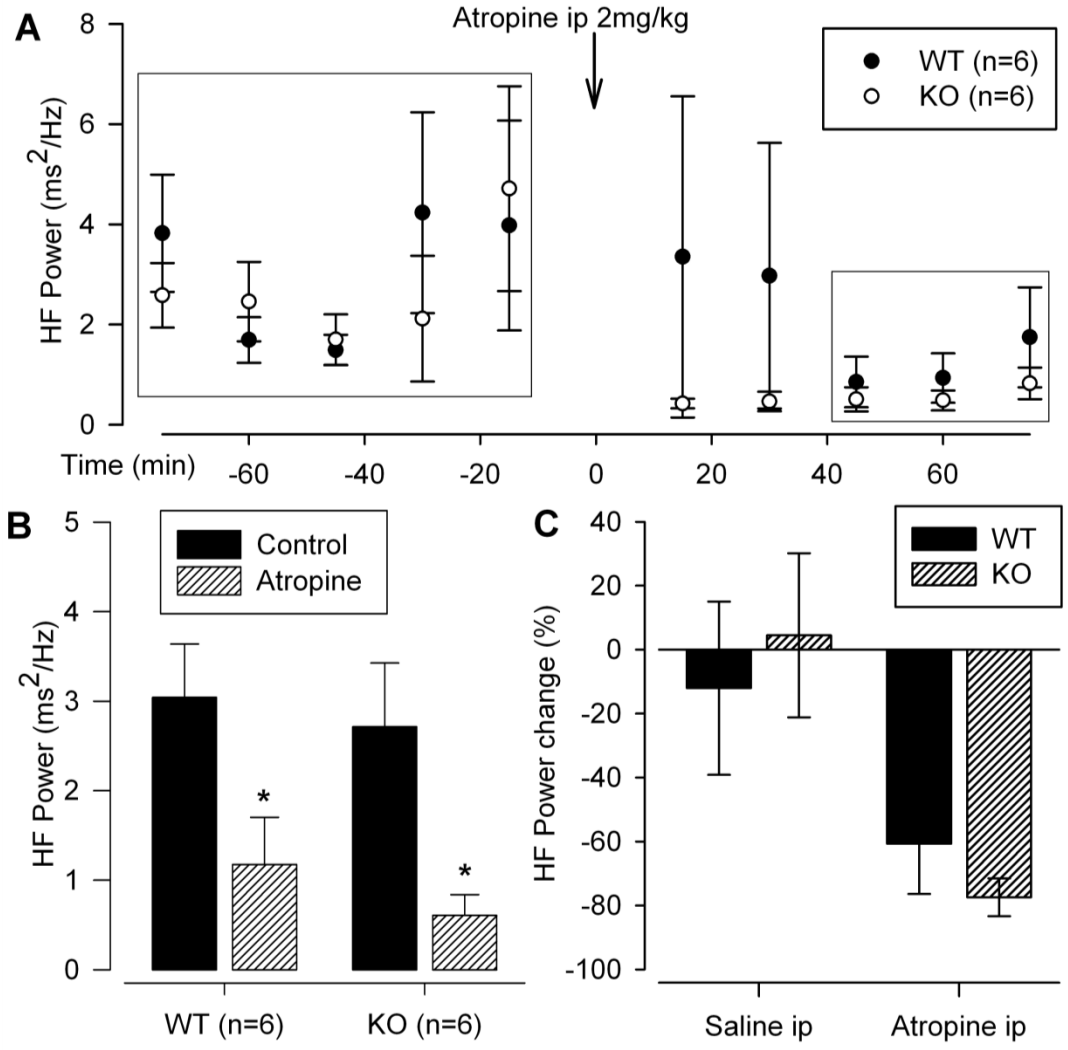

Figure 4.8. Heart rate variability (HRV) responses to atropine in conscious *Gnasxl* knockout mice.
Heart rate was recorded from conscious *Gnasxl* knockout mice and wildtype siblings at high resolution (within 0.2 ms). FFT spectra were produced from 3-minute sections of clean and stable heart rate resampled at 20 Hz using Welch's algorithm with 32-second windows with 50 % overlap. HF power was used as an indicator of parasympathetic stimulation of the cardiovascular system, and was calculated between 1.0 and 5.0 Hz. Atropine was injected at 2 mg/kg ip.
(A) Response in HF power to atropine over time.
(B) Both wildtypes and knockouts had a significant drop in HF power after atropine injection (*p≤0.05 by paired t-test, n=6).
(C) Both wildtypes and knockouts had comparable percentage decreases in HF power in response to atropine.

4.3.2.3 HRV control at night in conscious Gnasxl knockouts

HRV parameters were calculated for wildtypes and knockouts during the 5-hour period between 20:00 and 01:00, as this is when the mice had high levels of heart rate and activity (Figure 3.5A/C). A minimum of ten 3-minute windows were used for each mouse, and the average value for each parameter used as a representative value for that mouse. In this way, knockouts were found to have elevated LF/HF ratio at night (Figure 4.9; 1.79 ±0.18 vs 1.23 ±0.14, KO vs WT; $p \leq 0.05$ by t-test, n=9/12), as well as trends for decreased HF power and increased SDNN and Poincaré SD2.

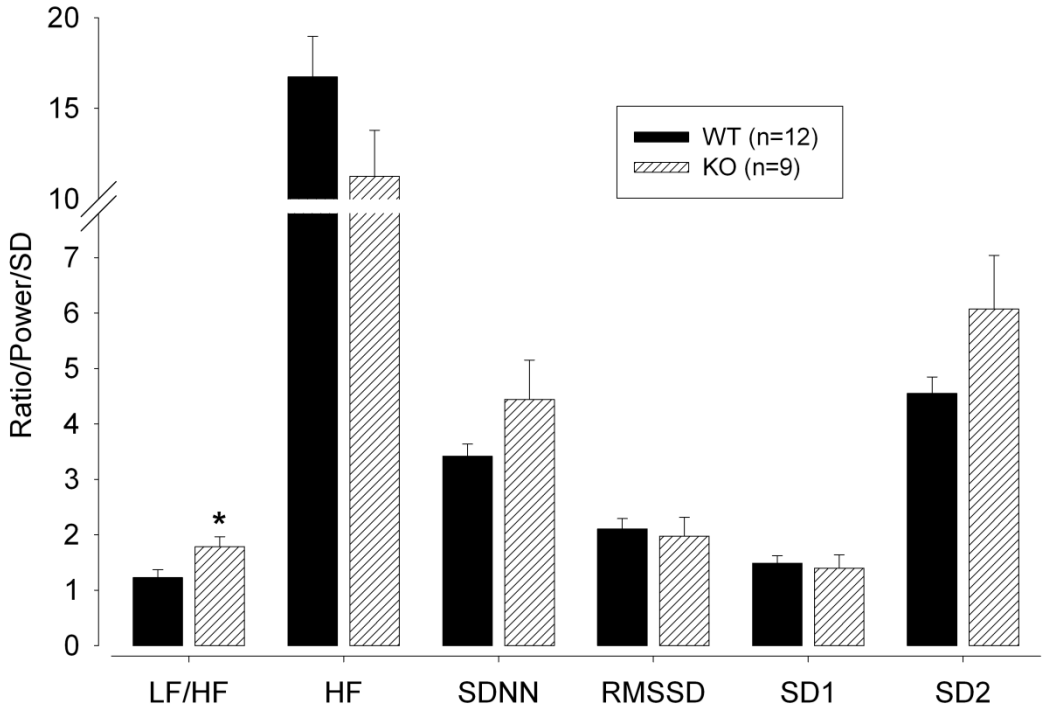

Figure 4.9. Basal heart rate variability (HRV) parameters in *Gnasxl* knockouts at night.
Heart rate was recorded in adult *Gnasxl* knockout mice and wildtype siblings. A number of HRV parameters were analysed from at least ten 3-minute sections of heart rate per mouse. HF power and LF/HF ratio were calculated from FFT spectra using banding of LF 0.15-1.0 Hz, HF 1.0-5.0 Hz. SDNN and RMSSD are the standard time-domain analyses (standard deviation of normal RR intervals and root mean square of successive differences, respectively). SD1 and SD2 are the two standard deviation parameters from Poincaré plots. LF/HF ratio was significantly increased in KO compared to WT (*p≤0.05 by t-test). There are no units for LF/HF; HF power has units of ms^2/Hz; the rest have units of ms.

4.4 Discussion

In Chapter 3 it was shown that mice lacking XLαs have elevated blood pressure and heart rate, likely due to elevated sympathetic stimulation. In this chapter support for this finding was sought through the use of HRV analysis to probe in more detail the sources of autonomic control of the cardiovascular system in *Gnasxl* knockout mice. In particular the specifics of SNS versus PNS stimulation, and how the paradoxic autonomic responses from Chapter 3 may have been caused.

HRV analysis offers additional information concerning cardiovascular control than simply investigating blood pressure or heart rate. It has been used diagnostically in human patients and as a predictive tool to predict cardiac pathology, such as ventricular tachycardia (Huikuri *et al.*, 1993).

HRV has also been used extensively in research to investigate cardiovascular control in rodents, but the parameters used for HRV in mice are less certain than in humans (Gehrmann *et al.*, 2000). A wide range of methodologies are used in the literature, so in order to use HRV analysis in this investigation the different HRV methods first had to be validated to provide valid and reliable outcomes.

Firstly two time-domain HRV parameters were investigated: the standard deviation of normal RR intervals (SDNN), and the root mean square of successive differences (RMSSD). These parameters are the simplest to calculate, but can still provide information on autonomic control. SDNN is simply a measure of the deviation of a heart rate series over time. It increases in line with heart rate "drift" over time, thereby providing a rough

estimate of the degree of long-term (or low frequency) variation in heart rate, which corresponds mainly to sympathetic stimulation of the cardiovascular system. The typical examples in Figure 4.2A demonstrate that SDNN decreases after inhibition of the SNS due to reserpine injection.

RMSSD, on the other hand, roughly quantifies beat-to-beat variation in heart rate, thereby giving a crude estimate of the short-term (or high frequency) variation in heart rate, which would be expected to more closely correspond to parasympathetic stimulation of the cardiovascular system. The typical examples in Figure 4.2A demonstrate that RMSSD decreases significantly after loss of parasympathetic inhibition by atropine, but there is little effect of reserpine injection. These effects were seen consistently across a sample of wildtype mice (Figure 4.2B/C), except that there was a non-significant decrease in SDNN after atropine injection, which might result in skewed quantification of the SNS.

Secondly nonlinear HRV analysis with Poincaré plots was investigated. This is essentially a different (and possibly more robust) method of investigating the short- and long-term changes in heart rate variation (Deepak, 2011). The corresponding parameters from a Poincaré plot are SD1, which quantifies short-term heart rate variation, and SD2, which quantifies long-term heart rate variation (Figure 4.3Ai for a typical Poincaré plot).

Loss of sympathetic stimulation of the cardiovascular system after reserpine injection resulted in a reduction in SD2 on the Poincare plot, while SD1 remained high (Figure 4.3Aii). On the other hand, loss of parasympathetic stimulation after atropine injection resulted in a reduction in SD1, while SD2

remained high (Figure 4.3Aiii). These effects were seen consistently across a sample of wildtype mice (Figure 4.3B/C), except that there was a non-significant decrease in SD2 after atropine, which might result in skewed quantification of the SNS, as with the SDNN.

Thirdly frequency-domain HRV analyses were investigated using fast Fourier transforms (FFTs), as well as both autoregressive and Lomb power spectra. Lomb spectra have the added benefit that they function on unevenly spaced data, which means that the heart rate series doesn't need to be resampled (Lomb, 1976; Moody, 1993).

Frequency domain HRV analyses can provide the most information about heart rate variability, but require more support and validation from experiment. Briefly, power spectra use complex mathematical algorithms to quantify the degree of variability in heart rate that is contributed by different frequencies in variation. Hence, the total power of an FFT spectrum is directly proportional to the standard deviation of the time series analysed, split into frequency components.

Previous studies have attempted to standardise the parameters used to define the LF and HF bands of power spectra in mice (Thireau *et al.*, 2008), however there is by no means any consensus among different researchers. Therefore, typical bandings were used as a guide, but empirical validation was required to define the parameters used in this study.

Having tested and validated various HRV analyses, it was found that all three types of power spectra produced valid responses to both reserpine and atropine (Figures 4.4-6). However, the autoregressive spectra had a

decrease in LF/HF ratio after atropine that approached significance (Figure 4.5C; 1.4 ±0.2 to 0.9 ±0.2 ms^2/Hz; p=0.085 by paired t-test, n=6). Therefore, and additionally due to the difficulty producing Lomb spectra and the widespread use of FFT's in the literature, FFT power spectra were used to analyse HRV in the *Gnasxl* knockout mouse.

Firstly, the LF/HF ratio was used as a marker of sympathovagal balance; LF/HF ratio was significantly reduced after reserpine injection in both wildtypes and knockouts (Figure 4.7B), but knockouts had a significantly greater % decrease in LF/HF ratio (Figure 4.7C). This confirms that the elevated blood pressure and heart rate in *Gnasxl* knockouts shown in the previous chapter is not caused by peripheral effects, such as different vascular properties or receptor density (Young & Davisson, 2011), but is in fact caused by elevated SNS stimulation of the cardiovascular system.

The parasympathetic contribution to HRV in the *Gnasxl* knockout mouse was evaluated by HF power response to atropine injection. Atropine caused a significant decrease in HF power in both wildtypes and knockouts that was consistent between genotypes (Figure 4.8B). This might seem counterintuitive in light of the elevated heart rate response to atropine in the knockouts, but in fact this could shed light on the mechanism involved: that after loss of PNS stimulation in the knockouts, the elevated SNS activity in these animals would be more prominent, resulting in a reflex increase in cardiovascular output.

The results so far have shown that *Gnasxl* knockout mice have elevated SNS stimulation of the cardiovascular system, but the PNS seems

unaffected. However, these results only reflect the day period, when the mice are less active, as this is the time when the injections were performed.

Therefore, basal levels of autonomic stimulation were investigated during the active night period, when *Gnasxl* knockouts were found to have significantly elevated LF/HF as well as a trend for decreased HF power (Figure 4.9). This suggests that the knockouts might have consistently higher SNS activity at night, and it could be interesting to pursue this result by injection of reserpine and atropine during the night and investigating cardiovascular and HRV responses. The knockouts also had a trend for increased SDNN and Poincaré SD2, which would also correlate with elevated SNS stimulation of the cardiovascular system.

In summary, the HRV changes in *Gnasxl* knockout mice support the results from chapter 3 showing that *Gnasxl* knockouts have elevated sympathetic stimulation of the cardiovascular system, and confirm that this is due to a central effect changing SNS activity. This suggests that XLαs normally inhibits central control of SNS activity, and therefore lack of XLαs increases basal SNS stimulation of the cardiovascular system.

5 Investigating XLαs signalling pathways mediating cardiovascular control

5.1 Introduction

XLαs is a signalling protein known to control metabolism via the sympathetic nervous system (SNS) (Xie *et al.*, 2006), and is expressed in a number of key brain regions involved in SNS control (Krechowec *et al.*, 2012). However, arguably the most challenging aspect of investigating XLαs signalling is the lack of known signalling partner.

It is known where XLαs is expressed, and the likely downstream signalling (ie. via adenylate cyclase), but it is unknown which receptor(s) it might couple to *in vivo*. This question has been previously addressed with respected to location (ie. a signalling partner for XLαs must be expressed in the same cell (Krechowec *et al.*, 2012)), but co-staining XLαs with known GPCRs in the brain has elicited little success.

5.1.1 XLαs signalling

A number of studies have investigated the role of XLαs signalling in vitro, which have shown that XLαs is potentially capable of coupling to a few known GPCRs, including β_2-AR and PTHR (Liu *et al.*, 2011). However, there is no known $G_s\alpha$-coupled GPCR that gives a lean phenotype similar to XLαs

when mutated, therefore there are no viable options for possible XLαs signalling partners among known GPCRs.

In this chapter, the approach used is to test the response to agonists of neuronal receptors of interest. This experiment is limited to choosing known GPCRs with known agonists, which are unlikely to couple directly to XLαs. Of particular interest is the response of the melanocortin pathway, which has such a profound effect on energy balance, and has been investigated in detail with respect to $G_s\alpha$ coupling.

5.1.2 Melanocortin pathways

The melanocortin system is a well known mediator of food intake, metabolism and SNS control of the cardiovascular system (Balthasar *et al.*, 2005), and was interesting to investigate. It has been shown previously that the MC4R couples via $G_s\alpha$ (Chen *et al.*, 2009). However, the situation remains unclear, particularly in the PVN, where $G_s\alpha$ control the cardiovascular system, but MC4R is known to have potent effects on energy expenditure (Chen *et al.*, 2011).

In this study, the MC4R pathway will be investigated by ICV injection of the classic melanocortin agonist melanotan II (MTII) (Irani & Haskell-Luevano, 2005), recording blood pressure and heart rate responses. MC4R signalling will also be investigated in conscious mice by ip injection, and using electrocardiogram (ECG) telemeters to record heart rate.

For peripheral injections, MTII could not be used, as it activates MC3R as well as MC4R, and would therefore cause off-target peripheral effects; for

example, MC3Rs are found on the heart (Chhajlani, 1996), and MTII will therefore have direct cardiac effects if injected peripherally. Therefore, the agonist Ro27-3225 was used, as this has been shown to cause central activation of MC4R when injected peripherally, and has 100-fold higher affinity for MC4R than the MC3R (Benoit *et al.*, 2000).

5.1.3 GLP-1 pathways

The other pathway tested was the glucagon-like peptide 1 (GLP-1) signalling pathway. GLP-1 is an incretin hormone, which signals peripherally to control insulin signalling and glucose homeostasis (Holst, 2007). However, a separate GLP-1 signalling system is also found in the brain, where GLP1 acts as a peptide neurotransmitter to control food intake, metabolism and the cardiovascular system (Yamamoto *et al.*, 2002; Baggio *et al.*, 2004).

Additionally, the expression pattern of the GLP-1 receptor closely mirrors that of XLαs, including the medullary raphe nuclei and the hypothalamic PVN (Merchenthaler *et al.*, 1999), making it a likely candidate for involvement in XLαs signalling. Peripheral injection of Exendin-4, a protease-resistant GLP1 analogue, has been shown to activate central GLP-1 receptors and result in increase SNS activity, causing elevated blood pressure and heart rate (Yamamoto *et al.*, 2002).

The doses used for all three of these drugs are taken from the literature, with the aim of producing a robust cardiovascular response. For central injections, mice were anaesthetised urethane-chloralose and drugs were injected ICV; blood pressure and heart rate responses were recorded. For peripheral injections, ECG telemetry was used; heart rate responses were recorded,

and for more information about the response to Exendin-4, heart rate variability (HRV) was investigated by fast Fourier transform (FFT) power spectral analysis.

5.1.4 Aims

The aim of this chapter is to use cardiovascular responses to investigate how loss of XLαs might impact on known neuropeptide signalling pathways; specifically, it is likely that *Gnasxl* knockouts will be sensitive to pathways that stimulate the SNS. The outcome of this experiment might afford the first indication of how XLαs signalling might mediate its effects in mice, and provide a stepping stone for further investigations into the mechanism of XLαs function in the mouse. Three techniques will be used to achieve this: blood pressure recording in anaesthetised mice with ICV injection; heart rate recording in conscious mice with ip injection; and finally HRV analysis in conscious mice with ip injection.

5.2 Methods

Adult male *Gnasxl*$^{m+p-}$ knockout mice and wildtype siblings were used for this experiment. Cardiovascular recordings were performed, as described in chapter 2, by ECG telemetry in conscious mice and by arterial cannulation in urethane-chloralose anaesthetised mice. Blood pressure, heart rate and heart rate variability were analysed as described in chapters 2-4.

Anaesthetised mice were injected ICV with 0.5 µg Exendin-4 or 600 pmol MTII in 1 µl volume, dissolved in aCSF. The coordinates for ICV injections were calculated from Paxinos and Franklin (Paxinos & Franklin, 2001),

according to the following distances from Bregma: 0.2mm caudal, 1.0 mm lateral and 3.7 mm vertical from the surface of the skull. At the end of the experiment 1 µl of 1 % (w/v) Chicago Blue (Sigma) was injected at the same coordinates to confirm correct injection.

Conscious mice were injected intraperitoneally with sterile 0.9 % saline, 1 µg/kg and 50 µg/kg Exendin-4, or they were injected intravenously (tail vein) with 0.9 % saline and 50 µg/kg Ro27-3225. All drugs were diluted according to body weight into sterile 0.9 % saline and injected in 50 µl volume. If mice were given multiple drug injections, at least two days were left between each to allow the previous drug to be metabolised and excreted.

5.3 Results

5.3.1 Control of melanocortin signalling in Gnasxl knockout mice

The role of melanocortin signalling in cardiovascular control in *Gnasxl* knockouts was investigated by ICV injection of MTII in anaesthetised *Gnasxl* knockout mice, recording blood pressure and heart rate responses. Further investigations were performed by ip injection of the MC4R agonist Ro27-3225 in conscious *Gnasxl* knockout mice, recording heart rate responses.

5.3.1.1 Blood pressure and heart rate responses to central MTII injection in anaesthetised Gnasxl knockout mice

The classic melanocortin agonist MTII was injected ICV in anaesthetised, cannulated adult mice. MTII was expected to increased blood pressure and heart rate via activation of the SNS (Haynes *et al.*, 1999). Typical blood pressure responses to 600 pmol MTII ICV are shown in Figure 5.1A for

wildtype (top) and knockout (bottom). Both show clear blood pressure responses within a couple of minutes of injection.

However, the blood pressure change is not so clear when averaged over time for a sample of animals, as shown in Figure 5.1B. Linear trendlines for BP before and after injection (Figure 5.1C) show that blood pressure is on a steady decline before injection. The trend lines show that, at least in knockouts, there appears to be a change in the general decrease in BP over time. However, no significant BP responses could be quantified due to the downward trend and the high variability in response between subjects.

There was a general increase in average heart rate after MTII injection for both wildtype and knockout (Figure 5.2A). However, mean heart rate was only significantly increased in knockout (Figure 5.2B; 612 ±45 to 651 ±39 bpm, $p \leq 0.05$ by paired t-test, n=6), but not in wildtype mice (Figure 5.2B; 597 ±40 to 616 ±30 bpm, n=5). There was no significant difference in heart rate change between wildtype and knockout mice (Figure 5.2C; 39 ±10 vs 19 ±9 bpm, KO vs WT; n=6/5).

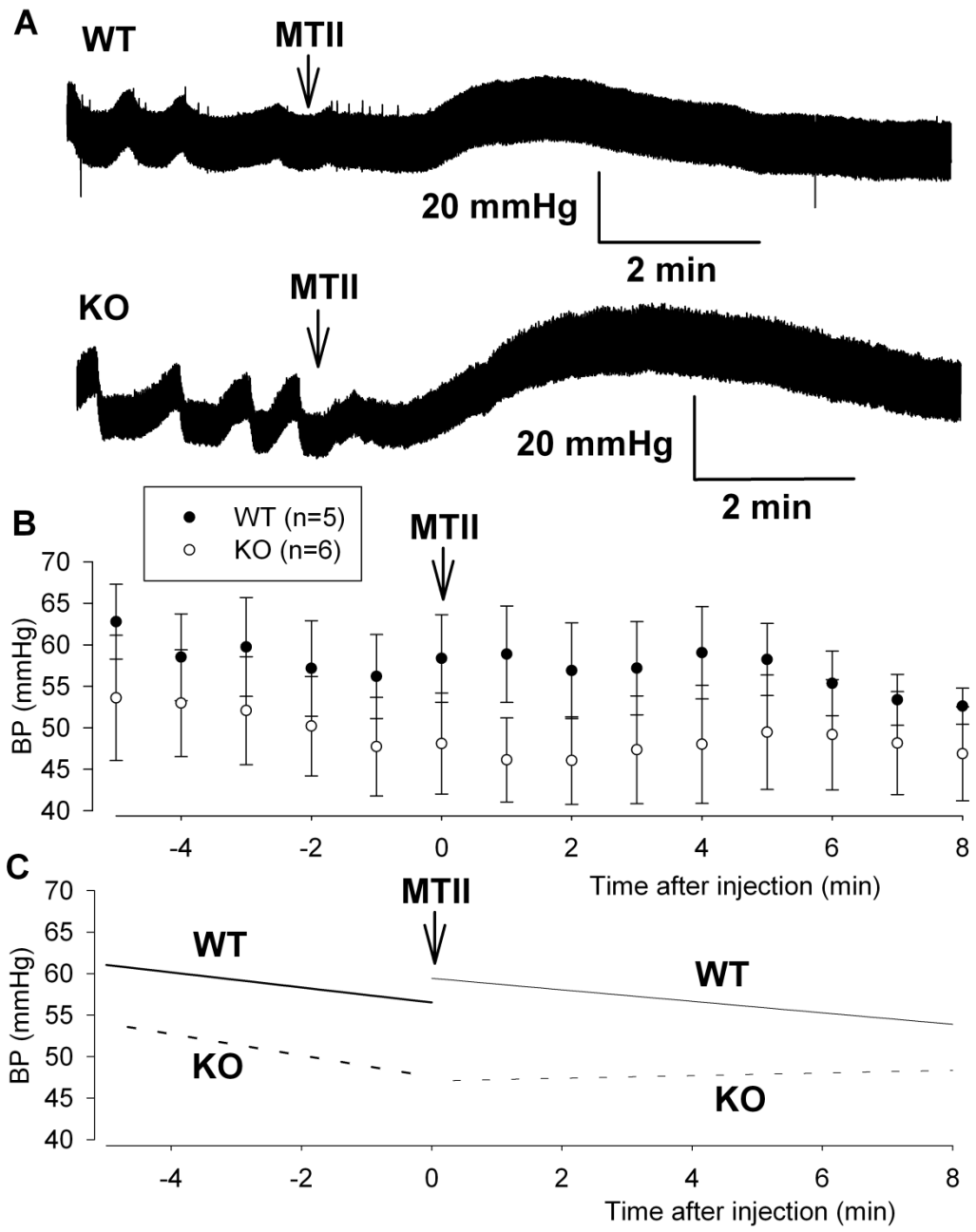

Figure 5.1. Blood pressure responses to central MTII in anaesthetised *Gnasxl* knockout mice.

Blood pressure was recorded from urethane-chloralose anaesthetised *Gnasxl* knockout mice and wildtype siblings. The melanocortin MC3/4R agonist MTII was injected ICV at 600pmol in aCSF.

(A) Typical traces of blood pressure responses to MTII in WT (top) and KO (bottom).

(B) Mean blood pressure responses over time.

(C) Linear regression lines of blood pressure responses for WT (solid line) and KO (dashed line).

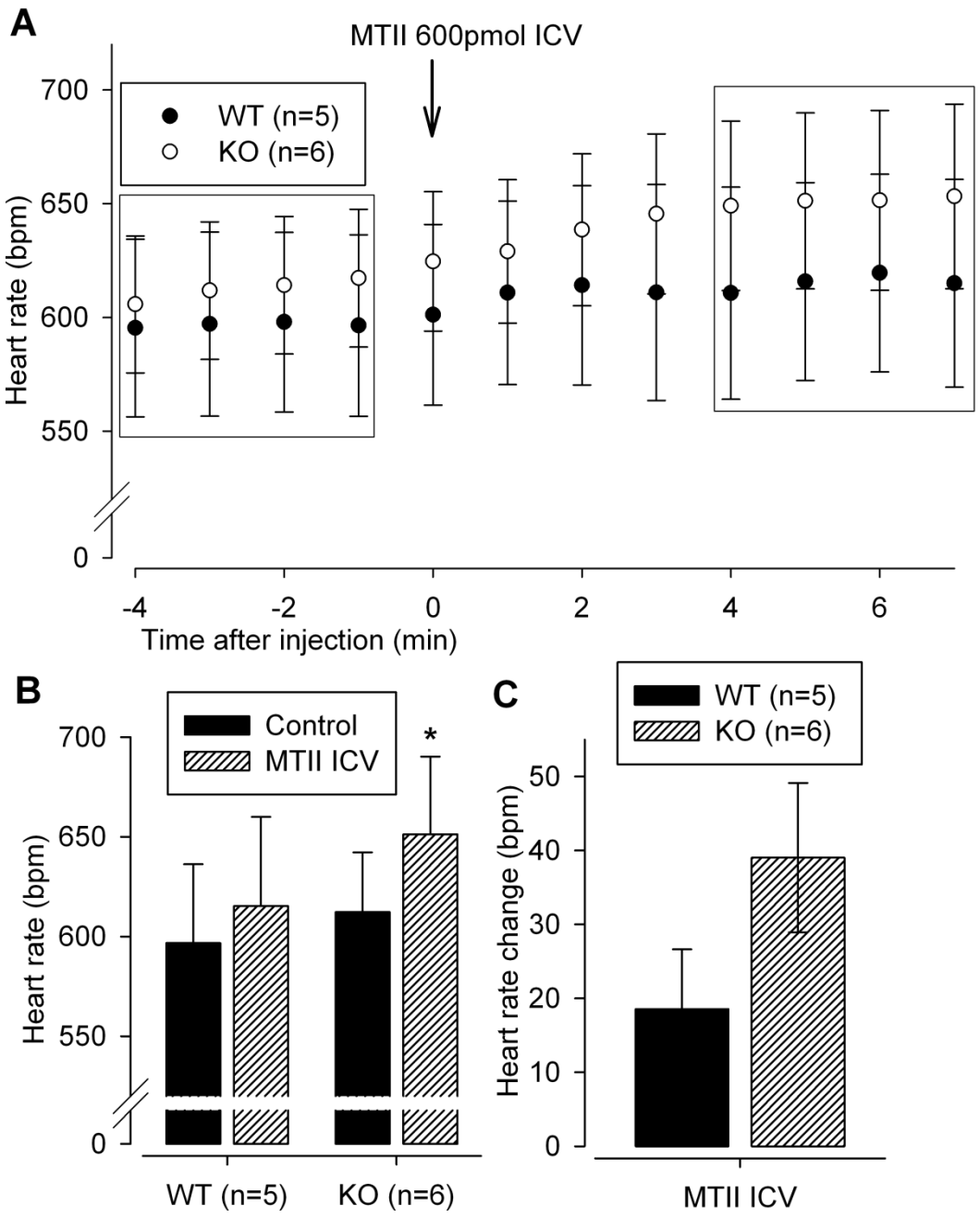

Figure 5.2. Heart rate responses to central MTII in anaesthetised *Gnasxl* knockout mice.

Heart rate was recorded from urethane-chloralose anaesthetised *Gnasxl* knockout mice and wildtype siblings. The melanocortin MC3/4R agonist MTII was injected ICV at 600pmol in aCSF.

(A) Average heart rate response over time for *Gnasxl* knockouts and wildtype siblings.

(B) Heart rate was significantly increased in knockouts but not in wildtypes (*p≤0.05 by paired t-test, n=6).

(C) There was no significant difference in average heart rate change between wildtypes and knockouts.

5.3.1.2 Heart rate responses to peripheral Ro27-3225 injection in conscious Gnasxl knockout mice

The synthetic melanocortin agonist Ro27-3225 was injected peripherally at a dose of 50 µg/kg. However, there was no obvious change in heart rate in wildtypes or knockouts, other than the usual increase due to handling stress (Figure 5.3A). On average, heart rate remained constant in both wildtypes (Figure 5.3B; 577 ±90 to 572 ±63 bpm; n=4) and in knockouts (Figure 5.3B; 597 ±34 to 559 ±34 bpm; n=3) after injection of Ro27-3225, and there was no significant difference in response between the two (Figure 5.3C; -14 ±67 vs -5 ±85 bpm, KO vs WT; n=3/4). The lack of effect is possibly due to difficulties in performing the tail vein injections, which stress the mice more than usual, and it is not always possible to inject the full dose of drug.

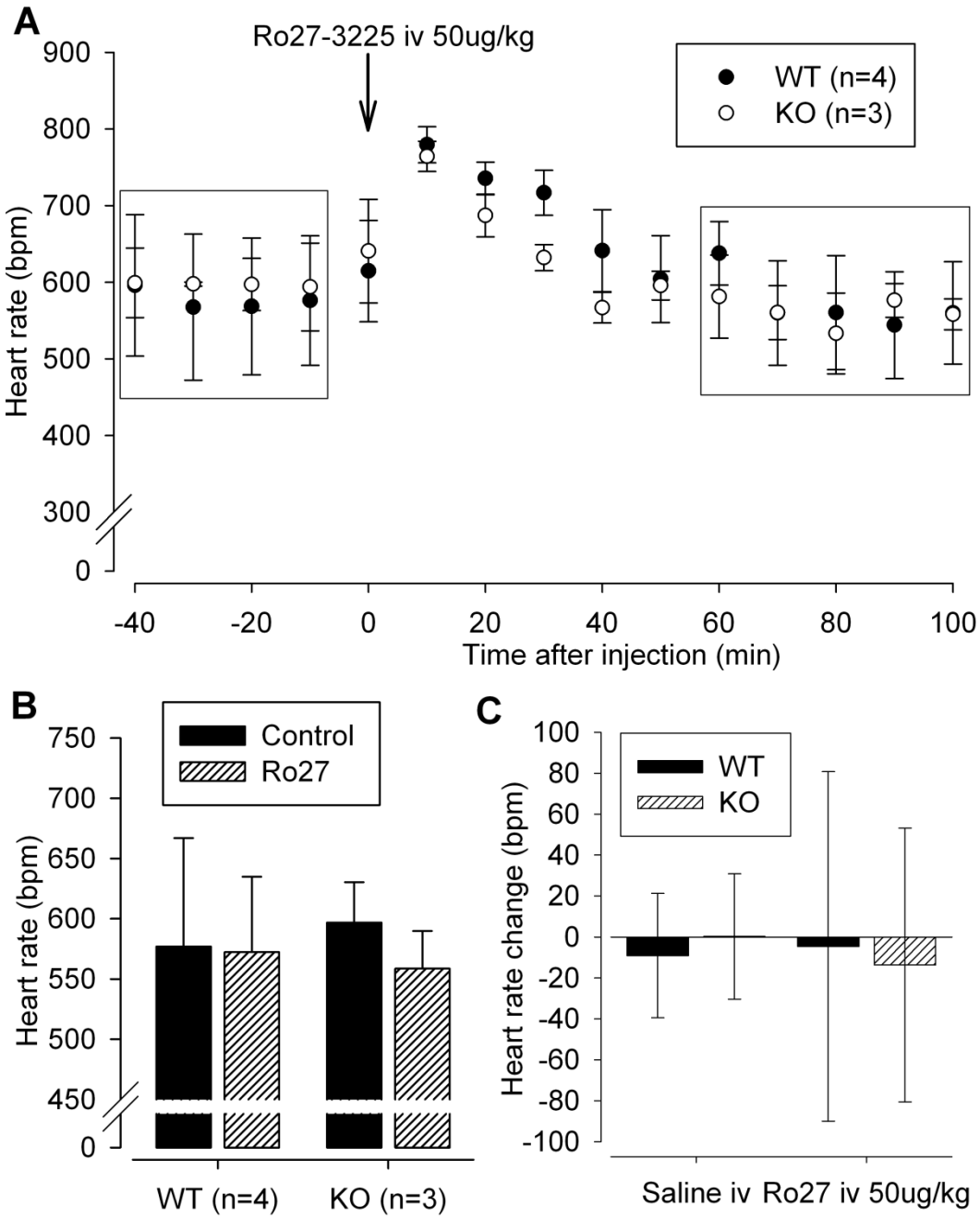

Figure 5.3. Heart rate response to Ro27-3225 in conscious *Gnasxl* knockout mice.

Heart rate was recorded using ECG telemetry from conscious *Gnasxl* knockout mice and wildtype siblings. The melanocortin MC4R-specific agonist Ro27-3225 was injected at 50 µg/kg iv.

(A) Heart rate response to Ro27-3225 over time.

(B) Mean heart rate before and after Ro27-3225.

(C) Both wildtypes and knockouts had no change in heart rate in response to Ro27-3225.

5.3.2 Control of GLP-1 signalling in Gnasxl knockout mice

The role of glucagon-like peptide 1 (GLP-1) signalling in cardiovascular control in *Gnasxl* knockouts was investigated by ICV injection of the GLP-1 receptor agonist Exendin-4 in to anaesthetised *Gnasxl* knockout mice, recording blood pressure and heart rate responses. Further investigations were performed by ip injection of the Exendin-4 in conscious *Gnasxl* knockout mice, recording heart rate responses, as well as HRV analysis using FFT spectra to investigate the specific contribution of the sympathetic and parasympathetic branches of the autonomic nervous system.

5.3.2.1 Blood pressure and heart rate responses to central Exendin-4 injection in anaesthetised Gnasxl knockout mice

Exendin-4 was injected ICV in anaesthetised, cannulated adult mice, at a dose of 0.5 µg. Typical blood pressure responses to 0.5 µg Exendin-4 ICV are shown in Figure 5.4A for wildtype (top) and knockout (bottom). Both show clear blood pressure responses within a couple of minutes of injection. However, the blood pressure change is not so clear when averaged over time, as shown in Figure 5.4B. Linear trendlines for BP before and after injection (Figure 5.4C) show that blood pressure is on a steady decline before injection. However, no objective BP responses could be quantified due to the downward trend and the high variability in response between subjects. After injection, there appears to be a decrease in the BP decline over time, but there is no way of distinguishing between wildtype and knockout mice.

There was a general increase in average heart rate after ICV Exendin-4 injection for both wildtype and knockout (Figure 5.5A). Mean heart rate was significantly increased in knockout after ICV Exendin-4 (Figure 5.5B; 615 ±9 to 633 ±6 bpm, $p \leq 0.05$ by paired t-test n=8), but not in wildtype (Figure 5.5B; 557 ±29 to 585 ±38 bpm, n=6). There was no significant difference in heart rate change between wildtype and knockout (Figure 5.5C).

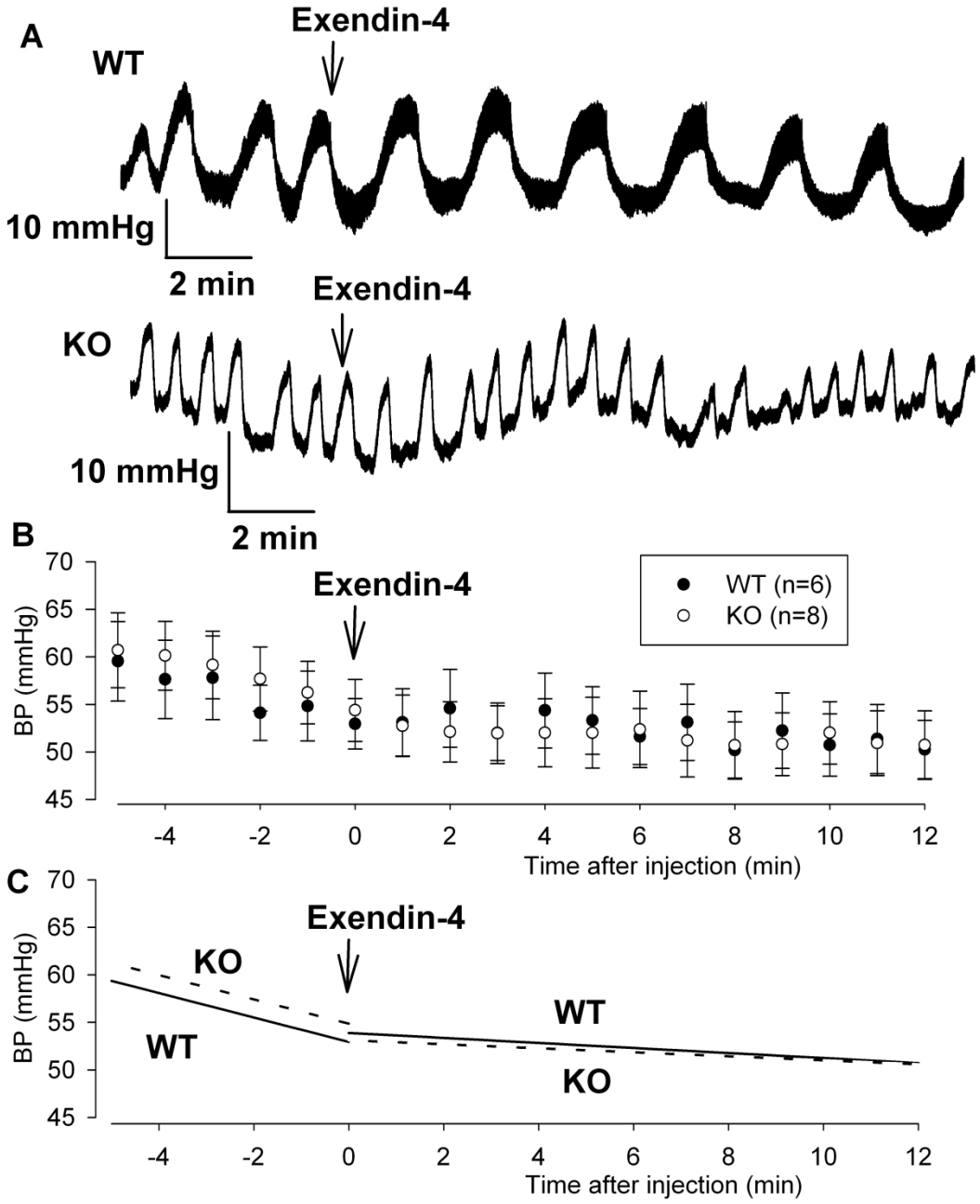

Figure 5.4. Blood pressure responses to central Exendin-4 in anaesthetised *Gnasxl* knockout mice.

Blood pressure was recorded from urethane-chloralose anaesthetised *Gnasxl* knockout mice and wildtype siblings. The protease-resistant GLP1R agonist Exendin-4 was injected ICV at 500ng in aCSF.

(A) Typical traces of blood pressure responses to Exendin-4 in WT (top) and KO (bottom).

(B) Mean blood pressure responses over time.

(C) Linear regression lines of blood pressure responses for WT (solid line) and KO (dashed line).

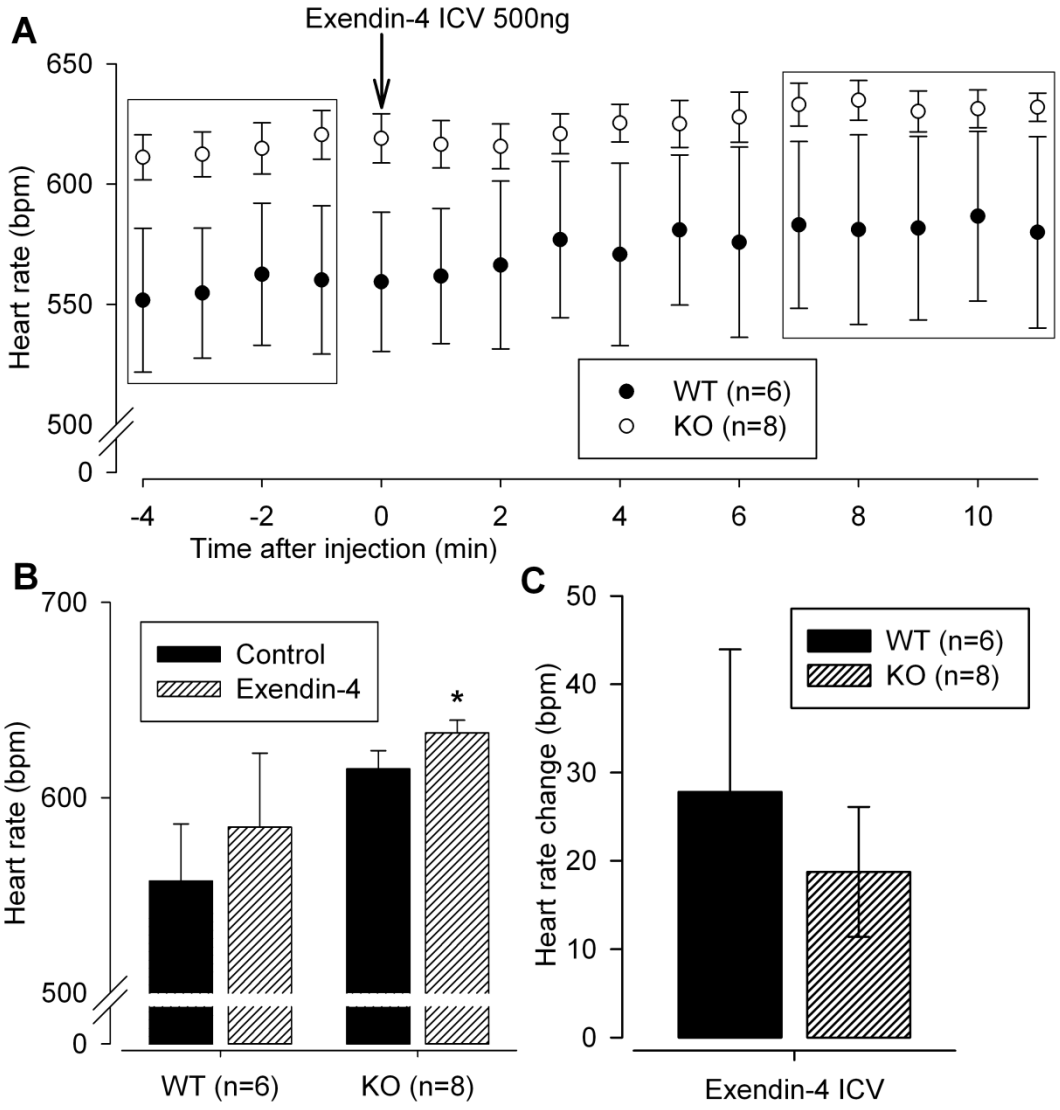

Figure 5.5. Heart rate responses to central Exendin-4 in anaesthetised *Gnasxl* knockout mice.
The protease-resistant GLP1R agonist Exendin-4 was injected 500ng ICV into urethane-chloralose anaesthetised *Gnasxl* knockout mice and wildtype siblings.
(A) Average heart rate response over time for *Gnasxl* knockouts and wildtype siblings.
(B) Heart rate was significantly increased in knockouts but not in wildtypes (*p≤0.05 by paired t-test).
(C) There was no difference in average heart rate change between wildtypes and knockouts.

5.3.2.2 Heart rate responses to peripheral Exendin-4 injection in conscious Gnasxl knockout mice

Exendin-4 is a protease-resistant analogue of GLP1, which is reported to cross the BBB and activate central SNS control of the cardiovascular system following peripheral injection. Exendin-4 was injected at 1 µg/kg, which is a low dose as in (Yamamoto *et al.*, 2002), but little lasting effect was seen in either wildtype or knockout (Figure 5.6A). We then injected Exendin-4 at 50 µg/kg, similar to (Sowden *et al.*, 2007) or a high dose in (Yamamoto *et al.*, 2002), which produced a sustained HR increase in knockout (Figure 5.6B; $p \leq 0.05$, n=7) but not wildtype mice (Figure 5.6B; n=7). 50 µg/kg Exendin-4 produced a significantly greater HR increase in knockout than in wildtype mice (Figure 5.6C; 72 ±23 vs 12 ±20 bpm in KO vs WT, $p \leq 0.05$ by t-test). This was further investigated by HRV analysis to probe the specific changes in autonomic control that caused the hypersensitivity response to Exendin-4 in *Gnasxl* knockout mice.

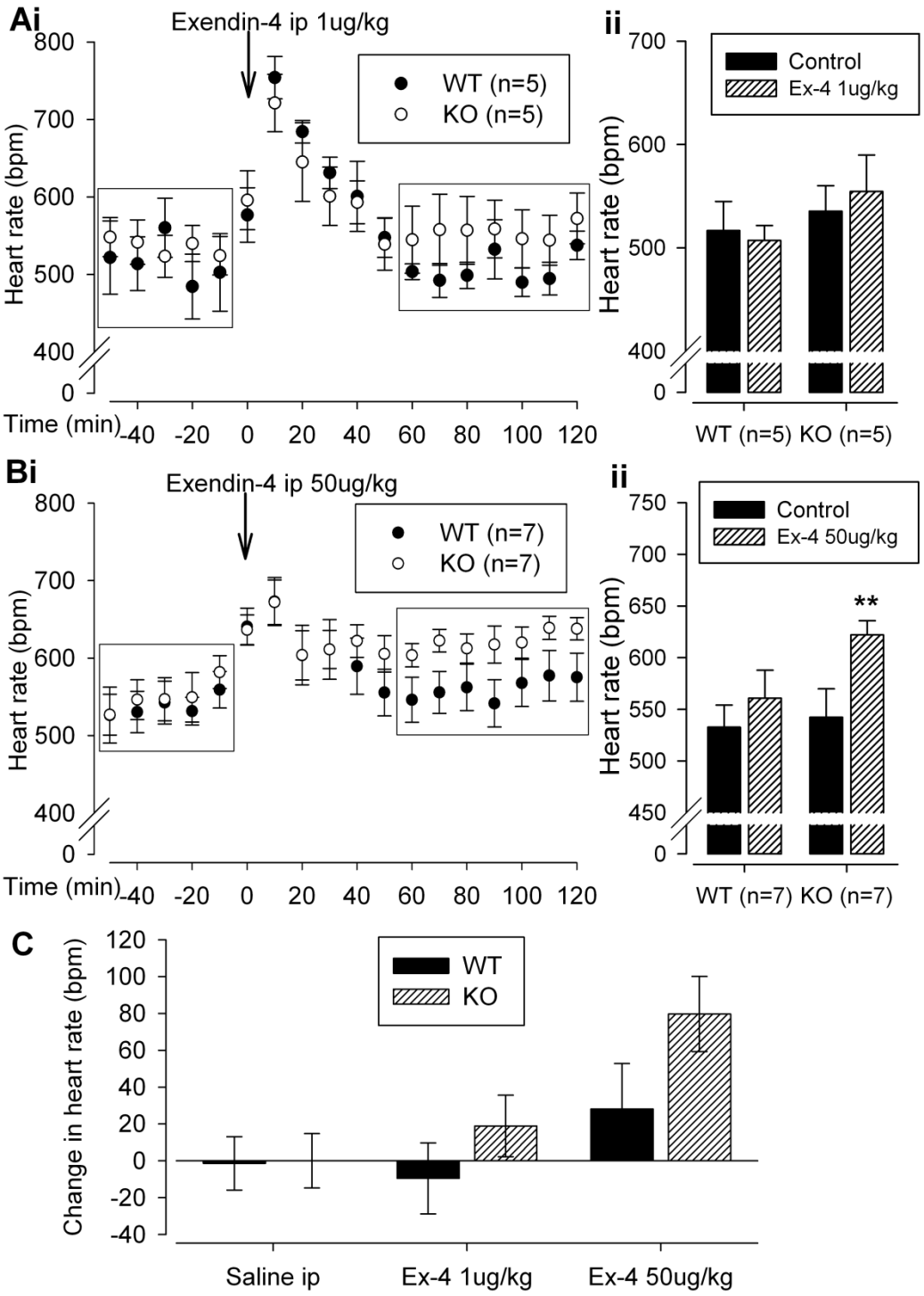

Figure 5.6. Heart rate responses to Exendin-4 in conscious *Gnasxl* knockout mice.

The protease-resistant GLP1R agonist Exendin-4 was injected 1µg/kg and 50µg/kg ip into conscious *Gnasxl* knockout mice and wildtype siblings.

(A) (i) Heart rate response to Exendin-4 over time at 1µg/kg, and (ii) average heart rates.

(B) (i) Heart rate response to Exendin-4 over time at 50µg/kg, and (ii) average heart rates; heart rate is significantly elevated in knockouts after 50µg/kg Exendin-4 (**p≤0.01 by paired t-test, n=7).

(C) Heart rate change in wildtypes and knockouts in response to Exendin-4 50µg/kg.

5.3.2.3 Heart rate variability responses to peripheral Exendin-4 injection in conscious Gnasxl knockout mice

Firstly, the sympathetic HRV responses were investigated as the LF/HF ratio from FFT spectra, which didn't change noticeably after injection (Figure 5.7A). This was supported by quantification of the LF/HF ratio before and after Exendin-4 injection (Figure 5.7B), and there was no difference in percentage change compared to saline (Figure 5.7C).

Secondly, the parasympathetic HRV responses were investigated as the change in HF power from FFT spectra. HF power was dramatically reduced in wildtype and knockout following Exendin-4 injection (Figure 5.8A). This was a significant change in wildtype mice (Figure 5.8B; 6.3 ±2.3 to 1.4 ±0.4 ms^2/Hz; $p \leq 0.05$ by paired t-test, n=7), but not in knockout mice due to high variability in the starting HF power.

However, when compared as percentage change in HF power after Exendin-4 injection, both wildtype and knockout had a highly significant percentage decrease in HF power (Figure 5.8C; -76 ±4 and -77 ±9 % for WT and KO; $p \leq 0.001$ by paired t-test, n=7/7), with no difference between the two.

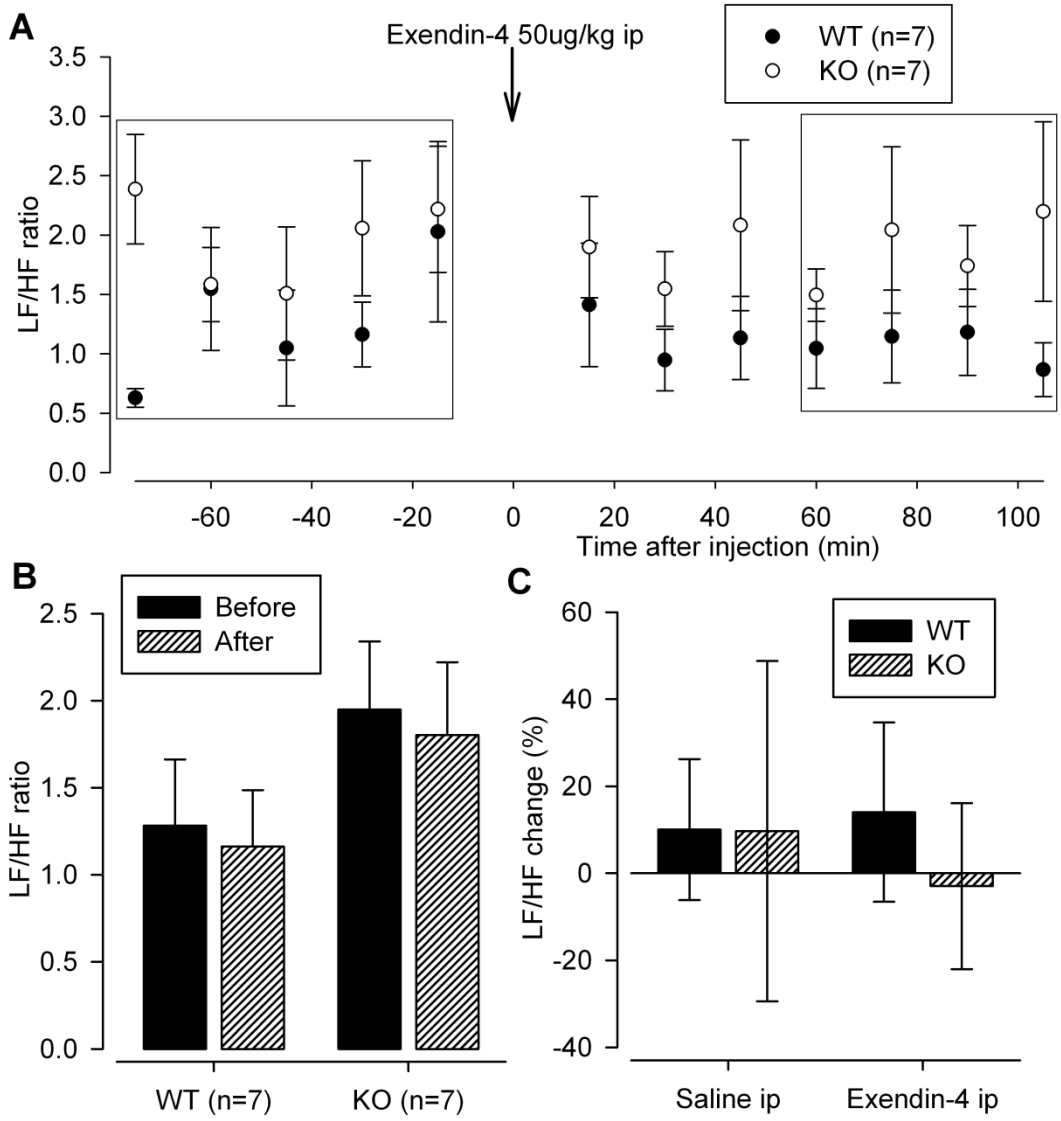

Figure 5.7. Sympathetic-mediated HRV responses to Exendin-4 in conscious *Gnasxl* knockout mice.
The protease-resistant GLP1R agonist Exendin-4 was injected 50µg/kg ip into conscious *Gnasxl* knockout mice and wildtype siblings.
(A) LF/HF ratio response to Exendin-4 over time; boxes show regions averaged in (B).
(B) Mean LF/HF before and after Exendin-4 in wildtypes and knockouts.
(C) Mean percentage changes to LF/HF in response to Exendin-4 in wildtypes and knockouts.

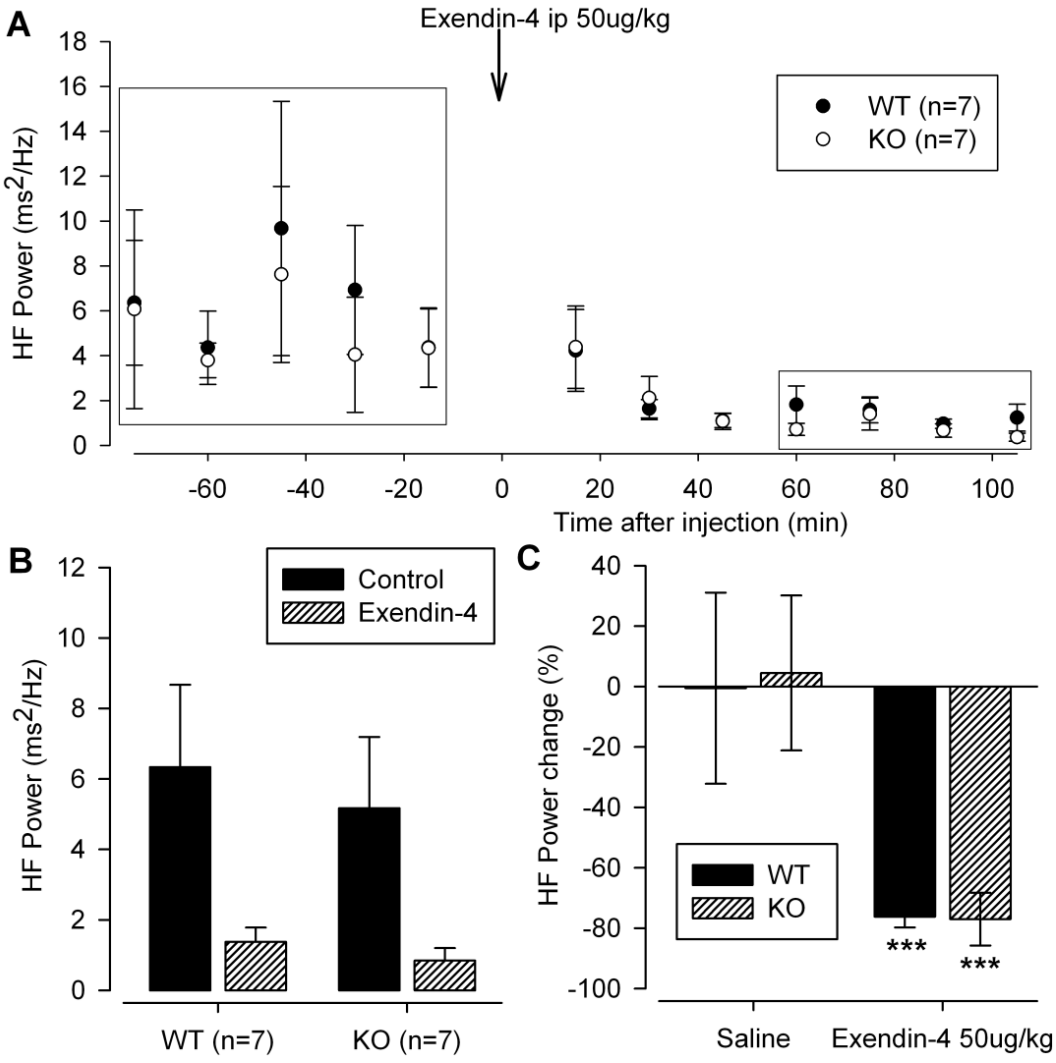

Figure 5.8. High frequency HRV responses to Exendin-4 in conscious *Gnasxl* knockout mice.
The protease-resistant GLP1R agonist Exendin-4 was injected 50µg/kg ip into conscious *Gnasxl* knockout mice and wildtype siblings.
(A) HF power response to Exendin-4 over time; boxes show regions averaged in (B).
(B) Mean HF power before and after Exendin-4 in wildtypes and knockouts.
(C) Both wildtypes and knockouts have a significant % decrease in HF power (***p≤0.001 by paired t-test, n=7).

5.4 Discussion

The aim of this chapter was to investigate neuronal signalling pathways that might be disrupted in *Gnasxl*$^{m+p-}$ knockout mice. Cardiovascular responses were recorded to agonists for the central melanocortin receptor MC4R and the GLP1 receptor.

The melanocortin system is a well known mediator of appetite, metabolism and the cardiovascular system via control of the SNS (Hall *et al.*, 2010). There are numerous members of the melanocortin family of receptors, which are expressed in different regions of the body. The main receptor involved in SNS control in the brain is the MC4R, and it is this receptor that was hypothesised to possibly be deregulated in *Gnasxl*$^{m+p-}$ knockouts, and therefore was the receptor of interest for this investigation. The classic MC3/4R agonist MTII was injected ICV, and the blood pressure and heart rate responses were recorded.

Although there were good BP responses to MTII (Figure 5.1A), high variability between animals and a declining basal blood pressure meant there was no objective way of discerning a significantly different BP response between wildtype and knockout mice. However, linear trendlines through the average blood pressure showed that there might be a more substantial change in the declining BP trend in knockouts than in wildtypes.

The heart rate responses to MTII were also investigated, which showed a much clearer effect than the blood pressure response, and in this case the knockouts had a significant increase in heart rate, which was not seen in the wildtypes. This result suggests that the knockouts might be sensitive to

MC4R signalling, as hypothesised in the introduction. However, due to the inconclusive BP response, I wanted to confirm this in conscious mice using telemetry.

For the telemetry experiment an agonist was needed that could be injected peripherally but would act centrally to activate specifically the MC4R preferentially over the other melanocortin receptors. The synthetic compound Ro27-3225 was chosen as an agonist that is specific for the MC4R, and has over 100-fold higher affinity for MC4R than MC3R (Benoit *et al.*, 2000).

Ro27-3225 has also been reported to improve cardiovascular parameters when injected peripherally, in this case in response to haemorrhagic shock (Giuliani *et al.*, 2007). No direct cardiovascular responses to Ro27-3225 have been previously reported, so the dose was taken from Giuliani et al. where it was injected iv at 54 nmol/kg. This is equivalent to 42.4 µg/kg, so I rounded this up to 50 µg/kg. However, the iv injections were technically challenging and resulted in ambiguous and inconclusive cardiovascular responses (Figure 5.3).

Exendin-4 is a well-known agonist to the GLP1R, and is in clinical use in Type II diabetes to improve glucose metabolism and insulin sensitivity, for example as the drug Exenatide (www.byetta.com). Exendin-4 was injected ICV in anaesthetised, cannulated adult mice, and blood pressure and heart rate responses were recorded.

However, as with the MTII ICV injections, the baseline blood pressure and BP response to Exendin-4 were highly variable, and the baseline BP was declining over time, which made it impossible to discern any objective

significantly different blood pressure changes (Figure 5.4). Using linear trendlines, it was possible to discern an effect on the blood pressure, essentially a lessening of the BP decline. However, there was no difference between the wildtypes and knockouts.

Heart rate responses were also investigated (Figure 5.5); heart rate generally increased in wildtypes and knockouts, but was only significant in knockouts. However, the effect compared to wildtypes was inconclusive, so the cardiovascular effects in conscious mice were investigated next.

Exendin-4 is widely used as a GLP1R agonist in cardiovascular studies in conscious animals, and is reported to cross the BBB (Kastin & Akerstrom, 2003) and to activate central GLP1 receptors to produce an increase in SNS stimulation of peripheral effectors (Nogueiras *et al.*, 2009; Perez-Tilve *et al.*, 2010). Reports of the use of Exendin-4 in cardiovascular studies varies, so we tried two different doses of Exendin-4, as from (Yamamoto *et al.*, 2002; Sowden *et al.*, 2007).

Low dose Exendin-4 produced a trend towards elevated HR in knockout compared to wildtype mice (Figure 5.6A); high dose Exendin-4 produced a significantly elevated HR in knockout compared to wildtype (Figure 5.6B). This was very interesting as it mirrors the elevated cardiovascular response to activation of the MC4R in knockouts shown earlier. This suggests that lack of XLαs results in hypersensitivity to such SNS-increasing neural pathways.

To investigate this further, the heart rate variability responses to Exendin-4 50 µg/kg were investigated, using LF/HF ratio as a marker of sympathetic activity, and HF power as a marker of parasympathetic activity. Using these

markers, with the same parameters as those defined in chapter 3, no change in LF/HF ratio was found in response to Exendin-4, in wildtype or knockout (Figure 5.7). This result is contrary to most of the previously published studies which show that peripheral Exendin-4 injections causes an increase in central SNS control, including elevated sympathetic stimulation of muscle (Barrucha *et al.*, 2008) and white adipose tissue (Nogueiras *et al.*, 2009) and activation of sympathetic preganglionic neurones of the spinal cord (Yamamoto *et al.*, 2002).

However, Griffioen *et al.* showed that the cardiovascular effects of peripheral Exendin-4 are caused by a decrease in parasympathetic activity, as calculated by HRV analysis (Griffioen *et al.*, 2011). This effect was also seen here; both wildtype and knockout mice had a highly significant decrease in HF power in response to Exendin-4. This suggests that Exendin-4 produces a decrease in parasympathetic stimulation of the cardiovascular system.

This might provide an explanation for the hypersensitive HR response of the knockouts for Exendin-4, when the results of chapters 3 and 4 are taken into account. In the same way as seen here with Exendin-4, atropine caused an equivalent reduction in parasympathetic HRV in wildtypes and knockouts, but caused an elevated heart rate response in knockouts. This is interesting given that XLαs is expressed in both the NTS and the nucleus ambiguus, the main sites for control of PNS output. The involvement of XLαs neurones in this Exendin-4 response will be investigated in Chapter 6.

6 Investigating the role of XLαs in neuronal c-fos responses to Exendin-4

6.1 Introduction

In the previous chapter it was shown that mice lacking XLαs were hypersensitive to Exendin-4, specifically that they had a greater heart rate response to Exendin-4. There are a number of ways to further investigate the neuronal signalling involved in this interesting result. In this chapter, the possible effects of loss of XLαs to neuronal signalling are investigated by immunohistochemistry staining for the early response marker c-fos.

6.1.1 c-fos

c-fos is a so-called early response gene that can be used as a useful indicator of neuronal activity, for a review of c-fos studies into cardiovascular control see Dampney and Horiuchi 2003 (Dampney & Horiuchi, 2003). It encodes the transcription factor Fos that is transiently highly expressed in response to stimulus (Figure 6.1); in neurones, this is likely to be depolarisation of the membrane. Fos, together with its partner Jun, control expression of so-called “late-response” genes, such as neurotransmitters.

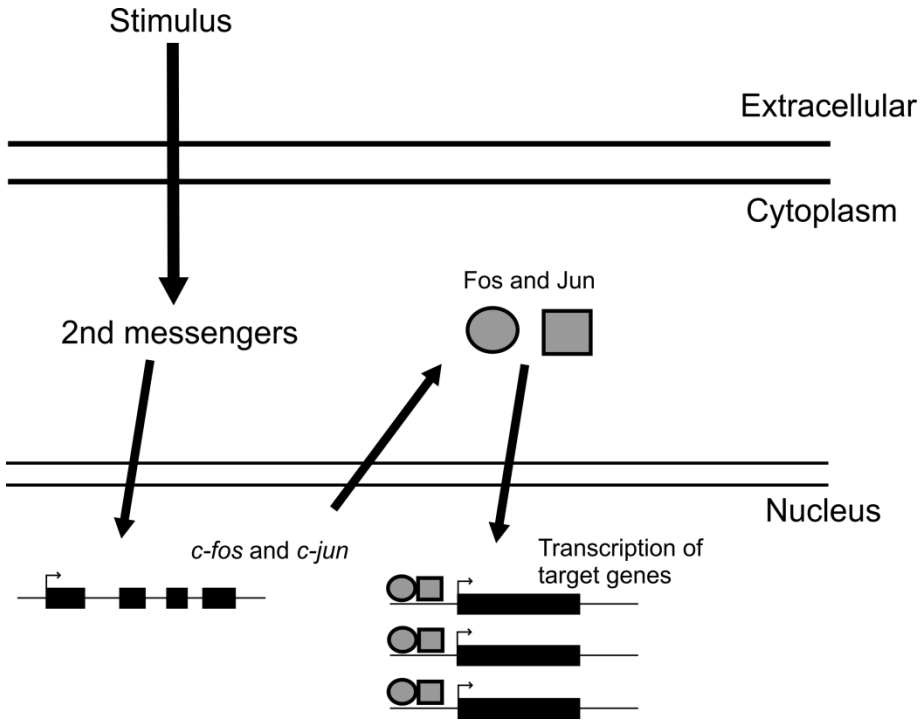

Figure 6.1. Diagram showing transcription control by Fos.
A stimulus, for example depolarisation or neurotransmitters in a neurone, stimulates transcription of *c-fos* and *c-jun*, via 2nd messengers such as Ca^{2+} and GTP. *c-fos* and *c-jun* are transcribed to the transcription factors Fos and Jun, respectively, which activate transcription of "late-response" genes, such as neurotransmitters. Modified from (Dampney & Horiuchi, 2003).

6.1.2 Benefits of using c-fos

There are a number of benefits of using c-fos as a marker of neuronal activation (Dampney & Horiuchi, 2003). Briefly, individual neurones can be identified by immunohistochemical staining for c-fos, and additionally population responses can be quantified. This is better than other techniques that typically allow for either population responses or individual responses, for example by 2-deoxy-D-glucose uptake or patch clamping, respectively.

Furthermore, the signal-to-noise ratio is good, as the basal levels of Fos are low but become highly expressed in response to stimulus. Fos can be used as a response in conscious mice; in fact, anaesthetics can reportedly cause high levels of background (Dampney *et al.*, 1995), so responses in conscious mice are preferable. Finally, and arguably the most significant benefit, is that it is possible to co-stain Fos against markers of neuronal cell types, for example it is possible to quantify neuronal responses in only catecholaminergic neurones (Yamamoto *et al.*, 2002).

6.1.3 Limitations of using c-fos

There are however a number of limitations to using Fos quantification. Not all neurones respond equally to stimulus, for example neurones in the substantia nigra apparently do not produce Fos at all (Dragunow & Faull, 1989). Additionally, strong and sustained stimulation of the neurone is required to produce a Fos response, which has a number of implications.

Firstly, it is possible that particular neurones are involved in a response, but the stimulus wasn't sustained enough to produce a Fos response. Secondly,

the hierarchy of response becomes unclear; it becomes challenging to differentiate between primary or secondary order neurones. Thirdly, the source of stimulus is unclear, for example because of converging pathways. A number of early-response genes have been investigated in this capacity, but Fos has been shown to provide the most reliable response (Lanteri-Minet *et al.*, 1994).

6.1.4 c-fos studies involving Exendin-4

A number of studies have investigated the c-fos responses to Exendin-4. Yamamoto *et al.* investigated the cardiovascular as well as neuronal c-fos responses to Exendin-4 (Yamamoto *et al.*, 2002). They showed that both peripheral and central injections of Exendin-4 caused a significant increase in blood pressure and heart rate in rats. They proceeded to investigate the c-fos responses to Exendin-4, and found that peripherally and centrally injected Exendin-4 resulted in similar activation of a number of brain regions involved in autonomic control, including the PVN, LC, NTS and AP, and the ventrolateral medulla (CVLM and RVLM).

Further investigations showed that Exendin-4 activated, among others, spinally-projecting catecholaminergic neurones of the medulla. Studies have since confirmed the overall c-fos results, particularly showing that the PVN, NTS and AP consistently respond to Exendin-4 (Baggio *et al.*, 2004; Baraboi *et al.*, 2011).

6.1.5 Aims

The aim of this chapter is to use Fos immunostaining to investigate neuronal activation in response to Exendin-4 with respect to absence of XLαs, focussing on the nucleus of the solitary tract (NTS) and area postrema (AP) in the hindbrain, and the paraventricular nucleus (PVN) and amygdala of the hypothalamus. It is expected that *Gnasxl* knockouts will have a greater neuronal response, particularly in regions crucial for SNS control such as the PVN. The c-fos responses specifically in XLαs-expressing neurones will also be investigated, in order to determine the involvement of XLαs in the hypersensitive heart rate response to Exendin-4.

6.2 Methods

Adult male *Gnasxl*$^{m+p-}$ knockout mice and wildtype siblings were injected ip with 50 µg/kg Exendin-4. 2 hours after injection, mice were terminally anaesthetised with pentobarbitone and then perfused with 4 % PFA. The brains were carefully removed and placed in 4 % PFA overnight at 4 °C then dehydrated in 30 % sucrose solution at 4 °C until they were cut on a cryostat to 12 µm. Sections were stored at -80 °C until use. To investigate the global change in number of c-fos responsive neurones, c-fos was stained by immunohistochemistry using low concentration 1° antibody Rabbit α c-fos (1:50k) and Vectastain biotinylated secondary antibody. This method was used to give strong staining (Vectastain) only in neurones that express high levels of c-fos (1:50k 1°). Numbers of c-fos positive nuclei were counted from 2-3 sections per regions, and quantified as numbers of positive cells per section per side.

c-fos responses in specific populations of neurones were investigated using immunofluorescence with higher concentration of 1° Rabbit α c-fos (1:2000) costained with Goat α XLαs (in wildtype mice only). Further details of all protocols can be found in Chapter 2.

6.3 Results

6.3.1 c-fos responses to Exendin-4 in *Gnasxl* knockout mice

c-fos responses to 50 µg/kg Exendin-4 were quantified by immunohistochemistry staining in *Gnasxl* knockouts and wildtype siblings.

6.3.1.1 Hindbrain c-fos responses

High levels of c-fos response were seen in both the area postrema (AP) and the medial nucleus of the solitary tract (mNTS), at approximately 7.6 mm caudal to Bregma, according to (Paxinos & Franklin, 2001). Typical c-fos responses to Exendin-4 for a wildtype and a knockout are shown in Figure 6.2A. There were no c-fos responses in response to saline (Figure 6.2B). Numbers of c-fos positive nuclei were quantified, and no significant difference was found between wildtypes and knockouts in either the mNTS (Figure 6.2C; 43 ±7 vs 30±9, WT vs KO, n=5) or the AP (Figure 6.2C; 26 ±3 vs 23 ±6, WT vs KO, n=5).

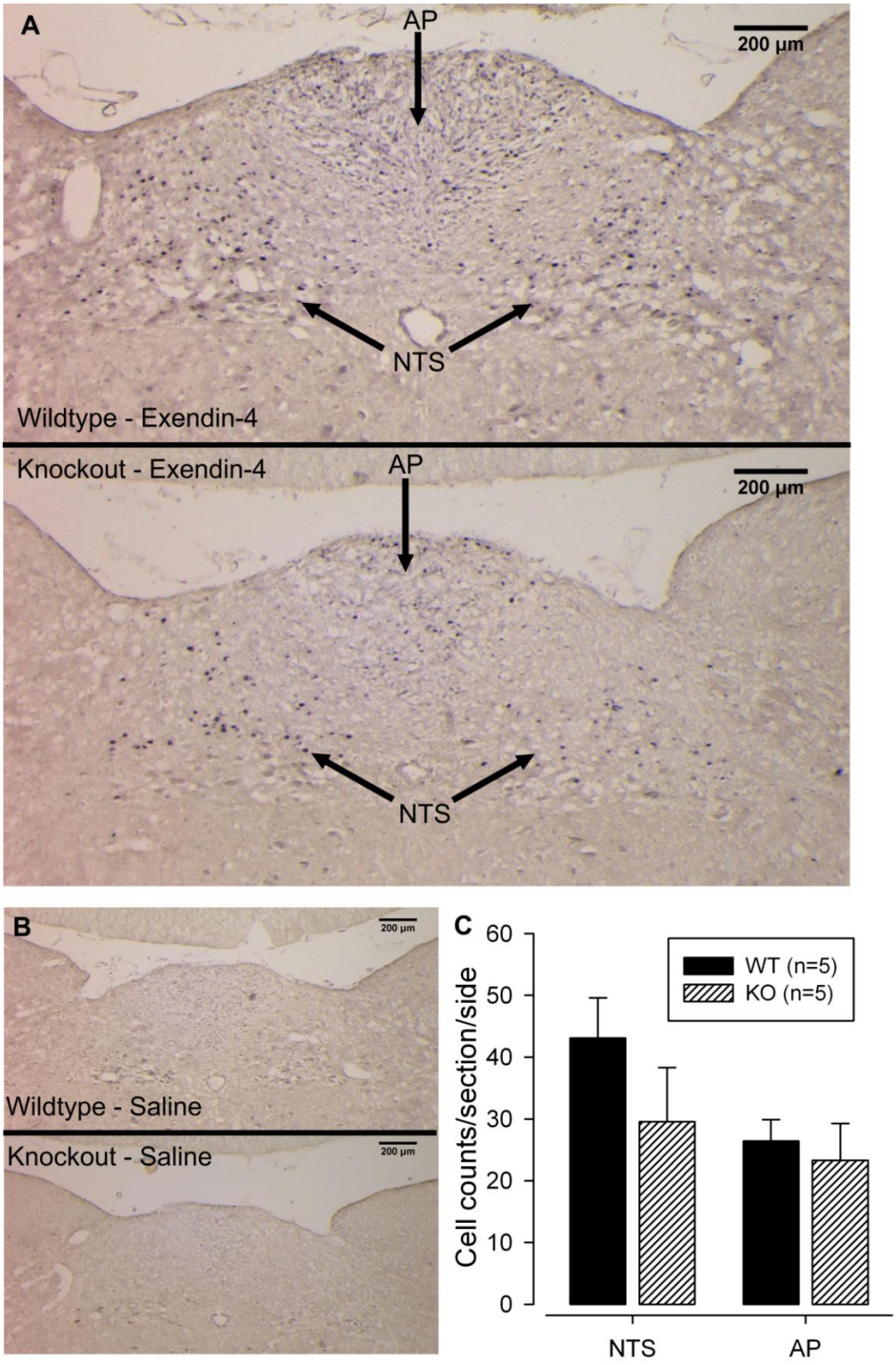

Figure 6.2. c-fos responses to Exendin-4 in the NTS and area postrema.
Neuronal c-fos responses 2 hours after injection of 50 µg/kg Exendin-4 ip in *Gnasxl* knockouts and wildtype siblings.
(A) Typical c-fos responses in wildtypes (WT) and knockouts (KO) in response to Exendin-4, at 7.6 mm caudal to bregma, according to (Paxinos & Franklin, 2001).
(B) Control stainings showing no c-fos responses to saline in WT or KO.
(C) Average c-fos counts for the nucleus of the solitary tract (NTS) and the area postrema (AP) around the coordinates shown.

6.3.1.2 Hypothalamic c-fos responses

High levels of c-fos response were seen in the paraventricular nucleus (PVN), at approximately 0.8 mm caudal to Bregma, according to (Paxinos & Franklin, 2001). Typical responses to Exendin-4 for a wildtype and a knockout are shown in Figure 6.3A. There were no c-fos responses in response to saline (Figure 6.3B). Numbers of c-fos positive nuclei were quantified, and no significant difference was found between wildtypes and knockouts (Figure 6.3C; 46 ±21 vs 37 ±8, WT vs KO, n=5).

The amygdala also showed distinctive c-fos responses, at approximately 0.9 mm caudal to Bregma, according to (Paxinos & Franklin, 2001). Typical responses to Exendin-4 for a wildtype and a knockout are shown in Figure 6.4A. There were no c-fos responses in response to saline (Figure 6.4B). Numbers of c-fos positive nuclei were quantified, and no significant difference was found between wildtypes and knockouts (Figure 6.4C; 24 ±8 vs 24 ±6, WT vs KO, n=5).

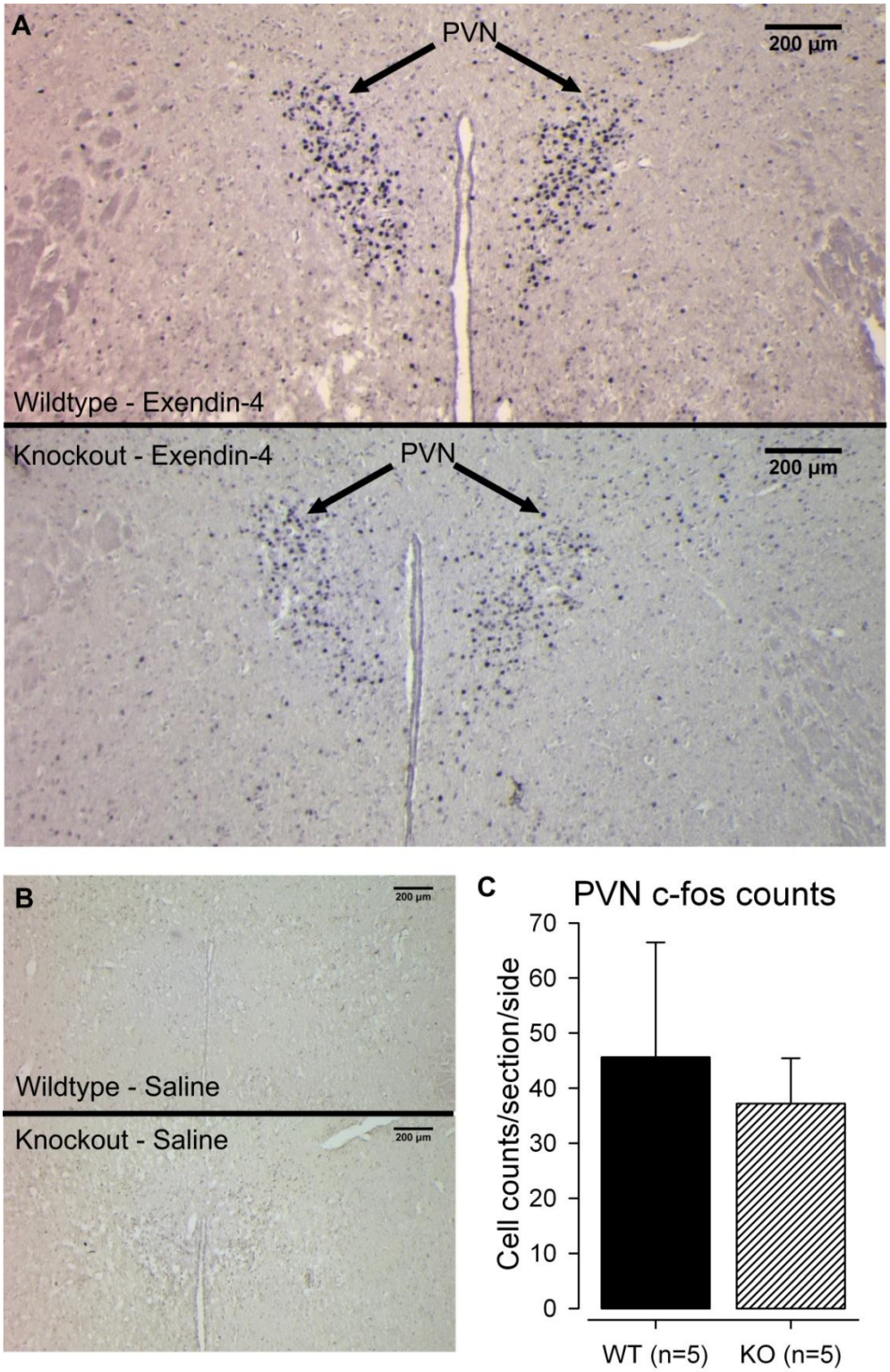

Figure 6.3. c-fos responses to Exendin-4 in the PVN.
Neuronal c-fos responses 2 hours after injection of 50 µg/kg Exendin-4 ip in *Gnasxl* knockouts and wildtype siblings.
(A) Typical c-fos responses in wildtypes (WT) and knockouts (KO) in response to Exendin-4, at 0.8 mm caudal to bregma, according to (Paxinos & Franklin, 2001).
(B) Control stainings showing no c-fos responses to saline in WT or KO.
(C) Average c-fos counts for the paraventricular nucleus (PVN) around the coordinates shown.

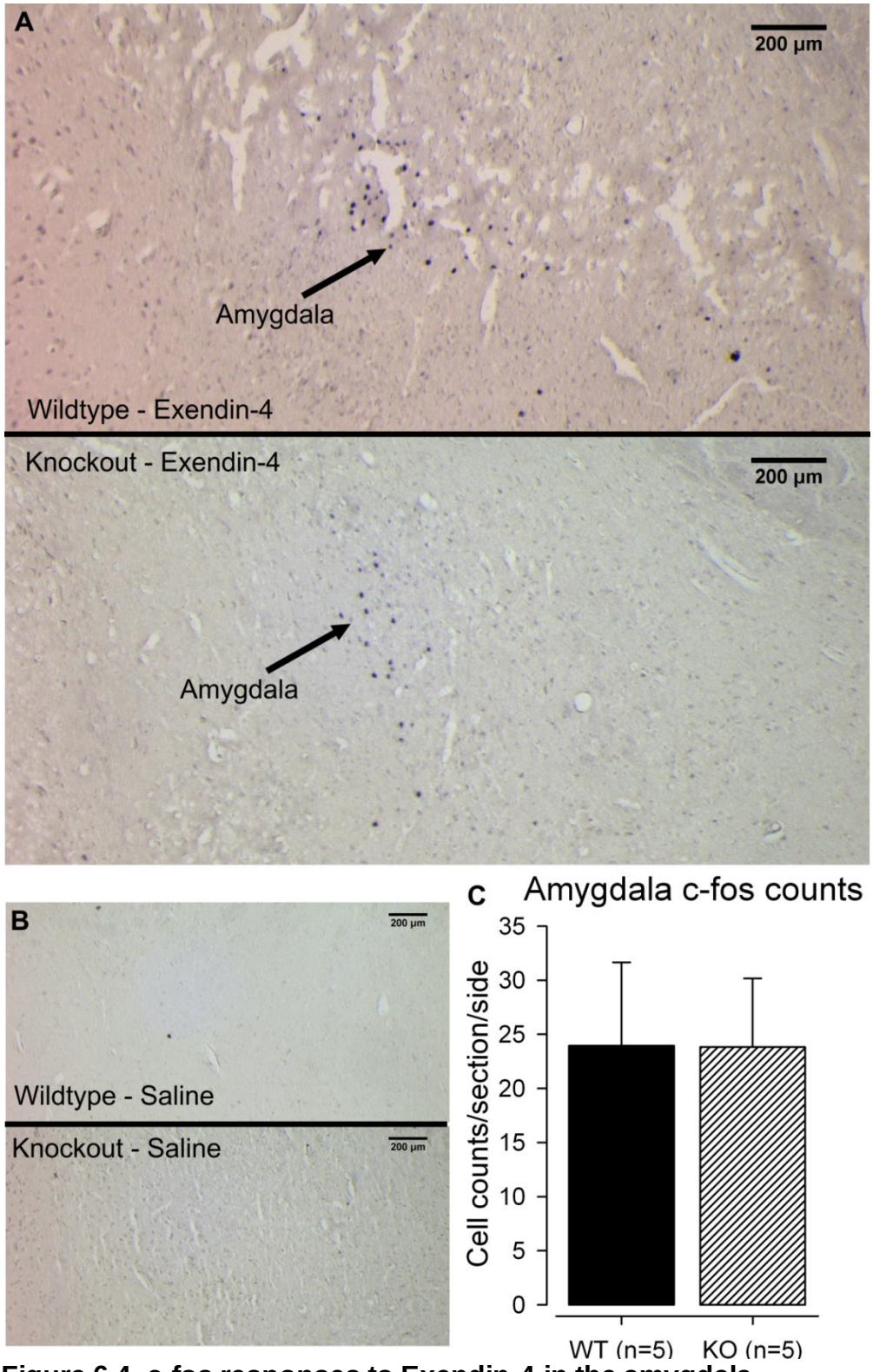

Figure 6.4. c-fos responses to Exendin-4 in the amygdala.
Neuronal c-fos responses 2 hours after injection of 50 µg/kg Exendin-4 ip in *Gnasxl* knockouts and wildtype siblings.
(A) Typical c-fos responses in wildtypes (WT) and knockouts (KO) in response to Exendin-4, at 0.9 mm caudal to bregma, according to (Paxinos & Franklin, 2001).
(B) Control stainings showing no c-fos responses to saline in WT or KO.
(C) Average c-fos counts for the amygdala around the coordinates shown.

6.3.2 c-fos responses to Exendin-4 in XLαs-expressing neurones

c-fos responses to 50 µg/kg Exendin-4 were quantified by immunofluorescence (IF) co-staining against XLαs.

6.3.2.1 Hindbrain c-fos responses in XLαs neurones

IF co-staining in the AP at approximately the same region as shown in the IHC staining showed that there were some c-fos positive XLαs neurones (Figure 6.5A). At the same caudal location, in the mNTS where there were many c-fos positive neurones and few XLαs-positive neurones, many of the XLαs neurones were positive for c-fos (Figure 6.6). However, more anterior in the NTS, at approximately 6.8 mm caudal to Bregma, where the majority of the XLαs-positive neurones of the NTS are to be found, there were few c-fos positive neurones, and no double positive cells (Figure 6.7).

6.3.2.2 Hypothalamic c-fos responses in XLαs neurones

There was a very interesting pattern in the PVN, where the XLαs-positive neurones are found around the periphery of the nucleus, and all the c-fos positive cells were found in the central area of the PVN (Figure 6.8A). In fact there was such a distinction in the populations of neurones that despite there being a large number of both there were no XLαs neurones positive for c-fos. This was also true in the amygdala, although there were fewer numbers of positive cells in this area (Figure 6.9A).

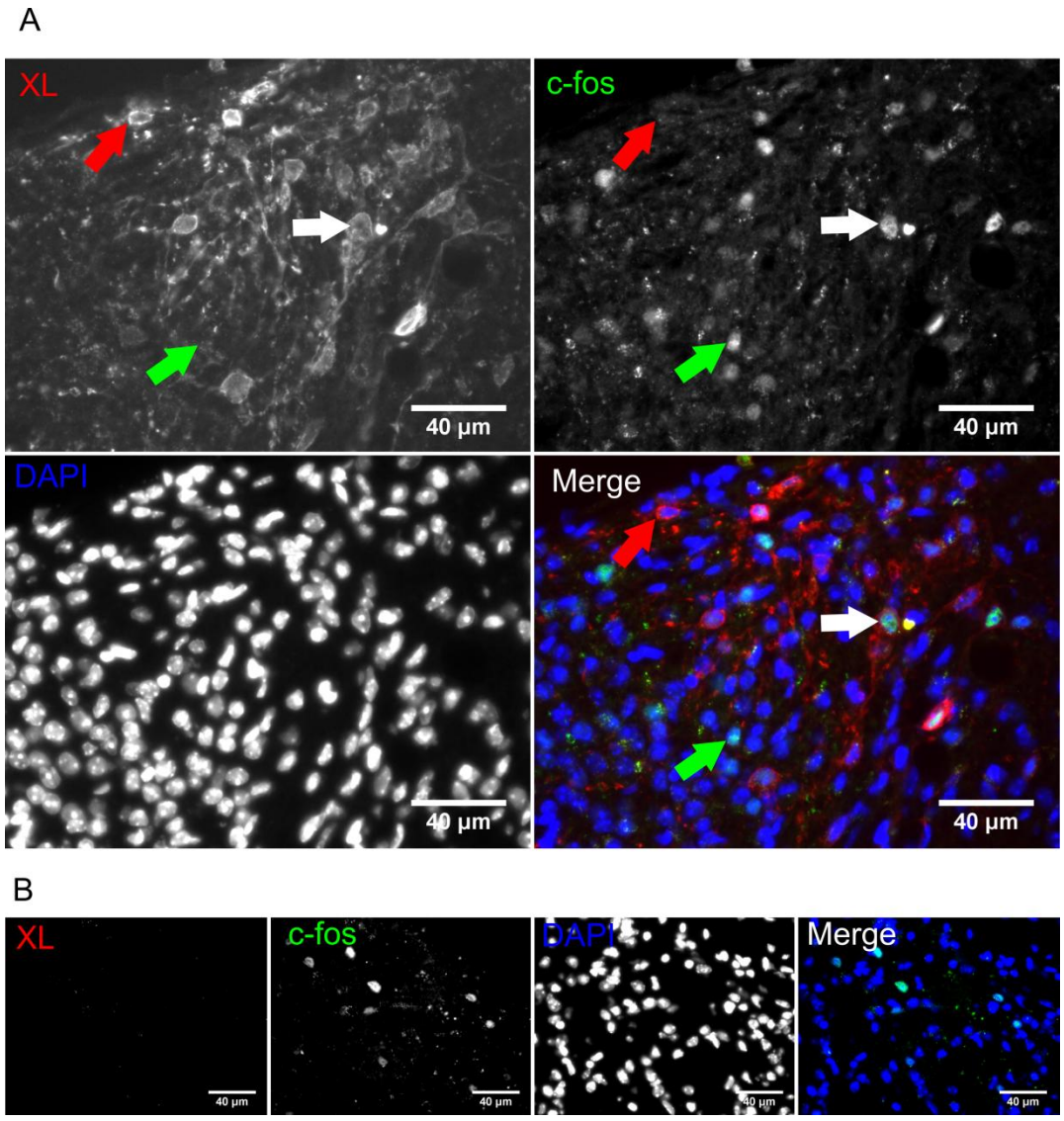

Figure 6.5. c-fos responses to Exendin-4 in XLαs-expressing neurones of the area postrema.

Neuronal c-fos responses 2 hours after injection of 50 µg/kg Exendin-4 ip in XLαs-expressing neurones.

(A) Typical c-fos response in the area postrema (AP) of a wildtype mouse, showing XLαs-expressing neurones (red), c-fos (green) and the nuclear stain DAPI (blue). Green arrow, neurone expressing c-fos; red arrow, neurone expressing XLαs; white arrow, neurone co-expressing c-fos and XLαs.

(B) Typical c-fos response in the same region of the AP in a *Gnasxl* knockout mouse, showing c-fos responses but no XLαs staining.

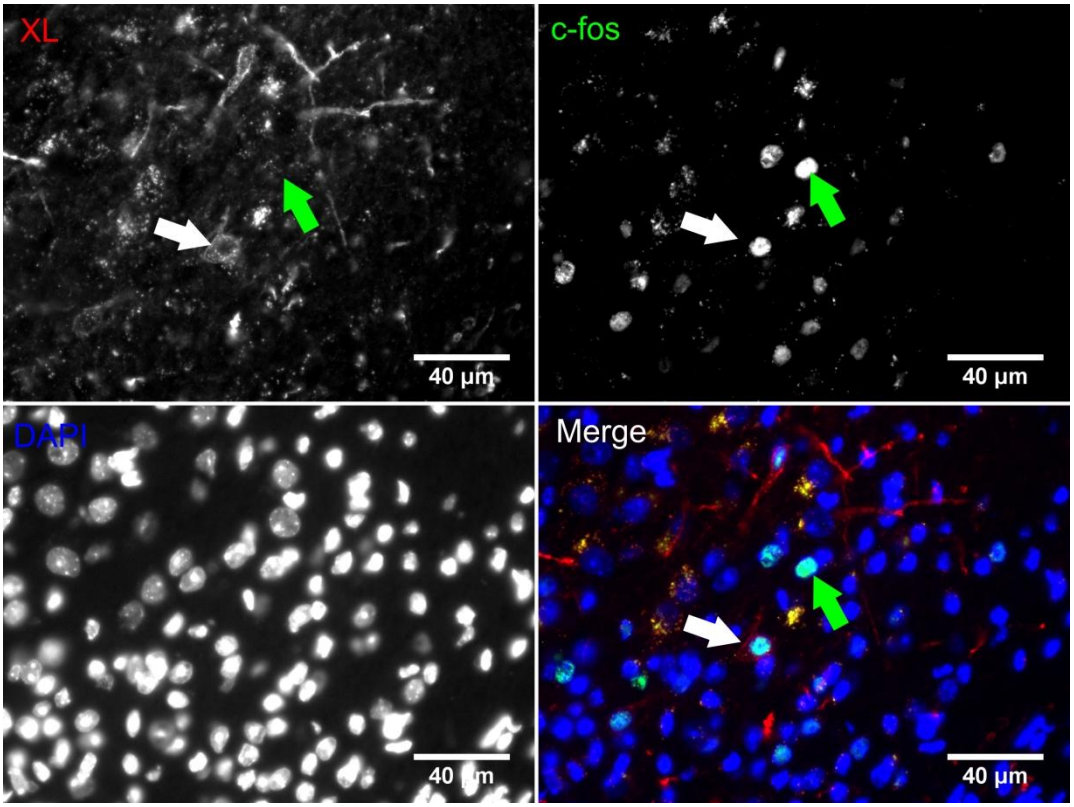

Figure 6.6. c-fos responses to Exendin-4 in XLαs-expressing neurones of the medial NTS.
Neuronal c-fos responses 2 hours after injection of 50 µg/kg Exendin-4 ip in XLαs-expressing neurones. Typical c-fos response in the medial region of the nucleus of the solitary tract (NTS) of a wildtype mouse, at approximately 7.6 mm caudal to Bregma according to (Paxinos & Franklin, 2001). Staining shows XLαs-expressing neurones (red), c-fos (green) and the nuclear stain DAPI (blue). Green arrow, neurone expressing c-fos; white arrow, neurone co-expressing c-fos and XLαs.

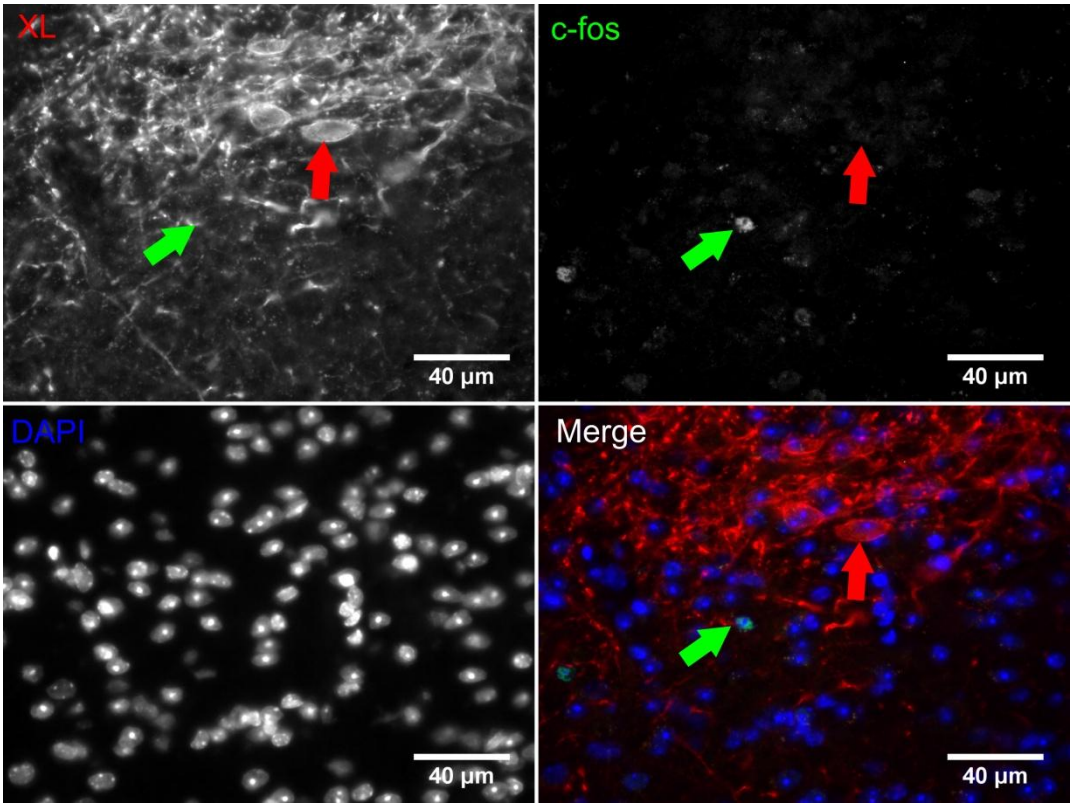

Figure 6.7. c-fos responses to Exendin-4 in XLαs-expressing neurones of the anterior NTS.
Neuronal c-fos responses 2 hours after injection of 50 µg/kg Exendin-4 ip in XLαs-expressing neurones. Typical c-fos response in the anterior region of the nucleus of the solitary tract (NTS) of a wildtype mouse, at approximately 6.8 mm caudal to Bregma according to (Paxinos & Franklin, 2001). Staining shows XLαs-expressing neurones (red), c-fos (green) and the nuclear stain DAPI (blue). Green arrow, neurone expressing c-fos; red arrow, neurone expressing XLαs.

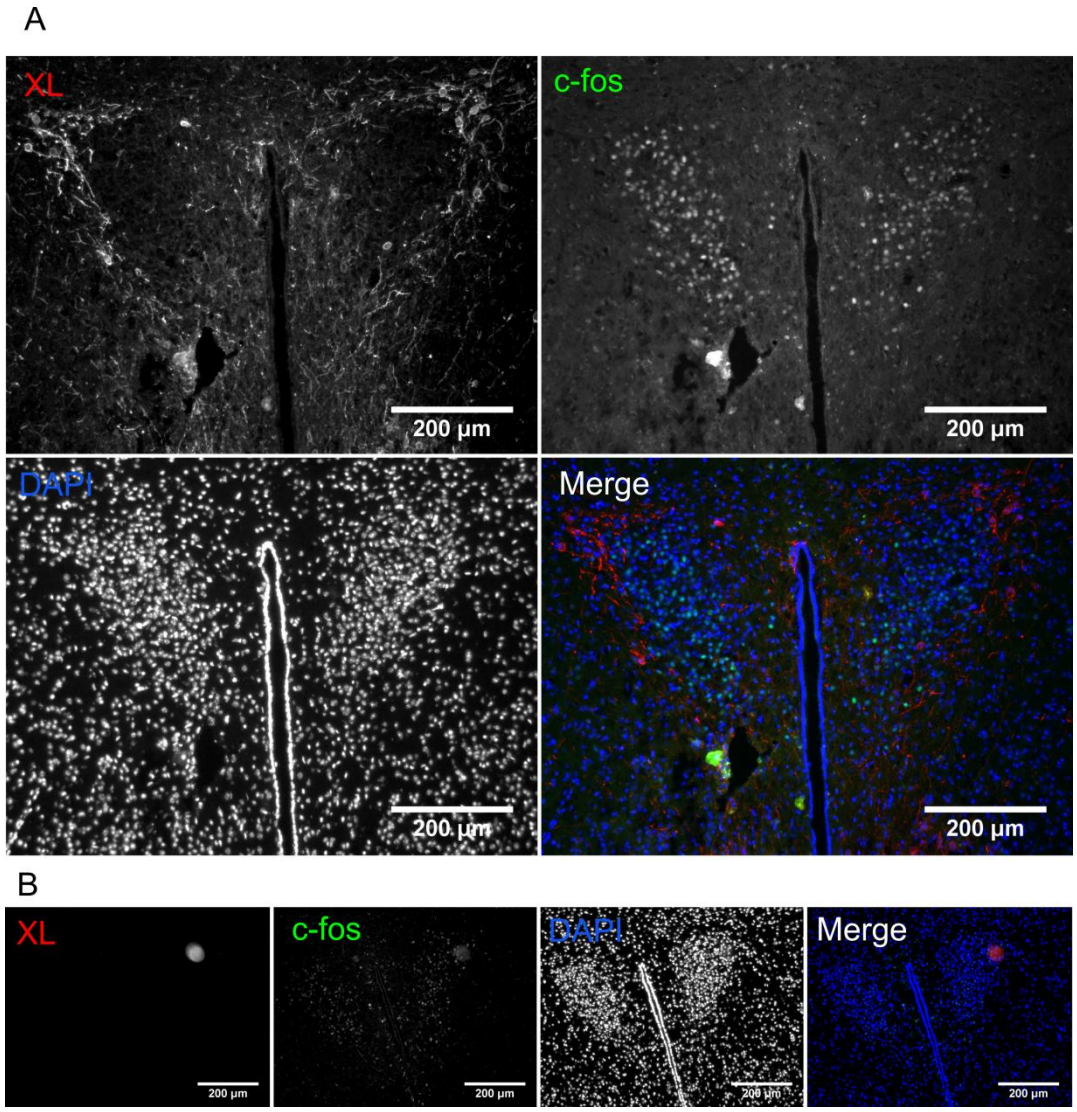

Figure 6.8. c-fos responses to Exendin-4 in XLαs-expressing neurones of the PVN.
Neuronal c-fos responses 2 hours after injection of 50 µg/kg Exendin-4 ip in XLαs-expressing neurones.
(A) Typical c-fos response in the paraventricular nucleus of the hypothalamus (PVN) of a wildtype mouse, showing XLαs-expressing neurones (red), c-fos (green) and the nuclear stain DAPI (blue).
(B) Typical c-fos response in the same region of the PVN in a *Gnasxl* knockout mouse, showing c-fos responses but no XLαs staining.

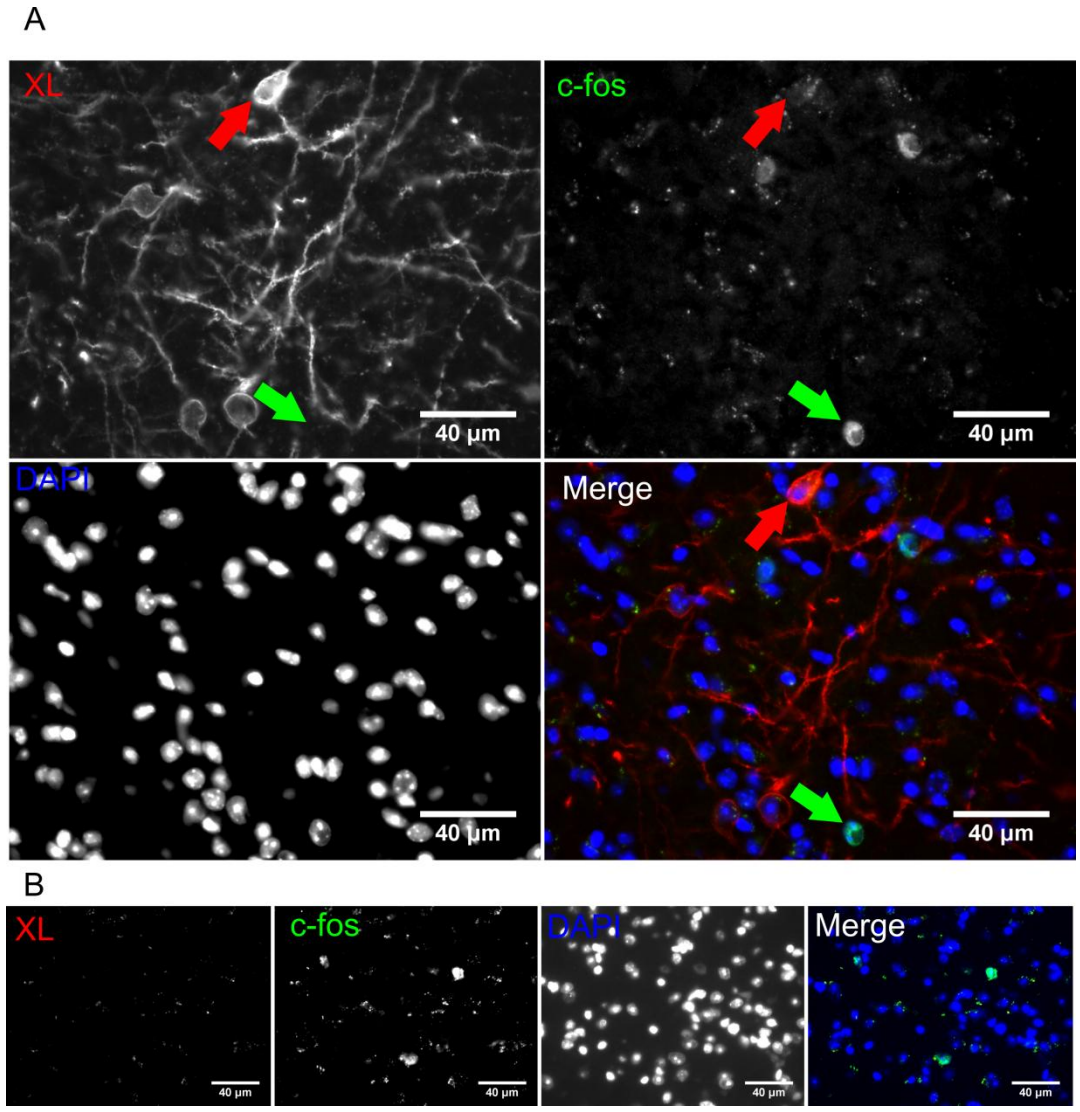

Figure 6.9. c-fos responses to Exendin-4 in XLαs-expressing neurones of the amygdala.
Neuronal c-fos responses 2 hours after injection of 50 µg/kg Exendin-4 ip in XLαs-expressing neurones.
(A) Typical c-fos response in the amygdala of a wildtype mouse, showing XLαs-expressing neurones (red), c-fos (green) and the nuclear stain DAPI (blue). Green arrow, neurone expressing c-fos; red arrow, neurone expressing XLαs.
(B) Typical c-fos response in the same region of the amygdala in a *Gnasxl* knockout mouse, showing c-fos responses but no XLαs staining.

6.4 Discussion

A number of previous studies have shown that peripheral injection of Exendin-4 consistently induces a c-fos response in a number of nuclei critical in the integration and control of SNS signalling, including the AP and NTS in the hindbrain, and the PVN and amygdala in the hypothalamus (Yamamoto *et al.*, 2002; Baggio *et al.*, 2004; Baraboi *et al.*, 2011). Robust c-fos responses were seen in all these nuclei in this study, with little difference in overall numbers of activated neurones between *Gnasxl* knockouts and wildtype siblings, except in the mNTS where there was a definite trend for a decrease in activated neurones in the knockouts (Figures 6.2-4). This is interesting in light of the hypersensitive cardiovascular response to Exendin-4 seen in the knockouts in Chapter 5, as one might expect an increase in neuronal activation in the knockouts; for example as seen in Baraboi *et al.* where higher doses of Exendin-4 injected resulted in increased responses of c-fos mRNA and physiological parameters (Baraboi *et al.*, 2011). Therefore, to investigate this further the c-fos response to Exendin-4 was examined specifically in XLαs-expressing neurones in wildtype mice.

The only region with any number of c-fos responsive XLαs neurones was the AP (Figure 6.5), although a couple of XLαs-positive neurones in the mNTS were also positive for c-fos (Figure 6.6). This suggests that XLαs might play a role in integration of the signal from Exendin-4, especially due to expression in the AP which is a circumventricular organ and can respond directly to circulating factors. However, in the more anterior NTS regions where XLαs expression is widespread, there were few activated neurones,

and no c-fos positive XLαs neurones (Figure 6.7), which would suggest that XLαs has little or no role to play in integration of vagal inputs via the NTS. However, this wouldn't discount a role of XLαs-expressing neurones in mediating inhibition of the parasympathetic neurones, which is a possible mechanism of cardiovascular control by Exendin-4 (Griffioen *et al.*, 2011), as neuronal inhibition doesn't stimulate a c-fos response (Dampney & Horiuchi, 2003).

The most interesting result was in the PVN, where XLαs is expressed around the periphery of the nucleus, and all the c-fos positive neurones were found in a distinct population in the centre of the PVN (Figure 6.8). This shows clear separation of the XLαs-positive PVN neurones from those that become activated in response to Exendin-4, which suggests that XLαs might play a secondary role in the signalling pathway. For example, there are known to be populations of GABAergic neurones in the PVN which supply inhibitory input to spinally-projecting SNS control neurones (for a review see (Nunn *et al.*, 2011)).

The lack of c-fos responses in XLαs-expressing neurones was also seen in the amygdala, where there was no overlap between XLαs-positive and c-fos responsive neurones (Figure 6.9). This suggests that XLαs-expressing neurones do not signal directly in a response pathway to activation of GLP-1R, but are instead found in a different pathway and affect downstream signalling independently.

7 Identification of a clone for generating a conditional *Gnasxl* knockout mouse

7.1 Introduction

A useful biological tool to study gene function is the generation of knockout mice. However, it has limitations, including potential early lethality for critical genes. This technology has been improved through the use of conditional targeting approaches, which typically involves the addition of flanking sequences to the region of interest that can then be acted upon by a recombinase to permanently remove the intervening DNA. A classic example is the cre-loxp recombination system.

7.1.1 cre-loxP mediated recombination

cre recombinase acts upon a pair of loxp recognition sites, which are 20-bp sequences that are recognised by the enzyme and undergo recombination (Lewandoski, 2001). This allows the production of conditionally targeted mice that have loxp sites recombinantly targeted to a gene or genetic region of interest; a conditionally targeted mouse should be functionally wildtype, but can be crossed with a mouse expressing cre under the control of a promoter of interest. This will then cause the DNA flanked by loxp sites to be

permanently cleaved out, but solely in those cells that express cre enzyme (Lewandoski, 2001).

However, there are complications with this technique, for example cre-expressing mice can have ectopic or “leaky” expression of cre enzyme, which would cause undesired recombination (Lewandoski, 2001). Additionally, as the target is permanently cleaved from the DNA, cre expression during embryonic development can result in widespread gene deletion in the adult.

The benefits of conditional targeting technology with respect to studying function of *Gnasxl* are abundant. Firstly, it will be possible to specifically delete *Gnasxl* in the brain, but not in peripheral tissues, providing final confirmation that the *Gnasxl*$^{m+p-}$ knockout phenotype is caused by central effects; this would be done using a nestin-cre mouse line (Tronche *et al.*, 1999). Secondly, it will be possible to knock out *Gnasxl* in particular populations of neurones, which would go a long way to narrowing down the site of action, and mechanism, of XLαs function. Targets of particular interest would be GABAergic neurones (using VGAT-cre) (Vong *et al.*, 2011) and PVN neurones (using Sim1-cre) (Balthasar *et al.*, 2005). The possibilities are diverse and ever-increasing as more cre lines are produced.

An additional benefit of conditional gene targeting technology is that it is possible to add a marker to the conditional allele that becomes expressed upon cre recombination (Livet *et al.*, 2007). Of particular interest is one of the wide range of fluorescent proteins that are currently available, as these will identify the neurones in brain slices, allowing patch clamping of only the

neurones of interest (Vong *et al.*, 2011). In addition, there are very good immunohistochemistry antibodies available against fluorescent proteins (Llewellyn-Smith *et al.*).

7.1.2 Conditional targeting of *Gnasxl*

In the case of *Gnasxl*, there is no possibility of a simple conditional targeting approach due to the highly complex nature of the regulation of *Gnasxl* expression, in particular the imprinting control region that is found in the early 5' region of *Gnasxl* and further upstream (Williamson *et al.*, 2006). It would therefore be essential to come up with a targeting strategy that doesn't affect this upstream control region. One such strategy is to use a conditional gene trap approach, which was placed downstream of *Gnasxl* exon 1 (Krechowec *et al.*, 2012).

The conditional gene trap approach uses 2 pairs of mutually incompatible loxp sites (Lee & Saito, 1998), which causes a permanent inversion of the intervening DNA sequence upon cre recombination (Krechowec *et al.*, 2012). It is called a gene trap because inversion of the intervening DNA activates a previously silent splice acceptor site that "captures" splicing from exon 1 of *Gnasxl* and is followed by a stop codon, resulting in premature termination of the protein.

The conditional *Gnasxl* gene-trap was unexpectedly found to cause an approximate 90 % knock-down of *Gnasxl*, resulting in a *Gnasxl* hypomorph that showed the characteristic knockout phenotype even in the "wildtype" un-recombined state (Krechowec *et al.*, 2012). This made it useless for investigating *Gnasxl* function, but the genetrap was constructed using a lacz

marker, which can be used to produce robust staining (XGal staining), and was used to give additional insight into the changing neonatal-to-adult phenotype of *Gnasxl* (Krechowec *et al.*, 2012). The knock-down effects to *Gnasxl* were found to be caused by the location of the inserted gene-trap (ie. in the A20 exon), which was known to be a rarely used splice acceptor site (Hayward *et al.*, 1998), but has since been shown to include enhancer functions for *Gnasxl* expression (unpublished data from other lab members).

7.1.3 Aims

Conditional targeting of *Gnasxl* is still of interest, so a new targeting approach was employed, where the targeting cassette was inserted much further downstream in the intron. Additionally the lacz marker was replaced with a red fluorescent protein, which would be of use for patch clamping experiments. The construct was transfected into mouse embryonic stem (ES) cells, and the aim of this chapter is to identify a correctly targeted ES cell clone using Southern blotting.

7.2 Methods

1152 ES cell colonies (ie. twelve 96-well plates) were placed in tail lysis buffer at 55 °C for 12 hours; DNA was extracted using isopropanol precipitation and ethanol cleaning, then dissolved in 50 µl TE. Once the DNA was fully dissolved, 20 µl was used in a Bgl II restriction enzyme digest overnight at 37 °C. Samples were run on a 0.8 % agarose gel for 18 hours at 40 V to give good separation of large (ie. more than 15 kb) DNA fragments. DNA was then transferred to a Hybond N^+ membrane (GE Healthcare) by semi-dry blotting for 48 hours. Details of the probes used are given below

(Table 7.1); details of probe hybridisation and colour development are given in Chapter 2.

Probe	Primers used	Probe size	Probe target
XL 5' 1	XL5' F1 and XL5' R2	425 bp	Region 5' of XL targeting cassette
XL 5' 2	XL5' F3 and XL5' R1	320 bp	Region 5' of XL targeting cassette
neo 1	neo F1 and neo R1	415 bp	neomycin resistance gene
neo 2	neo F2 and neo R2	470 bp	neomycin resistance gene

Table 7.1. Probes used for Southern blotting.
The primers used for each probe used in Southern blotting, as well as the size and target of each probe.

7.3 Results

1152 ES cell colonies were screened by Southern blot for correct insertion of the targeting cassette; two positive hits were then confirmed as being correctly targeted by blotting after restriction digest across the 5' and 3' homologous arms.

7.3.1 Screening ES cells colonies

7.3.1.1 Selecting restriction enzymes

Using the plasmid editing program ApE, the region of cassette insertion was screened for restriction enzymes that would cut genomic DNA outside of the homologous arms, but not within the arms or the insert itself. Bgl II was found to fit these criteria, producing a fragment of approximately 15.3 kb in the wildtype genome and 18.7 kb in the correctly targeted genome (Figure 7.1A).

7.3.1.2 Designing probes

Two probes were produced by Dig synth PCR, as described previously, using a plasmid containing the appropriate genomic DNA and the XL 5' probe primers (Table 7.1). Full details of the probes used are in Table 7.1 showing the size, target and primers used for each probe. The XL 5' probes were designed to bind between the Bgl II restriction site and the 5' homologous arm (Figure 7.1A).

7.3.1.3 Results from Southern blot screen

Of the 1152 clones screened, 2 positive hits were found (Figure 7.1B), both of which showed a second band at 18 kb that was not seen in any of the other samples.

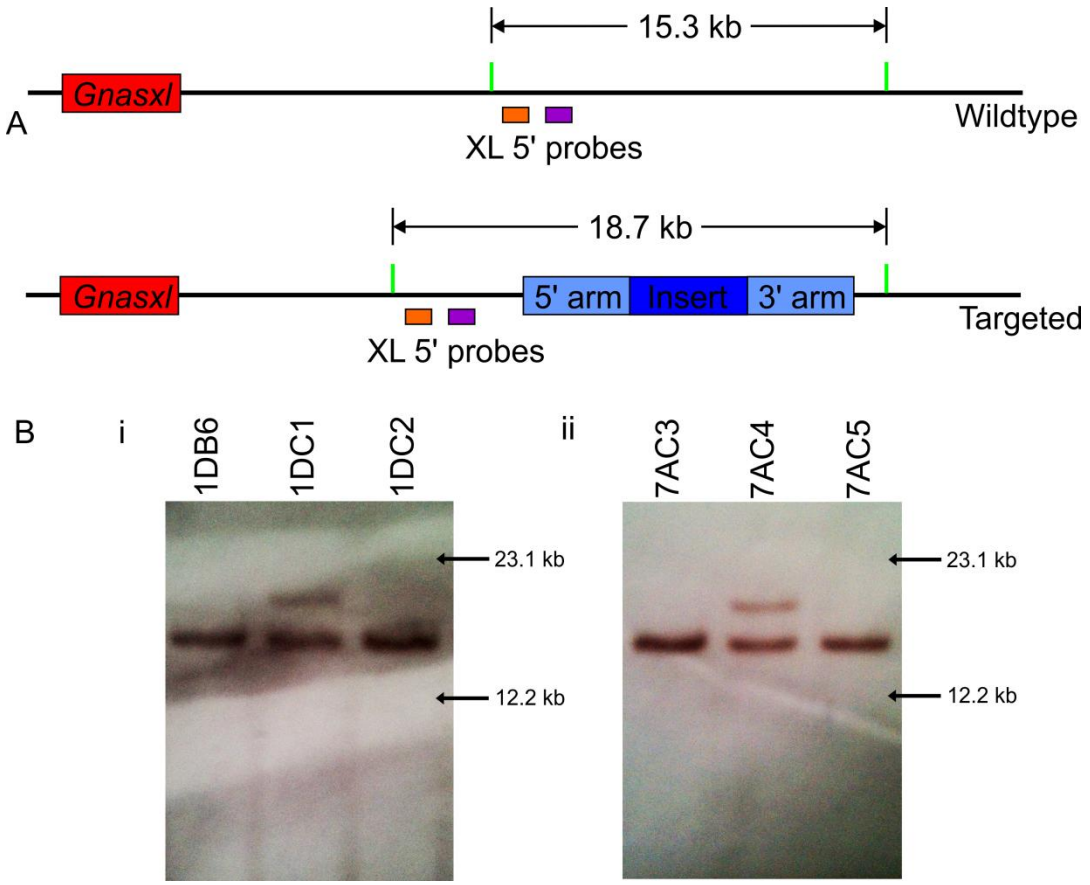

Figure 7.1. Southern blot screen for correctly targeted ES cell clones.
(A) Schematic showing restriction sites for Bgl II (green) in WT (top) and correctly targeted (bottom) genomic DNA. The probes used are shown in purple and orange, and the size of the visualised fragments is shown.
(B) Two positive hits were found in the screen: clones 1DC1 (i) and 7AC4 (ii), which are shown alongside the neighbouring, negative, samples.

7.3.2 Confirming hits from Southern blot screen

7.3.2.1 Selecting restriction enzymes

Using ApE, two restriction enzymes were found that would cut in one of the homologous arms on one side, and outside the homologous arms on the other side: Bgl I and Spe I, as shown in Figure 7.2A.

7.3.2.2 Designing probes

Two probes were produced by Dig synth PCR against the neomycin resistance gene, using an appropriate plasmid as target DNA. Full details of the probes used are in Table 7.1 showing the size, target and primers used for each probe.

7.3.2.3 Results from confirmatory Southern blot

Both of the positive hits from the ES cell screen were tested for correct insertion. Each sample was digested with Spe I and Bgl I in separate reactions. Each digest had a band in the expected position to confirm correct targeting (Figure 7.2B).

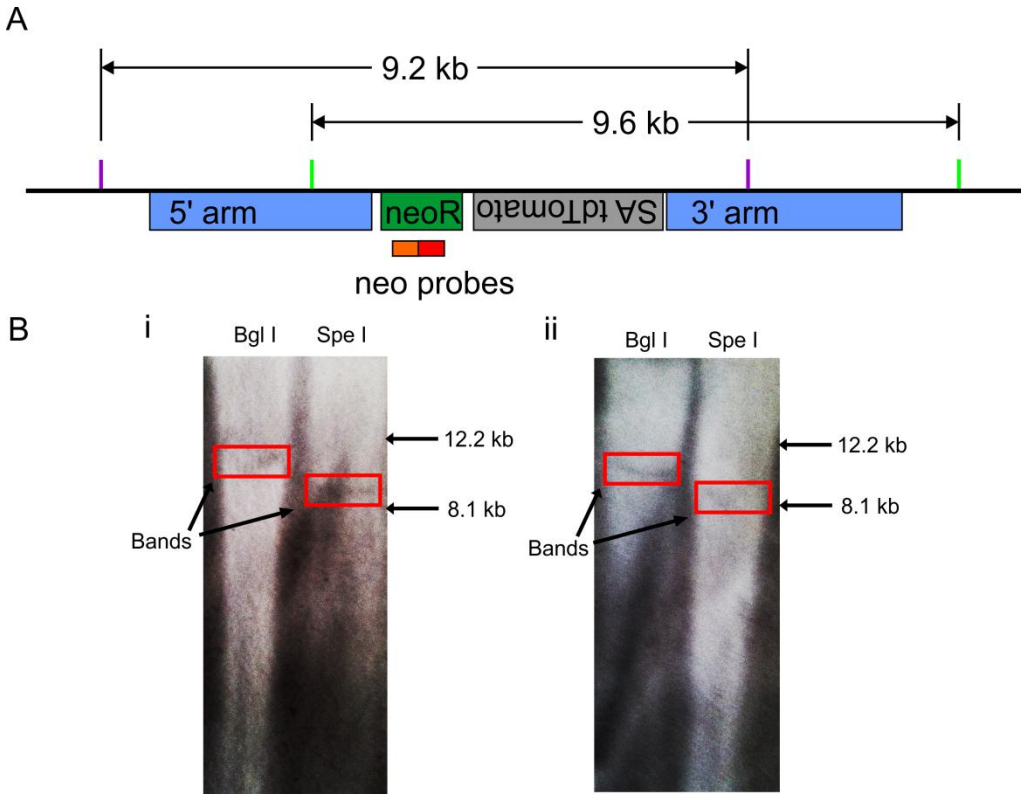

Figure 7.2. Confirmatory Southern blot of identified ES cell clones.
(A) Schematic showing restriction sites for Bgl I (green) and Spe I (purple) of a correctly targeted clone, showing a simplified targeting construct and surrounding genomic DNA. The probes used are shown in orange and red, and the size of the fragments, provided correct targeting, are shown. The construct contains an inverted splice acceptor (SA) before a red fluorescent protein (tdTomato), which are flanked by double loxp sites, which serve to invert the intervening DNA upon cre recombination, see Krechowec *et al.* for further information (Krechowec *et al.*, 2012). Loxp sites and flp sites have been omitted for clarity.
(B) (i) Clone 1DC1 and (ii) clone 7AC4 both had bands at the correct distance when digested with each Bgl I and Spe I.

7.4 Discussion

The aim of this chapter was to identify a correctly targeted ES cell clone that could be used to produce a conditional *Gnasxl* knockout mouse. This was done by Southern blot screening, and two clones were discovered (Figure 7.1). Confirmation was provided by an additional Southern blot using restriction enzymes chosen to test correct location of each homologous arm with respect to the surrounding genomic DNA (Figure 7.2).

The next step will be to culture the successful clones to produce colonies that could then be injected into blastocysts, which would be implanted into pseudopregnant females, and hopefully the modified genetic material be transmitted by chimaeras born via the gametes to produce a stable mouse line.

Further experiments would include conditionally knocking out *Gnasxl* in specific populations of neurones using cre-driver lines, for example in PVN neurones (Balthasar *et al.*, 2005). Additionally, due to the incorporation of a fluorescent protein marker in the gene trap, it will be possible to perform patch clamp experiments targeting those *Gnasxl* neurones that have been inactivated. Overall, this mouse line, when generated, will provide abundant exciting avenues for further experimentation.

8 Discussion

8.1 Autonomic control in mice lacking XLαs

A previous study suggested that *Gnasxl* knockout mice have a global increase in SNS activity (Xie *et al.*, 2006). Here it was shown that anaesthetised knockouts had elevated blood pressure (Figure 3.2), confirmed to be caused by increased SNS stimulation by injection of the sympatholytic reserpine (Figure 3.3). This was supported by elevated heart rate in conscious knockouts (Figure 3.5), and a significant heart rate response to reserpine (Figure 3.6). Interestingly, the knockouts also had a significant response to the parasympatholytic atropine (Figure 3.7), suggesting paradoxically that the knockouts had both increased SNS and PNS stimulation of the cardiovascular system.

A recent study by Gayen *et al.* investigated the role of the SNS in the hypertensive phenotype of the Chromogranin A knockout mouse (Gayen *et al.*, 2009). Mice lacking the secretory protein Chromogranin A have elevated levels of circulating catecholamines in plasma; this correlates to the elevated levels of excreted catecholamines seen in mice lacking XLαs (Xie *et al.*, 2006). Gayen *et al.* showed that the Chromogranin A knockout had elevated blood pressure and heart rate in conscious freely-moving conditions, but this difference was lost under anaesthesia. The authors suggest that this effect was caused by loss of the normally elevated SNS activity in the knockouts.

This situation could be recapitulated in the *Gnasxl* knockouts. The elevated blood pressure in knockouts could have been detected only because of the anaesthetic used and the dose-matching used in the cannulation experiment. Gayen *et al.* also investigated the heart rate changes to SNS and PNS inhibition of the cardiovascular system, by injection of propranolol and atropine, respectively. The Chromogranin A knockouts were found to be hypersensitive compared to wildtypes in response to both, similar to the effects seen in XLαs knockouts. Gayen *et al.* suggested that this hypersensitivity might be caused either by diminished baroreceptor function, or by heightened activity of both the SNS and PNS.

Cardiovascular control in *Gnasxl* knockouts was further investigated by HRV analysis using FFTs, which were validated in wildtype mice to give valid frequency ranges for HF power to indicate PNS activity and LF/HF ratio to indicate SNS activity (Figure 4.4). Following injection in conscious mice, *Gnasxl* knockouts had a greater LF/HF response to reserpine than wildtypes (Figure 4.7), but a similar HF power response to atropine (Figure 4.8). This implied that the increased blood pressure and heart rate in *Gnasxl* knockouts was caused by elevated SNS stimulation of the cardiovascular system; however, this does not discount other underlying mechanisms, for example changes to baroreflex function or the renin-angiotensin system.

Additionally, there was no change to PNS stimulation, suggesting that the heart rate response to atropine may have been a result of heightened SNS stimulation. However, baroreceptor function was not investigated; as suggested by Gayen *et al.* diminished baroreceptor function might give the cardiovascular responses seen.

8.2 Neuronal signalling via XLαs

The possible signalling pathways involved in XLαs control of the cardiovascular system was investigated by injection of melanocortin and GLP-1R agonists. Knockouts had a hypersensitive heart rate response both to centrally injected MTII in anaesthetised mice (Figure 5.2) and peripherally injected Exendin-4 in conscious mice (Figure 5.6). Further analysis of HRV indicated that Exendin-4 caused a highly significant decrease in HF power in both wildtypes and knockouts (Figure 5.8), suggesting the hypersensitive heart rate response may be caused in a similar way to the response to atropine. For a summary of the physiological parameters and responses in *Gnasxl* knockouts measured in this study, see Table 8.1.

Treatment	Method	Parameter	Result	Figure
Basal	Cannulation	BP	↑in KO	3.3
		HR	no significant difference	3.3
		T_b	↑in KO	3.9
	Telemetry	HR	↑in KO at night	3.6
		Activity	no significant difference	3.6
	HRV (FFT)	LF/HF	↑in KO at night	4.9
		HF	no significant difference at night	4.9
Reserpine	Cannulation	BP	greater ↓ in KO	3.4
	Telemetry	HR	greater ↓ in KO	3.7
	HRV (FFT)	LF/HF	greater ↓ in KO	4.7
Atropine	Telemetry	HR	greater ↑ in KO	3.8
	HRV (FFT)	HF	equivalent ↓ in WT and KO	4.8
MTII/Ro27	Cannulation	BP	no significant difference	5.1
		HR	↑response in KO	5.2
	Telemetry	HR	no significant difference	5.3
Exendin-4	Cannulation	BP	no significant difference	5.4
		HR	↑response in KO	5.5
	Telemetry	HR	greater ↑ in KO	5.6
	HRV (FFT)	LF/HF	no significant difference	5.7
		HF	equivalent ↓ in WT and KO	5.8
	c-fos	AP	equivalent ↑ in WT and KO	6.2
		NTS	equivalent ↑ in WT and KO	6.2
		PVN	equivalent ↑ in WT and KO	6.3
		Amygdala	equivalent ↑ in WT and KO	6.4

Table 8.1. Summary of physiological data.
Basal physiological parameters and responses to treatment in adult *Gnasxl* knockouts and wildtype siblings.

The earlier part of this study showing elevated SNS stimulation of the cardiovascular system in *Gnasxl* knockouts was interesting as it confirmed a previous hypothesis that the mice have a systemic increase in SNS activity, as well as providing further evidence of the opposite phenotypes between mice lacking $G_s\alpha$ and those lacking XLαs. The opposing phenotypes of *Gnasxl* and *Gnas* knockouts were further supported by the hypersensitive heart rate response of *Gnasxl* to the MC4R agonist MTII, as mice lacking $G_s\alpha$ are resistant to MTII. Furthermore, the hypersensitive heart rate response to Exendin-4 suggests that the hypersensitivity to SNS-stimulating neuropeptides may be a common phenotype in *Gnasxl* knockouts.

Neuronal signalling responses to Exendin-4 were investigated by immunohistochemistry staining for c-fos, which showed similar responses between wildtypes and knockouts in a number of brain regions involved in SNS control of the cardiovascular system (Figures 6.2-4). Interestingly, although XLαs was expressed in a number of the brain regions that responded to Exendin-4, the only response in XLαs positive neurones was in NTS regions with few XLαs neurones and in the AP. Any c-fos response in XLαs-expressing neurones was conspicuously absent in the hypothalamus, specifically in the PVN and the amygdala. These data suggest that XLαs might function via a secondary effect to increase sensitivity of downstream signalling pathways.

A possible mechanism of XLαs action is shown in Figure 8.1, which proposes that XLαs is expressed in neurones secondary to the main action of GLP-1R (or other neuropeptide) pathways. Of particular interest is the expression of XLαs in a population of PVN neurones adjacent to many Exendin-4-

responsive neurones. This suggests that XLαs might provide tonic inhibitory input to downstream SNS control neurones, for example via GABA. A previous study showing the ability of XLαs to continue signalling at the plasma membrane longer than $G_s\alpha$ might even suggest a mechanism for how these neurones remain tonically active (Liu *et al.*, 2011). Loss of XLαs would therefore result in a decrease in tonic GABA release, resulting in hyperactive and hypersensitive downstream SNS control neurones.

The hypersensitivity of *Gnasxl* knockouts to agonists for GLP-1R and MC4R suggests a second mechanism in which *Gnasxl* acts in inhibitory neurones to dampen SNS outflow, separate from the main GLP-1 or melanocortin signalling pathways (Figure 8.2). In this scheme, loss of XLαs would result in constitutively elevated SNS outflow, as well as increasing sensitivity to GLP-1R or MC4R agonists, but only by indirect means.

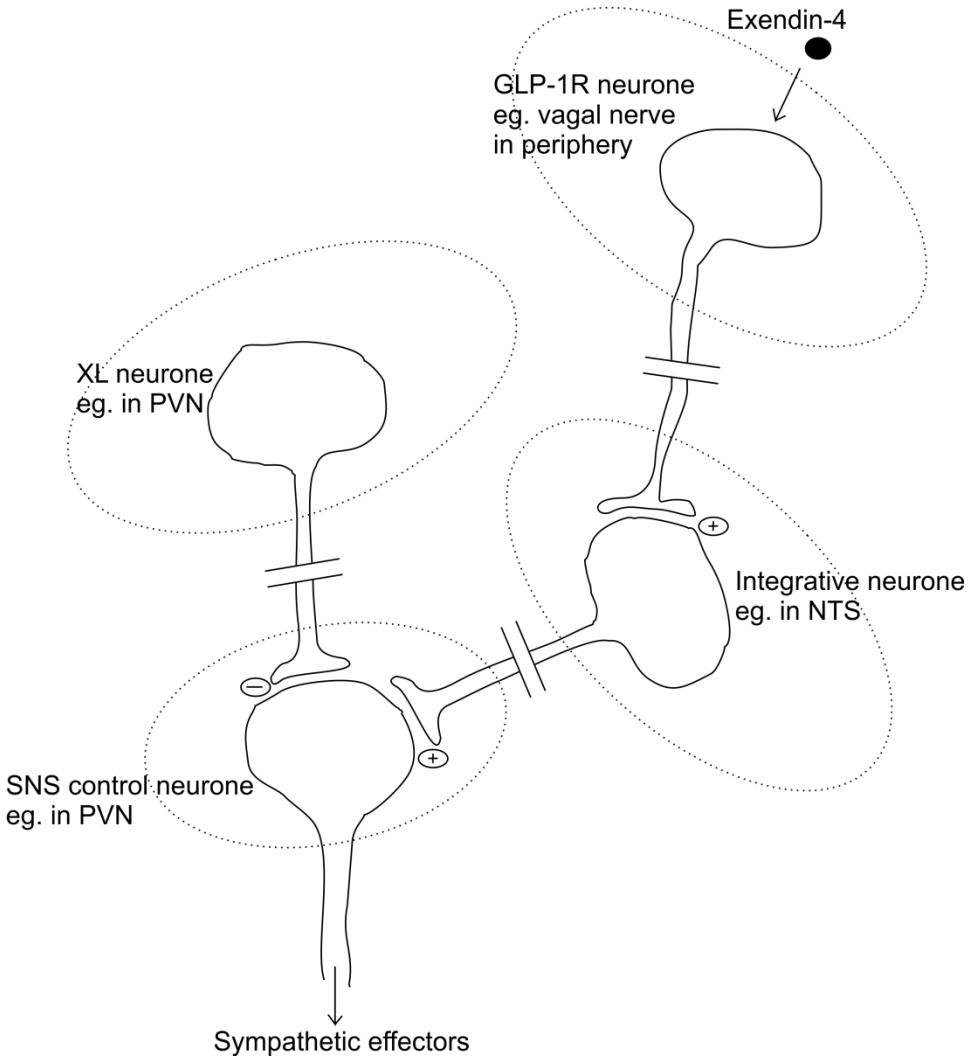

Figure 8.1. Scheme depicting how XLαs might signal in response to Exendin-4: part I.
In this scheme, XLαs is expressed in a PVN neurone that is separate to the main GLP-1R signalling pathway. The XLαs-expressing neurone provides a separate input to the same downstream SNS control neurones, possibly by constitutive inhibitory activity. In this way, loss of XLαs could result in chronically elevated SNS activity, as well as a hypersensitive response to Exendin-4 without resulting in activation of XLαs neurones.

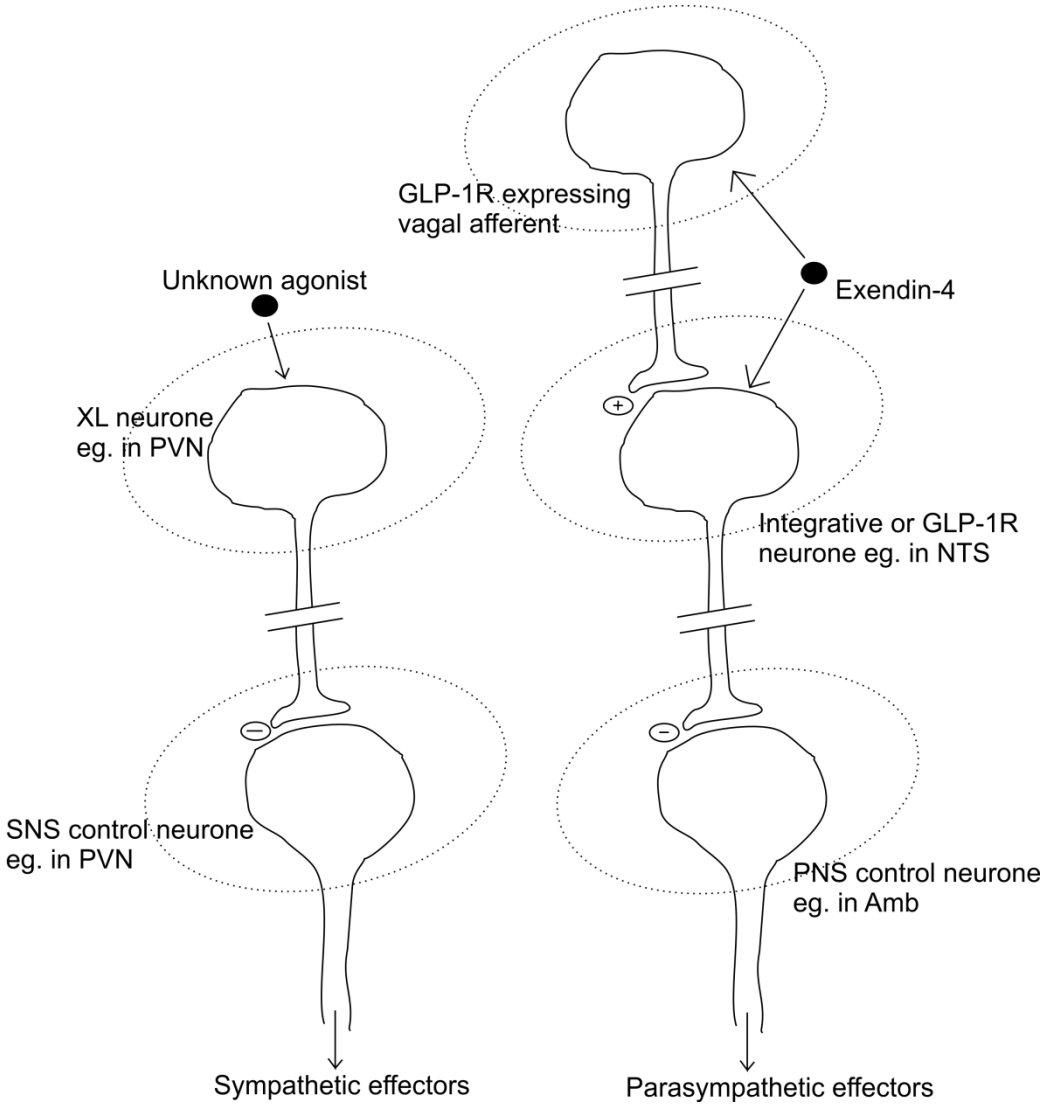

Figure 8.2. Scheme depicting how XLαs might signal in response to Exendin-4: part II.
In this scheme, XLαs is expressed in a pathway that inhibits SNS outflow, but is completely separate from the pathway that mediates the response to Exendin-4. The hypersensitivity to Exendin-4 in *Gnasxl* knockouts is caused by the dominant effect of heightened SNS outflow after inhibition of the PNS by Exendin-4.

8.3 Speculative discussion

8.3.1 Future work

This study poses many interesting questions about the mechanism by which XLαs functions. Although it suggests a secondary, or at least inhibitory, mechanism of some kind, there is still much that remains unknown. An interesting follow-up experiment would be to perform the IF co-localisation of c-fos response to Exendin-4 in *Gnasxl* knockouts with a marker for XLαs neurones. In this way, it would be possible to determine whether loss of XLαs changes the signalling behaviour of neurones that normally express it. This would be possible using a conditional knockout, similar to that described in chapter 7, which expresses a marker in neurones that have had XLαs knocked out.

There are a number of directions in which this work could be further investigated. Firstly would be the use of conditional knockouts for *Gnasxl*, which was the driving force behind Chapter 7. For example, it would be very interesting to knock out XLαs in GABAergic neurones, because the data shown here suggest that XLαs functions in an inhibitory manner. There are also strong indications that GABA signalling plays a major role in control of energy balance and in SNS control (Vong *et al.*, 2011).

Secondly would be patch clamp electrophysiology. Again, an interesting course of action would be to investigate GABAergic signalling, for example, GABAergic control of spinally-projecting neurones of the PVN. This could be done by recording electrophysiologically from retrogradely-labelled sympathetic-projecting neurones of the PVN. The other main

electrophysiology route would be using mouse models with GFP-labelled neurone populations. For example, using mice with fluorescently labelled GABA-ergic neurones, as these are likely to behave differently in mice lacking XLαs. Ideally, one would want to record from identified XLαs neurones, which would require the generation of a knockin mouse line expressing fluorescent proteins under the control of the *Gnasxl* promoter. However, this would enable a researcher to test what XLαs-expressing neurones responds to (eg. neuropeptides such as GLP-1 or metabolic signals such as glucose).

Thirdly, it would be interesting to use *in situ* hybridisation to investigate orphan GPCRs that might couple to XLαs. For example, the orphan receptor Gpr101 has been shown to have an expression pattern almost identical to XLαs, and is likely to influence cAMP signalling (Bates *et al.*, 2006). Provided a likely GPCR could be identified, this could be followed up by a knockout mouse specific to that receptor, and further studies involving double knockouts or targeted knockouts using a *Gnasxl*-cre line.

An interesting feature of the $G_s\alpha$ mutations is the dose-dependent aspect of the phenotype. Paternally inherited *Gnas* mutations cause AHO in human patients, and a similar phenotype in mice, even though there is heterozygous expression of $G_s\alpha$. Additionally, the recent paper by Fernandez-Rebollo et al. suggests that there is a dose-dependent effect of XLαs (Fernandez-Rebollo *et al.*, 2012). It would be interesting to investigate the effect of XLαs over-expression in adults, to see if this recapitulates the XLαs knockout phenotype (as suggested by the Fernandez-Rebollo paper), and whether the signalling effects are the same as seen in the knockouts, ie. would XLαs

overexpression result in elevated SNS activity and hypersensitivity to Exendin-4?

8.3.2 Broader implications

There is no direct medical relevance for this work, as there is no known pathology associated with mutation of XLαs in humans – although it is possible that the leanness and poor suckling behaviour associated with this mutation goes unnoticed in the clinical setting. However, due to the highly conserved nature of the *Gnas* locus, and the similarities in the effects of $G_s\alpha$ mutation between humans and mice, it seems likely that XLαs exerts effects in humans. This would make it an attractive drug target, as selective inhibition of XLαs would almost certainly results in reproducing the effects of the knockout, ie. to drastically increase energy expenditure and improve glucose tolerance, which would benefit obese patients.

The most interesting aspect of this work is the link between XLαs and hypersensitivity to Exendin-4. As mentioned earlier, Exendin-4 is in clinical use to improve management of type 2 diabetes. If the hypersensitivity in response to inhibition of XLαs was also seen in humans, this might make an XLαs antagonist additionally effective by improving the responsiveness to Exendin-4.

This work also provides the first, albeit indirect, evidence for a mechanism for the action of XLαs *in vivo*. It suggests an inhibitory role of XLαs-expressing neurones separate from the main pathways of metabolism and cardiovascular control via central neuropeptide signalling pathways. The expression pattern of XLαs in the PVN in the particular suggests these

neurones might be involved in tonic suppression of the SNS output, so an antagonist would result in both elevated SNS control of metabolism and hypersensitivity to the normal homeostatic control mechanisms.

In summary, this work provides insight into the little-known effects of the signalling protein XLαs and provides a platform for exciting further avenues of research.

Appendix

Publications from this work:

1. Nunn N, Womack M, Dart C, & Barrett-Jolley R (2011) Function and Pharmacology of Spinally-Projecting Sympathetic Pre-Autonomic Neurones in the Paraventricular Nucleus of the Hypothalamus. *Curr.Neuropharmacol.* **9**(2)**:** 262-277

2. Krechowec S, Burton K, Newlaczyl A, Nunn N, Vlatkovic N, & Plagge A (2012) Postnatal changes in the expression pattern of the imprinted signalling protein XLαs underlie the changing phenotype of deficient mice. *PLoS ONE* **7**(1): e29753

3. Nunn N, Feetham C, Plagge A, & Barrett-Jolley R (2012) Deregulated autonomic control causes elevated blood pressure, heart rate and body temperature in mice lacking the XLαs protein of the *Gnas* locus. *PLoS ONE* (Under Review)

Abstracts from this work:

1. Nunn N, Barrett-Jolley R, & Plagge A (2009) Brown adipose tissue development and cardiovascular parameters in Gnasxl knock-out mice. *Proceedings of the British Pharmacological Society* **7**(3): 49P

2. Burton K, Nunn N, Krechowec S, Barrett-Jolley R & Plagge A (2010) Hypothalamic expression pattern and molecular and physiological markers indicate elevated sympathetic stimulation of metabolism in XLαs-deficient mice. Co-author and co-presenter of a poster

presented at the *Physiological Society meeting for Metabolism and Endocrinology*

3. Nunn N, Feetham CH, Barrett-Jolley R, & Plagge A (2011) Loss of the imprinted signalling protein XLαs in mice results in increased sympathetic stimulation of the cardiovascular system. Oral presentation to *22nd Mammalian Genetics and Development Workshop.* Published in *Genetical Research* **94**(1): 51-52

4. Nunn N, Feetham CH, Plagge A, & Barrett-Jolley R (2011) Investigation of cardiovascular parameters as indicators of sympathetic activity in lean and hypermetabolic gnasxl knock-out mice. *Proceedings of the Physiol Society* **23:** PC27

5. Nunn N, Feetham CH, Plagge A, & Barrett-Jolley R (2012) Hypermetabolic *Gnasxl* knock-out mice have increased sympathetic control of heart rate variability. *Proceedings of the Physiol Society* **27**: PC226

References

Adan RA, Cone RD, Burbach JP & Gispen WH (1994). Differential effects of melanocortin peptides on neural melanocortin receptors. *Mol Pharmacol* 46, 1182-1190.

Akselrod S, Gordon D, Ubel FA, Shannon DC, Berger AC & Cohen RJ (1981). Power spectrum analysis of heart rate fluctuation: a quantitative probe of beat-to-beat cardiovascular control. *Science* 213, 220-222.

Anand BK & Brobeck JR (1951). Localization of a "feeding center" in the hypothalamus of the rat. *Proc Soc Exp Biol Med* 77, 323-324.

Andresen M & Paton J (2011). The nucleus of the solitary tract: processing information from viscerosensory afferents. *Central regulation of autonomic functions.* 2nd edition, 23-46.

Baggio LL, Huang Q, Brown TJ & Drucker DJ (2004). Oxyntomodulin and glucagon-like peptide-1 differentially regulate murine food intake and energy expenditure. *Gastroenterology* 127, 546-558.

Bakris GL & Frohlich ED (1989). The evolution of antihypertensive therapy: an overview of four decades of experience. *J Am Coll Cardiol* 14, 1595-1608.

Balthasar N (2009). Feeding signals to the hungry mind. *Exp Physiol* 94, 857-866.

Balthasar N, Dalgaard LT, Lee CE, Yu J, Funahashi H, Williams T, Ferreira M, Tang V, McGovern RA, Kenny CD, Christiansen LM, Edelstein E, Choi B, Boss O, Aschkenasi C, Zhang CY, Mountjoy K, Kishi T, Elmquist JK & Lowell BB (2005). Divergence of melanocortin pathways in the control of food intake and energy expenditure. *Cell* 123, 493-505.

Baraboi ED, St-Pierre DH, Shooner J, Timofeeva E & Richard D (2011). Brain activation following peripheral administration of the GLP-1 receptor agonist exendin-4. *Am J Physiol Regul Integr Comp Physiol* 301, R1011-1024.

Barrucha AE, Charkoudian N, Andrews CN, Camilleri M, Sletten D, Zinsmeister AR & Low P (2008). Effects of glucagon-like peptide-1, yohimbine, and nitrergic modulation on sympathetic and parasympathetic activity in humans. *Am J Physiol Regul Integr Comp Physiol* 295, R874-R880.

Bastepe M, Gunes Y, Perez-Villamil B, Hunzelman J, Weinstein LS & Juppner H (2002). Receptor-mediated adenylyl cyclase activation through XLalpha(s), the extra-large variant of the stimulatory G protein alpha-subunit. *Molecular Endocrinology* 16, 1912-1919.

Bates B, Zhang L, Nawoschik S, Kodangattil S, Tseng E, Kopsco D, Kramer A, Shan Q, Taylor N, Johnson J, Sun Y, Chen HM, Blatcher M, Paulsen JE & Pausch MH (2006). Characterization of Gpr101 expression and G-protein coupling selectivity. *Brain Res* 1087, 1-14.

Baudrie V, Laude D & Elghozi JL (2007). Optimal frequency ranges for extracting information on cardiovascular autonomic control from the blood pressure and pulse interval spectrograms in mice. *Am J Physiol Regul Integr Comp Physiol* 292, R904-912.

Belle MD, Diekman CO, Forger DB & Piggins HD (2009). Daily electrical silencing in the mammalian circadian clock. *Science* 326, 281-284.

Benoit SC, Schwartz MW, Lachey JL, Hagan MM, Rushing PA, Blake KA, Yagaloff KA, Kurylko G, Franco L, Danhoo W & Seeley RJ (2000). A novel selective melanocortin-4 receptor agonist reduces food intake in rats and mice without producing aversive consequences. *J Neurosci* 20, 3442-3448.

Brito MN, Brito NA, Baro DJ, Song CK & Bartness TJ (2007). Differential activation of the sympathetic innervation of adipose tissues by melanocortin receptor stimulation. *Endocrinology* 148, 5339-5347.

Brobeck JR (1946). Mechanism of the development of obesity in animals with hypothalamic lesions. *Physiol Rev* 26, 541-559.

Brobeck JR, Tepperman J & Long CN (1943). Experimental Hypothalamic Hyperphagia in the Albino Rat. *Yale J Biol Med* 15, 831-853.

Camm AJ, Malik M, Bigger JT, Beithardt G, Cerutti S, Cohen RJ, Coumel P, Fallen EL, Kennedy HL, Kleiger RE, Lombardi F, Malliani A, Moss AJ, Rottman JN, Schmidt G, Schwartz PJ & Singer DH (1996). Heart rate variability. Standards of measurement, physiological interpretation, and clinical use. Task Force of the European Society of Cardiology and the North American Society of Pacing and Electrophysiology. *Eur Heart J* 17, 354-381.

Cannon B & Nedergaard J (2004). Brown adipose tissue: function and physiological significance. *Physiol Rev* 84, 277-359.

Card JP & Sved AF (2011). Central autonomic pathways. *Central regulation of autonomic functions.* 2nd edition, 3-22.

Carlsson A, Hillarp NA & Waldeck B (1963). Analysis of the Mg++-Atp Dependent Storage Mechanism in the Amine Granules of the Adrenal Medulla. *Acta Physiol Scand Suppl*, SUPPL215:211-238.

Carruba MO, Bondiolotti G, Picotti GB, Catteruccia N & Da Prada M (1987). Effects of diethyl ether, halothane, ketamine and urethane on sympathetic activity in the rat. *Eur J Pharmacol* 134, 15-24.

Cattanach BM, Peters J, Ball S & Rasberry C (2000). Two imprinted gene mutations: three phenotypes. *Hum Mol Genet* 9, 2263-2273.

Chen M, Berger A, Kablan A, Zhang J, Gavrilova O & Weinstein LS (2012). Gsalpha deficiency in the paraventricular nucleus of the hypothalamus partially contributes to obesity associated with gsalpha mutations. *Endocrinology* 153, 4256-4265.

Chen M, Gavrilova O, Liu J, Xie T, Deng C, Nguyen AT, Nackers LM, Lorenzo J, Shen L & Weinstein LS (2005). Alternative Gnas gene products have opposite effects on glucose and lipid metabolism. *Proceedings of the National Academy of Sciences of the United States of America* 102, 7386-7391.

Chen M, Nemechek NM, Mema E, Wang J & Weinstein LS (2011). Effects of deficiency of the G protein Gsalpha on energy and glucose homeostasis. *Eur J Pharmacol* 660, 119-124.

Chen M, Wang J, Dickerson KE, Kelleher J, Xie T, Gupta D, Lai EW, Pacak K, Gavrilova O & Weinstein LS (2009). Central nervous system imprinting of the G protein G(s)alpha and its role in metabolic regulation. *Cell Metab* 9, 548-555.

Chhajlani V (1996). Distribution of cDNA for melanocortin receptor subtypes in human tissues. *Biochem Mol Biol Int* 38, 73-80.

Chung KY, Rasmussen SG, Liu T, Li S, DeVree BT, Chae PS, Calinski D, Kobilka BK, Woods VL, Jr. & Sunahara RK (2011). Conformational changes in the G protein Gs induced by the beta2 adrenergic receptor. *Nature* 477, 611-615.

Coote JH (2007). Landmarks in understanding the central nervous control of the cardiovascular system. *Exp Physiol* 92, 3-18.

Corander MP, Fenech M & Coll AP (2009). Science of self-preservation: how melanocortin action in the brain modulates body weight, blood pressure, and ischemic damage. *Circulation* 120, 2260-2268.

Cowley MA, Smart JL, Rubinstein M, Cerdan MG, Diano S, Horvath TL, Cone RD & Low MJ (2001). Leptin activates anorexigenic POMC neurons through a neural network in the arcuate nucleus. *Nature* 411, 480-484.

Cypess AM, Lehman S, Williams G, Tal I, Rodman D, Goldfine AB, Kuo FC, Palmer EL, Tseng YH, Doria A, Kolodny GM & Kahn CR (2009). Identification and importance of brown adipose tissue in adult humans. *N Engl J Med* 360, 1509-1517.

Dalkara T, Irikura K, Huang Z, Panahian N & Moskowitz MA (1995). Cerebrovascular responses under controlled and monitored physiological

conditions in the anesthetized mouse. *J Cereb Blood Flow Metab* 15, 631-638.

Dampney RA, Coleman MJ, Fontes MA, Hirooka Y, Horiuchi J, Li YW, Polson JW, Potts PD & Tagawa T (2002). Central mechanisms underlying short- and long-term regulation of the cardiovascular system. *Clin Exp Pharmacol Physiol* 29, 261-268.

Dampney RA & Horiuchi J (2003). Functional organisation of central cardiovascular pathways: studies using c-fos gene expression. *Prog Neurobiol* 71, 359-384.

Dampney RA, Horiuchi J, Killinger S, Sheriff MJ, Tan PS & McDowall LM (2005). Long-term regulation of arterial blood pressure by hypothalamic nuclei: some critical questions. *Clin Exp Pharmacol Physiol* 32, 419-425.

Dampney RA, Li YW, Hirooka Y, Potts P & Polson JW (1995). Use of c-fos functional mapping to identify the central baroreceptor reflex pathway: advantages and limitations. *Clin Exp Hypertens* 17, 197-208.

Davern PJ, Jackson KL, Nguyen-Huu TP, La Greca L & Head GA (2010). Cardiovascular reactivity and neuronal activation to stress in Schlager genetically hypertensive mice. *Neuroscience* 170, 551-558.

Davern PJ, Nguyen-Huu TP, La Greca L, Abdelkader A & Head GA (2009). Role of the sympathetic nervous system in Schlager genetically hypertensive mice. *Hypertension* 54, 852-859.

Deepak KK (2011). Heart rate variability: Molecular mechanisms and clinical implications. *Heart rate and Rhythm*, 119-132.

Dimicco JA & Zaretsky DV (2007). The dorsomedial hypothalamus: a new player in thermoregulation. *Am J Physiol Regul Integr Comp Physiol* 292, R47-63.

Dragunow M & Faull R (1989). The use of c-fos as a metabolic marker in neuronal pathway tracing. *J Neurosci Methods* 29, 261-265.

Ecker PM, Lin CC, Powers J, Kobilka BK, Dubin AM & Bernstein D (2006). Effect of targeted deletions of beta1- and beta2-adrenergic-receptor subtypes on heart rate variability. *Am J Physiol Heart Circ Physiol* 290, H192-199.

Egan JJ, Greenberg AS, Chang MK, Wek SA, Moos MC, Jr. & Londos C (1992). Mechanism of hormone-stimulated lipolysis in adipocytes: translocation of hormone-sensitive lipase to the lipid storage droplet. *Proc Natl Acad Sci U S A* 89, 8537-8541.

Esler M & Kaye D (1998). Increased sympathetic nervous system activity and its therapeutic reduction in arterial hypertension, portal hypertension and heart failure. *J Auton Nerv Syst* 72, 210-219.

Ewing DJ, Martyn CN, Young RJ & Clarke BF (1985). The value of cardiovascular autonomic function tests: 10 years experience in diabetes. *Diabetes Care* 8, 491-498.

Fan W, Boston BA, Kesterson RA, Hruby VJ & Cone RD (1997). Role of melanocortinergic neurons in feeding and the agouti obesity syndrome. *Nature* 385, 165-168.

Farah VM, Joaquim LF & Morris M (2006). Stress cardiovascular/autonomic interactions in mice. *Physiol Behav* 89, 569-575.

Fernandez-Rebollo E, Maeda A, Reyes M, Turan S, Frohlich LF, Plagge A, Kelsey G, Juppner H & Bastepe M (2012). Loss of XLalphas (extra-large alphas) imprinting results in early postnatal hypoglycemia and lethality in a mouse model of pseudohypoparathyroidism Ib. *Proc Natl Acad Sci U S A* 109, 6638-6643.

Fisher JP, Young CN & Fadel PJ (2009). Central sympathetic overactivity: maladies and mechanisms. *Auton Neurosci* 148, 5-15.

Frohlich LF, Mrakovcic M, Steinborn R, Chung UI, Bastepe M & Juppner H (2010). Targeted deletion of the Nesp55 DMR defines another Gnas imprinting control region and provides a mouse model of autosomal dominant PHP-Ib. *Proc Natl Acad Sci U S A* 107, 9275-9280.

Gao Q & Horvath TL (2008). Neuronal control of energy homeostasis. *FEBS Lett* 582, 132-141.

Gayen JR, Gu Y, O'Connor DT & Mahata SK (2009). Global disturbances in autonomic function yield cardiovascular instability and hypertension in the chromogranin a null mouse. *Endocrinology* 150, 5027-5035.

Gehrmann J, Hammer PE, Maguire CT, Wakimoto H, Triedman JK & Berul CI (2000). Phenotypic screening for heart rate variability in the mouse. *Am J Physiol Heart Circ Physiol* 279, H733-740.

Giuliani D, Mioni C, Bazzani C, Zaffe D, Botticelli AR, Capolongo S, Sabba A, Galantucci M, Iannone A, Grieco P, Novellino E, Colombo G, Tomasi A, Catania A & Guarini S (2007). Selective melanocortin MC4 receptor agonists reverse haemorrhagic shock and prevent multiple organ damage. *Br J Pharmacol* 150, 595-603.

Goldberger AL, Amaral LA, Glass L, Hausdorff JM, Ivanov PC, Mark RG, Mietus JE, Moody GB, Peng CK & Stanley HE (2000). PhysioBank,

PhysioToolkit, and PhysioNet: components of a new research resource for complex physiologic signals. *Circulation* 101, E215-220.

Goldstein DS, Bentho O, Park MY & Sharabi Y (2011). Low-frequency power of heart rate variability is not a measure of cardiac sympathetic tone but may be a measure of modulation of cardiac autonomic outflows by baroreflexes. *Exp Physiol* 96, 1255-1261.

Gregg C, Zhang J, Weissbourd B, Luo S, Schroth GP, Haig D & Dulac C (2010). High-resolution analysis of parent-of-origin allelic expression in the mouse brain. *Science* 329, 643-648.

Griffioen KJ, Wan R, Okun E, Wang X, Lovett-Barr MR, Li Y, Mughal MR, Mendelowitz D & Mattson MP (2011). GLP-1 receptor stimulation depresses heart rate variability and inhibits neurotransmission to cardiac vagal neurons. *Cardiovasc Res* 89, 72-78.

Hall JE, da Silva AA, do Carmo JM, Dubinion J, Hamza S, Munusamy S, Smith G & Stec DE (2010). Obesity-induced hypertension: role of sympathetic nervous system, leptin, and melanocortins. *J Biol Chem* 285, 17271-17276.

Haynes WG, Morgan DA, Djalali A, Sivitz WI & Mark AL (1999). Interactions between the melanocortin system and leptin in control of sympathetic nerve traffic. *Hypertension* 33, 542-547.

Hayward BE, Kamiya M, Strain L, Moran V, Campbell R, Hayashizaki Y & Bonthron DT (1998). The human GNAS1 gene is imprinted and encodes distinct paternally and biallelically expressed G proteins. *Proc Natl Acad Sci U S A* 95, 10038-10043.

Hetherington AW & Ranson SW (1940). Hypothalamic lesions and adipocity in the rat. *Anat Rec* 78, 149.

Holst JJ (2007). The physiology of glucagon-like peptide 1. *Physiol Rev* 87, 1409-1439.

Huikuri HV, Valkama JO, Airaksinen KE, Seppanen T, Kessler KM, Takkunen JT & Myerburg RJ (1993). Frequency domain measures of heart rate variability before the onset of nonsustained and sustained ventricular tachycardia in patients with coronary artery disease. *Circulation* 87, 1220-1228.

Huso DL, Edie S, Levine MA, Schwindinger W, Wang Y, Juppner H & Germain-Lee EL (2011). Heterotopic ossifications in a mouse model of albright hereditary osteodystrophy. *PLoS One* 6, e21755.

Irani BG & Haskell-Luevano C (2005). Feeding effects of melanocortin ligands--a historical perspective. *Peptides* 26, 1788-1799.

Iversen LL, Glowinski J & Axelrod J (1965). The uptake and storage of H3-norepinephrine in the reserpine-pretreated rat heart. *J Pharmacol Exp Ther* 150, 173-183.

Janssen BJ, De Celle T, Debets JJ, Brouns AE, Callahan MF & Smith TL (2004). Effects of anesthetics on systemic hemodynamics in mice. *Am J Physiol Heart Circ Physiol* 287, H1618-1624.

Kass DA, Hare JM & Georgakopoulos D (1998). Murine cardiac function: a cautionary tail. *Circ Res* 82, 519-522.

Kastin AJ & Akerstrom V (2003). Entry of exendin-4 into brain is rapid but may be limited at high doses. *Int J Obes Relat Metab Disord* 27, 313-318.

Katona PG & Jih F (1975). Respiratory sinus arrhythmia: noninvasive measure of parasympathetic cardiac control. *J Appl Physiol* 39, 801-805.

Kaya AI, Ugur O, Oner SS, Bastepe M & Onaran HO (2009). Coupling of beta2-adrenoceptors to XLalphas and Galphas: a new insight into ligand-induced G protein activation. *Journal of Pharmacology and Experimental Therapeutics* 329, 350-359.

Kehlenbach RH, Matthey J & Huttner WB (1994). XL alpha s is a new type of G protein. *Nature* 372, 804-809.

Klemke M, Pasolli HA, Kehlenbach RH, Offermanns S, Schultz G & Huttner WB (2000). Characterization of the extra-large G protein alpha-subunit XLalphas. II. Signal transduction properties. *Journal of Biological Chemistry* 275, 33633-33640.

Krechowec SO, Burton KL, Newlaczyl AU, Nunn N, Vlatkovic N & Plagge A (2012). Postnatal Changes in the Expression Pattern of the Imprinted Signalling Protein XLalphas Underlie the Changing Phenotype of Deficient Mice. *PLoS One* 7, e29753.

Kuo JJ, da Silva AA, Tallam LS & Hall JE (2004). Role of adrenergic activity in pressor responses to chronic melanocortin receptor activation. *Hypertension* 43, 370-375.

Lanteri-Minet M, Weil-Fugazza J, de Pommery J & Menetrey D (1994). Hindbrain structures involved in pain processing as revealed by the expression of c-Fos and other immediate early gene proteins. *Neuroscience* 58, 287-298.

Laude D, Baudrie V & Elghozi JL (2008). Effects of atropine on the time and frequency domain estimates of blood pressure and heart rate variability in mice. *Clin Exp Pharmacol Physiol* 35, 454-457.

Laurent AC, Breckler M, Berthouze M & Lezoualc'h F (2012). Role of Epac in brain and heart. *Biochem Soc Trans* 40, 51-57.

Lee G & Saito I (1998). Role of nucleotide sequences of loxP spacer region in Cre-mediated recombination. *Gene* 216, 55-65.

Lewandoski M (2001). Conditional control of gene expression in the mouse. *Nat Rev Genet* 2, 743-755.

Li P, Cui B, Zhang L, Sun H, Liu T & Zhu G (2012). Melanocortin 3/4 receptors in paraventricular nucleus modulates sympathetic outflow and blood pressure. *Exp Physiol*.

Li YF & Patel KP (2003). Paraventricular nucleus of the hypothalamus and elevated sympathetic activity in heart failure: the altered inhibitory mechanisms. *Acta Physiol Scand* 177, 17-26.

Liu Z, Turan S, Wehbi VL, Vilardaga JP & Bastepe M (2011). Extra-long Galphas variant XLalphas protein escapes activation-induced subcellular redistribution and is able to provide sustained signaling. *J Biol Chem* 286, 38558-38569.

Livet J, Weissman TA, Kang H, Draft RW, Lu J, Bennis RA, Sanes JR & Lichtman JW (2007). Transgenic strategies for combinatorial expression of fluorescent proteins in the nervous system. *Nature* 450, 56-62.

Llewellyn-Smith IJ, Reimann F, Gribble FM & Trapp S (2011). Preproglucagon neurons project widely to autonomic control areas in the mouse brain. *Neuroscience* 180, 111-121.

Loewy AD (1991). Forebrain nuclei involved in autonomic control. *Prog Brain Res* 87, 253-268.

Lomb NR (1976). Least-squares frequency analysis of unevenly spaced data. *Astrophysics and Space Science* 39, 447-462.

Lonze BE & Ginty DD (2002). Function and regulation of CREB family transcription factors in the nervous system. *Neuron* 35, 605-623.

Madden CJ & Morrison SF (2009). Neurons in the paraventricular nucleus of the hypothalamus inhibit sympathetic outflow to brown adipose tissue. *Am J Physiol Regul Integr Comp Physiol* 296, R831-843.

Makita N, Sato J, Rondard P, Fukamachi H, Yuasa Y, Aldred MA, Hashimoto M, Fujita T & Iiri T (2007). Human G(salpha) mutant causes pseudohypoparathyroidism type Ia/neonatal diarrhea, a potential cell-specific role of the palmitoylation cycle. *Proc Natl Acad Sci U S A* 104, 17424-17429.

Malliani A, Pagani M, Lombardi F & Cerutti S (1991). Cardiovascular neural regulation explored in the frequency domain. *Circulation* 84, 482-492.

Malpas SC (2010). Sympathetic nervous system overactivity and its role in the development of cardiovascular disease. *Physiol Rev* 90, 513-557.

Matsumura K, Tsuchihashi T, Fujii K & Iida M (2003). Neural regulation of blood pressure by leptin and the related peptides. *Regul Pept* 114, 79-86.

Merchenthaler I, Lane M & Shughrue P (1999). Distribution of pre-pro-glucagon and glucagon-like peptide-1 receptor messenger RNAs in the rat central nervous system. *J Comp Neurol* 403, 261-280.

Moody GB (1993). Spectral analysis of heart rate without resampling. *Computers in Cardiology*, 715-718.

Mountjoy KG, Mortrud MT, Low MJ, Simerly RB & Cone RD (1994). Localization of the melanocortin-4 receptor (MC4-R) in neuroendocrine and autonomic control circuits in the brain. *Mol Endocrinol* 8, 1298-1308.

Niskanen JP, Tarvainen MP, Ranta-Aho PO & Karjalainen PA (2004). Software for advanced HRV analysis. *Comput Methods Programs Biomed* 76, 73-81.

Nogueiras R, Perez-Tilve D, Veyrat-Durebex C, Morgan DA, Varela L, Haynes WG, Patterson JT, Disse E, Pfluger PT, Lopez M, Woods SC, DiMarchi R, Dieguez C, Rahmouni K, Rohner-Jeanrenaud F & Tschop MH (2009). Direct control of peripheral lipid deposition by CNS GLP-1 receptor

signaling is mediated by the sympathetic nervous system and blunted in diet-induced obesity. *J Neurosci* 29, 5916-5925.

Nogueiras R, Wiedmer P, Perez-Tilve D, Veyrat-Durebex C, Keogh JM, Sutton GM, Pfluger PT, Castaneda TR, Neschen S, Hofmann SM, Howles PN, Morgan DA, Benoit SC, Szanto I, Schrott B, Schurmann A, Joost HG, Hammond C, Hui DY, Woods SC, Rahmouni K, Butler AA, Farooqi IS, O'Rahilly S, Rohner-Jeanrenaud F & Tschop MH (2007). The central melanocortin system directly controls peripheral lipid metabolism. *J Clin Invest* 117, 3475-3488.

Nunn N, Womack M, Dart C & Barrett-Jolley R (2011). Function and pharmacology of spinally-projecting sympathetic pre-autonomic neurones in the paraventricular nucleus of the hypothalamus. *Curr Neuropharmacol* 9, 262-277.

Ogawa Y, Masuzaki H, Ebihara K, Shintani M, Aizawa-Abe M, Miyanaga F & Nakao K (2002). Pathophysiogical role of leptin in lifestyle-related diseases. Studies with transgenic skinny mice overexpressing leptin. *J Diabetes Complications* 16, 119-122.

Ollmann MM, Wilson BD, Yang YK, Kerns JA, Chen Y, Gantz I & Barsh GS (1997). Antagonism of central melanocortin receptors in vitro and in vivo by agouti-related protein. *Science* 278, 135-138.

Ozaki N, Shibasaki T, Kashima Y, Miki T, Takahashi K, Ueno H, Sunaga Y, Yano H, Matsuura Y, Iwanaga T, Takai Y & Seino S (2000). cAMP-GEFII is a direct target of cAMP in regulated exocytosis. *Nat Cell Biol* 2, 805-811.

Palma-Rigo K, Jackson KL, Davern PJ, Nguyen-Huu TP, Elghozi JL & Head GA (2011). Renin-angiotensin and sympathetic nervous system contribution to high blood pressure in Schlager mice. *J Hypertens* 29, 2156-2166.

Papaioannou VE (2007). Heart rate variability, baroreflex function and heart rate turbulence: possible origin and implications. *Hellenic J Cardiol* 48, 278-289.

Parati G, Faini A & Valentini M (2006). Blood pressure variability: its measurement and significance in hypertension. *Curr Hypertens Rep* 8, 199-204.

Parati G, Saul JP, Di Rienzo M & Mancia G (1995). Spectral analysis of blood pressure and heart rate variability in evaluating cardiovascular regulation. A critical appraisal. *Hypertension* 25, 1276-1286.

Pasolli HA & Huttner WB (2001). Expression of the extra-large G protein alpha-subunit XLalphas in neuroepithelial cells and young neurons during development of the rat nervous system. *Neuroscience Letters* 301, 119-122.

Pasolli HA, Klemke M, Kehlenbach RH, Wang Y & Huttner WB (2000). Characterization of the extra-large G protein alpha-subunit XLalphas. I. Tissue distribution and subcellular localization. *Journal of Biological Chemistry* 275, 33622-33632.

Patel KP (2000). Role of paraventricular nucleus in mediating sympathetic outflow in heart failure. *Heart Fail Rev* 5, 73-86.

Paxinos G & Franklin KBJ (2001). The Mouse Brain in Stereotaxic Coordinates. *Academic Press*.

Perez-Tilve D, Gonzalez-Matias L, Aulinger BA, Alvarez-Crespo M, Gil-Lozano M, Alvarez E, Andrade-Olivie AM, Tschop MH, D'Alessio DA & Mallo F (2010). Exendin-4 increases blood glucose levels acutely in rats by activation of the sympathetic nervous system. *Am J Physiol Endocrinol Metab* 298, E1088-1096.

Peters J, Wroe SF, Wells CA, Miller HJ, Bodle D, Beechey CV, Williamson CM & Kelsey G (1999). A cluster of oppositely imprinted transcripts at the Gnas locus in the distal imprinting region of mouse chromosome 2. *Proc Natl Acad Sci U S A* 96, 3830-3835.

Plagge A, Gordon E, Dean W, Boiani R, Cinti S, Peters J & Kelsey G (2004). The imprinted signaling protein XL alpha s is required for postnatal adaptation to feeding. *Nature Genetics* 36, 818-826.

Plagge A, Kelsey G & Germain-Lee EL (2008). Physiological functions of the imprinted Gnas locus and its protein variants Galpha(s) and XLalpha(s) in human and mouse. *J Endocrinol* 196, 193-214.

Rossi J, Balthasar N, Olson D, Scott M, Berglund E, Lee CE, Choi MJ, Lauzon D, Lowell BB & Elmquist JK (2011). Melanocortin-4 receptors expressed by cholinergic neurons regulate energy balance and glucose homeostasis. *Cell Metab* 13, 195-204.

Sahm UG, Qarawi MA, Olivier GW, Ahmed AR, Branch SK, Moss SH & Pouton CW (1994). The melanocortin (MC3) receptor from rat hypothalamus: photoaffinity labelling and binding of alanine-substituted alpha-MSH analogues. *FEBS Lett* 350, 29-32.

Sakamoto A, Weinstein LS, Plagge A, Eckhaus M & Kelsey G (2009). GNAS haploinsufficiency leads to subcutaneous tumor formation with collagen and elastin deposition and calcification. *Endocr Res* 34, 1-9.

Savontaus E, Breen TL, Kim A, Yang LM, Chua SC, Jr. & Wardlaw SL (2004). Metabolic effects of transgenic melanocyte-stimulating hormone overexpression in lean and obese mice. *Endocrinology* 145, 3881-3891.

Seino S & Shibasaki T (2005). PKA-dependent and PKA-independent pathways for cAMP-regulated exocytosis. *Physiol Rev* 85, 1303-1342.

Senador D, Kanakamedala K, Irigoyen MC, Morris M & Elased KM (2009). Cardiovascular and autonomic phenotype of db/db diabetic mice. *Exp Physiol* 94, 648-658.

Silver AJ, Flood JF, Song AM & Morley JE (1989). Evidence for a physiological role for CCK in the regulation of food intake in mice. *Am J Physiol* 256, R646-652.

Smith GP, Jerome C & Norgren R (1985). Afferent axons in abdominal vagus mediate satiety effect of cholecystokinin in rats. *Am J Physiol* 249, R638-641.

Sowden GL, Drucker DJ, Weinshenker D & Swoap SJ (2007). Oxyntomodulin increases intrinsic heart rate in mice independent of the glucagon-like peptide-1 receptor. *Am J Physiol Regul Integr Comp Physiol* 292, R962-970.

Spiegel AM & Weinstein LS (2004). Inherited diseases involving g proteins and g protein-coupled receptors. *Annu Rev Med* 55, 27-39.

Stern J (2011). Autonomic and neuroendocrine roles of the paraventricular nucleus. *Central regulation of autonomic functions.* 2nd edition, 62-77.

Sunahara RK, Tesmer JJ, Gilman AG & Sprang SR (1997). Crystal structure of the adenylyl cyclase activator Gsalpha. *Science* 278, 1943-1947.

Takahashi H, Yoshika M, Komiyama Y & Nishimura M (2011). The central mechanism underlying hypertension: a review of the roles of sodium ions, epithelial sodium channels, the renin-angiotensin-aldosterone system, oxidative stress and endogenous digitalis in the brain. *Hypertens Res* 34, 1147-1160.

Tallam LS, da Silva AA & Hall JE (2006). Melanocortin-4 receptor mediates chronic cardiovascular and metabolic actions of leptin. *Hypertension* 48, 58-64.

Tallam LS, Stec DE, Willis MA, da Silva AA & Hall JE (2005). Melanocortin-4 receptor-deficient mice are not hypertensive or salt-sensitive despite obesity, hyperinsulinemia, and hyperleptinemia. *Hypertension* 46, 326-332.

Tesmer JJ, Sunahara RK, Gilman AG & Sprang SR (1997). Crystal structure of the catalytic domains of adenylyl cyclase in a complex with Gsalpha.GTPgammaS. *Science* 278, 1907-1916.

Thireau J, Zhang BL, Poisson D & Babuty D (2008). Heart rate variability in mice: a theoretical and practical guide. *Exp Physiol* 93, 83-94.

Thiyagarajan MM, Bigras E, Van Tol HH, Hebert TE, Evanko DS & Wedegaertner PB (2002). Activation-induced subcellular redistribution of G

alpha(s) is dependent upon its unique N-terminus. *Biochemistry* 41, 9470-9484.

Thrasher TN (2004). Baroreceptors and the long-term control of blood pressure. *Exp Physiol* 89, 331-335.

Tronche F, Kellendonk C, Kretz O, Gass P, Anlag K, Orban PC, Bock R, Klein R & Schutz G (1999). Disruption of the glucocorticoid receptor gene in the nervous system results in reduced anxiety. *Nat Genet* 23, 99-103.

Uechi M, Asai K, Osaka M, Smith A, Sato N, Wagner TE, Ishikawa Y, Hayakawa H, Vatner DE, Shannon RP, Homcy CJ & Vatner SF (1998). Depressed heart rate variability and arterial baroreflex in conscious transgenic mice with overexpression of cardiac Gsalpha. *Circ Res* 82, 416-423.

Virtanen KA, Lidell ME, Orava J, Heglind M, Westergren R, Niemi T, Taittonen M, Laine J, Savisto NJ, Enerback S & Nuutila P (2009). Functional brown adipose tissue in healthy adults. *N Engl J Med* 360, 1518-1525.

Vong L, Ye C, Yang Z, Choi B, Chua S, Jr. & Lowell BB (2011). Leptin action on GABAergic neurons prevents obesity and reduces inhibitory tone to POMC neurons. *Neuron* 71, 142-154.

Wedegaertner PB, Bourne HR & von Zastrow M (1996). Activation-induced subcellular redistribution of Gs alpha. *Mol Biol Cell* 7, 1225-1233.

Weinstein LS, Xie T, Zhang QH & Chen M (2007). Studies of the regulation and function of the Gs alpha gene Gnas using gene targeting technology. *Pharmacol Ther* 115, 271-291.

Weinstein LS, Yu S, Warner DR & Liu J (2001). Endocrine manifestations of stimulatory G protein alpha-subunit mutations and the role of genomic imprinting. *Endocr Rev* 22, 675-705.

Wettschureck N & Offermanns S (2005). Mammalian G proteins and their cell type specific functions. *Physiol Rev* 85, 1159-1204.

Williamson CM, Blake A, Thomas S, Beechey CV, Hancock J, Cattanach BM & Peters J (2012). World Wide Web Site - Mouse Imprinting Data and References - <http://www.har.mrc.ac.uk/research/genomic_imprinting/>. *MRC Harwell, Oxfordshire*.

Williamson CM, Turner MD, Ball ST, Nottingham WT, Glenister P, Fray M, Tymowska-Lalanne Z, Plagge A, Powles-Glover N, Kelsey G, Maconochie M & Peters J (2006). Identification of an imprinting control region affecting the expression of all transcripts in the Gnas cluster. *Nat Genet* 38, 350-355.

Xie T, Plagge A, Gavrilova O, Pack S, Jou W, Lai EW, Frontera M, Kelsey G & Weinstein LS (2006). The Alternative Stimulatory G Protein {alpha}-Subunit XL{alpha}s Is a Critical Regulator of Energy and Glucose Metabolism and Sympathetic Nerve Activity in Adult Mice. *Journal of Biological Chemistry* 281, 18989-18999.

Xu Y, Elmquist JK & Fukuda M (2011). Central nervous control of energy and glucose balance: focus on the central melanocortin system. *Ann N Y Acad Sci* 1243, 1-14.

Yamamoto H, Lee CE, Marcus JN, Williams TD, Overton JM, Lopez ME, Hollenberg AN, Baggio L, Saper CB, Drucker DJ & Elmquist JK (2002). Glucagon-like peptide-1 receptor stimulation increases blood pressure and heart rate and activates autonomic regulatory neurons. *J Clin Invest* 110, 43-52.

Young CN & Davisson RL (2011). In vivo assessment of neurocardiovascular regulation in the mouse: principles, progress, and prospects. *Am J Physiol Heart Circ Physiol* 301, H654-662.

Yu S, Gavrilova O, Chen H, Lee R, Liu J, Pacak K, Parlow AF, Quon MJ, Reitman ML & Weinstein LS (2000). Paternal versus maternal transmission of a stimulatory G-protein alpha subunit knockout produces opposite effects on energy metabolism. *J Clin Invest* 105, 615-623.

Zaretskaia MV, Zaretsky DV, Shekhar A & DiMicco JA (2002). Chemical stimulation of the dorsomedial hypothalamus evokes non-shivering thermogenesis in anesthetized rats. *Brain Res* 928, 113-125.

Zhang K, Li YF & Patel KP (2002). Reduced endogenous GABA-mediated inhibition in the PVN on renal nerve discharge in rats with heart failure. *Am J Physiol Regul Integr Comp Physiol* 282, R1006-1015.

Zhang Y, Proenca R, Maffei M, Barone M, Leopold L & Friedman JM (1994). Positional cloning of the mouse obese gene and its human homologue. *Nature* 372, 425-432.